Virginia Institute of Marine Science
esearch Experiences for Undergraduates
Final Research Papers 2019

Funded by the National Science Foundation

Table of Contents

Sediment Modeling: iRUSLE via Bayesian Melding

Kayla Rutherford
James Madison University

Mentor: Dr. Grace Chiu

2 August 2019

Synopsis

The RUSLE sediment modeling system of this project is still inactive due to coding complications, but the individual functions that form the system work as directed when tested except for one function that automates the entire model. Continued efforts are being made to solve these errors to produce a working computer implementation that models sediment movement across the Weany Creek subcatchment.

Abstract

The iRUSLE modeling system is devised to monitor sediment movement across the Weany Creek subcatchment to provide land management recommendations to landowners and policy makers. Due to Weany Creek's high grazing and pastures, it is susceptible to high soil erosion rates which lead to a decrease in the soil's water holding capacity. The modeling system uses data from field observations and simulated draws from probability distributions to produce sediment deposit outputs across the subcatchment to determine water holding capacity and better land management practices. The computer implementation of the modeling system is still

ongoing with coding errors and therefore has not been used to produce model outputs. Efforts are continuously being made to solve these errors to produce a working computer implementation. In summary, the modeling system is still inactive, but the individual functions that form the system work properly when tested, except for the function that automates the entire model.

Introduction

In an arid country such as Australia, fresh water is a key resource to be monitored. Monitoring this resource ensures a carrying capacity that is adequately accessible for commercial, household, and agricultural purposes. Soil erosion may decrease a soil's infiltration capacity to hold fresh water, and, therefore, erosion poses a threat towards water scarcity (Bartley *et al.*, 2006). When topsoil is washed downstream from rain events, there is a decrease in the total sediment deposit to capture rainwater. Ultimately, this increases the runoff rate during rain events and decreases a soil's infiltrating capacity. The type of vegetation patches (cover), may impact soil erosion and runoff rates, causing a decrease in water infiltration if the vegetation cover is low (Post *et al.*, 2006). Thus, sediment modeling must be carried out to monitor and predict changes in soil erosion rates.

Our region of study is Weany Creek, a 13.5 km^2 sub-catchment to the Burdekin catchment in Queensland adjacent to the Great Barrier Reef (Figure 1). It is highly subjected to soil erosion (Post *et al.*, 2006). The Burdekin catchment contains four major creeks including the creek of our study (Wilkinson et al., 2018). This catchment discharges sediment deposits into the Great Barrier Reef and may cause harmful impacts to the quality of life to the reef depending on its discharge. Weany Creek is one of the discharge sources.

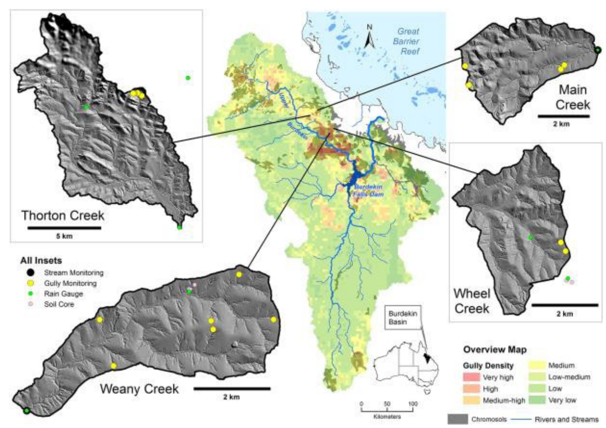

Figure 1: Burdekin Catchment located in northern Queensland, Australia, which contains the Weeny Creek subcatchment (Wilkinson et al., 2018) for observation and analysis in our project.

Weany Creek is composed of red, texture soils that overlie a granodiorite, an igneous rock similar to granite (Bartley *et al*., 2006). This soil has low fertility due to its surface textural properties and heavy grazing (Bartley *et al.,* 2006). Thus, this makes it susceptible to high soil erosion rates. For all the reasons described, data was taken using in-situ monitoring devices to monitor sediment and runoff loss after rain events collected by Post *et al.* (2006) (Figure 2). However, in-situ data cannot be collected at each individual map pixel to determine soil erosion, so a modeling system is devised. A main component of this modeling system is the Revised Universal Soil Loss Equation (RUSLE), with which one can approximate soil erosion and the total sediment deposit across all 499,318 map pixels that cover the Weany Creek subcatchment. However, data cannot be collected at each individual pixel to determine soil erosion, so a modeling system is devised.

The modeling system of this project (see Methods below) extends RUSLE to take actual weather and geomorphological data as inputs to produce simulated soil deposit outcomes to be analyzed. The output data analyzed from the extended modeling system will be used for scientific discovery to enhance grazing practices to farmers and landowners to reduce sediment runoff and preserve Weany Creek's holding capacity. In particular, using this modeling system, sediment movement is interpreted to understand how storms and cover type impact an area. One can hypothesize that having a higher cover type decreases soil erosion, because there are more roots to hold down the topsoil from incoming rainstorms. One can also hypothesize that an increase in a storm's kinetic energy should lead to an increase in soil erosion across Weany Creek.

Thus, to facilitate these broader objectives, my contribution to the project is to prepare a working model to analyze simulated outputs of sediment movement.

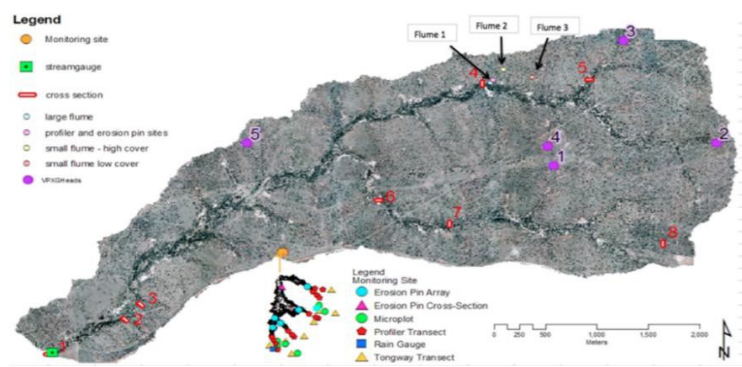

Figure 2: Weany Creek catchment monitored by Post *et al*. (2006).

Methods

Sediment modeling is done using integrated RUSLE (iRUSLE) (Chiu *et al*., 2013), a highly computational statistical modeling system, to model sediment movement in relation to sediment deposits. Its foundation is based on RUSLE and Bayesian melding (Poole & Raftery 2000). RUSLE is defined by the following (Renard *et al*., 1997):

Equation 1. $A = R * K * L * S * C * P$

A = estimated average soil loss in tonnes per acre per year

R = rainfall runoff erosivity factor

K = soil erodibility factor

L = slope length factor

S = slope steepness factor

C = cover management factor

P = support practice factor

A raster image consisting of 499,318 pixels is used to categorize cover type and spatial distribution on a scale between 1 and 4 described as ξ where 1 is extremely high cover and 4 is extremely low cover. The different cover types are used to understand how they correlate to sediment erosion during rain events. The A factor is only observed in isolated points on the map, while the other factors (except for C which is based on aerial photographs) are computed per pixel based on weather and geomorphological data.

Bayesian melding is a highly computationally intensive statistical technique used here to formulate probabilistic assessments of predicted values of soil erosion in conjunction with iRUSLE to determine soil erosion and sediment deposits across the Weany Creek catchment. It melds together several input values (collected data and solved values) to obtain posterior probability distributions of sediment deposits. The solved values are determined through knowledge-based estimates while collected data is data collected in the field.

The first input value is data collected by Post *et al*. during storm events (2006). These are the aforementioned-isolated field data on A, and pixel-wise weather, geomorphology, and photographic data. The second input includes substituted knowledge-based estimates of A using Equation 1 alone. These values are incorporated into the modeling system to retrieve a "melded output" for A, which is defined as sediment deposit.

The modeling system is produced by 'bayespackage', an R (R Core Team, 2013) package in conjunction between C++ and Rcpp (Eddelbuettel & Francois, 2011) code. Dr. Chiu, my mentor, implemented the Bayesian melding model (math equations) and prototyped the R implementation for the package. Dr. Josh Bowden, a CSIRO employee and original creator of 'bayespackage', produced the C++ code and corresponding Rcpp code and created an "alpha" software to upscale the prototyped version for application to the ~ 500K pixels in Weany Creek. My main task as the REU intern is to use the functions defined in the alpha 'bayespackage' and the '.RData' file (containing data inputs created by Dr.Chiu) to create a working "beta" implementation of the model for simulating sediment deposit outputs.

Results

In the final stages of running the "beta" version of the model, coding errors ceased the execution of results. From test running the individual functions within 'bayespackage', we can be assured that the individual functions work properly, except for the one function that is needed to automate the full model. There are ongoing efforts in trying to resolve the error, so the model can produce useable outputs.

Discussion

Details on Coding Errors

As stated, the model is currently inactive due to coding error. Through the process of implementing the "beta" version of the model, several other errors have been recognized and resolved including compilation, path, and function testing errors.

The original package was created in 2013 by my mentor Dr. Grace Chiu and Dr. Josh Bowden. However, the package was out of date and needed to be recompiled on a local high performance computing (HPC) system to run an intensive job on the HPC. Such a job was created to run the simulated model on the W&M/VIMS computing system. In the process of trying to recompile the package, a "restrict error" was received. The word 'restrict' was defined in the package to limit how a function is called within the code. This error was resolved using the following in the C++ code:

```
#if_STDC_VERSION_<199901L
#define restrict /*nothing*/
#endif
```

Once the package was compiled, it created a zip file called ‘bayespackage_1.0.tar.gz’ to be used inside R, a statistical program. Path errors were found when trying to compile the package such as “library not found”. This means that the specific file or extension of ‘RcppArmadillo’, another package used inside ‘bayespackage’ to employ a random number generator, couldn’t be found. However, when locating the extension of ‘RcppArmadillo’, it shows the extension was located in the path defined. The HPC staff and Dr. Josh Bowden were contacted to help correct this path error.

When the package was finally installed to R, the individual functions that form ‘bayespackage’ needed to be tested to ensure they worked properly. The data was interpreted to be used inside specific functions to create outputs. Inside the test functions, some pieces of data needed were not in the local environment, which caused complications when trying to run the functions. This data was later located, and the test functions were run accordingly. With the complete data in .RData, it was concluded that the individual functions run properly inside the package as directed.

When trying to run the full iRUSLE system by calling the function ‘draw_out_ind_J’ inside ‘bayespackage’, I received an HPC wall limit error (Figure 3). A wall limit error is defined as exceeding the time allotted to run a job. The job was set to run for an hour to produce draws, however it exceeded this time. This should not be the case with a correctly implemented modeling system. To diagnose the problem further, the output file was observed, which gave an outputted list of the number of storms, number of pixels, and number of draws, but did not produce any outputs on A (Figure 4). When looking more closely at the code, the function ‘setRNGseed’ – as commented by Dr. Josh Bowden – was to be run to activate the pseudo random number generator before running the ‘draw_out_ind_J’ function. However, when using this ‘setRNGseed’ function, it produced a segfault error: “memory not mapped” (Figure 5). A segfault error is defined as trying to access memory that it can’t access. Two hypotheses were devised:

1. The path file couldn’t be found to reach ‘RcppArmadillo’

2. setRNGseed is an older version and needs to be updated

Based upon the advice from the HPC staff, it was concluded that the error being produced is a coding error. Thus, this means that the first hypothesis shows to be false. The second hypothesis, that setRNGseed is an older version, is currently the area of study. Several solutions to replace this function have been trailed to no avail, but ongoing efforts are in place to find a solution.

Through continuous efforts to solve coding errors, a coding methodology was developed over the course of the program:

1. Which line?
2. What's the issue?
3. Who else has had this problem?
4. Copy the original code to a test code
5. Trial and error of changing code
6. Ask and get better help!

```
PBS Job Id: 5832831
Job Name:   test
Exec host:  vx01/0-11
Aborted by PBS Server
Job exceeded its walltime limit. Job was aborted
See Administrator for help
Exit_status=-11
resources_used.cput=01:00:16
resources_used.vmem=984100kb
resources_used.walltime=01:00:27
resources_used.mem=482788kb
resources_used.energy_used=0
req_information.task_count.0=1
req_information.lprocs.0=12
req_information.thread_usage_policy.0=allowthreads
req_information.hostlist.0=vx01:ppn=12
req_information.task_usage.0.task.0={"task":{"cpu_list":"0-11","mem_list":"0-1","cores":0,"threads":12,"host":"vx01"}}
Error_Path: vortex.sciclone.wm.edu:/sciclone/scr10/kmrutherford/iRUSLE/test.o5832831
Output_Path: vortex.sciclone.wm.edu:/sciclone/scr10/kmrutherford/iRUSLE/test.o5832831
```

Figure 3: Walltime limit error when trying to produce sediment deposit outputs from the modeling system.

```
>
> draw_out_ind_J1(p1.Theta.draws,covar.int,covar.sp.ls,1)
i_NumStorms: 18
NumDraws14: 10000
NumPix3: 499318
logscale : 1  TRUE
16 [vortex]
```

Figure 4: Running the model function 'draw_out_ind_J1' to produce outputs, however no outputs were given.

```
> setRNGseed
function ()
{
    .Call("setRNGseed", PACKAGE = "bayespackage")
}
<environment: namespace:bayespackage>
> setRNGseed()

 *** caught segfault ***
address 0x3, cause 'memory not mapped'

Possible actions:
1: abort (with core dump, if enabled)
2: normal R exit
3: exit R without saving workspace
4: exit R saving workspace
Selection:
```

Figure 5: The function setRNGseed produced a segfault error, meaning it's trying to access memory it can't access.

Software Manual

A READ-Me file was created to provide detailed notes and instructions on how to run the modeling system for iRUSLE users. Inside this file, it provides step by step instructions on how to compile the package on the W&M/VIMS HPC system. It includes notes taken on email conversations between personnel such as Dr. Josh Bowden and HPC staff regarding error complications. Definitions were defined regarding variables in the model and how they relate to the code. The data inputs were explained regarding how they are used inside the code and where to use them to run which functions. It also includes notes taken on errors received along the way and how they were solved. Lastly, a comparison was done between the iRUSLE-Bayesian melding model equations and the 'bayespackage' code. An explanation was given on where these equations were found inside the code and what they were producing.

Future Work

Although the "beta" version of the model is still not functional, continuous efforts will be made in the near future to solve the ongoing errors. Once the model implementation has been successfully configured and outputs have been analyzed, there will be efforts to produce a publication. It will be used to provide land management recommendations in relation to land use practices. Weany Creek is known for its high grazing and farmland which leads to its high soil erosion rates. Providing landowners, farmers, and policy makers better land management solutions, will mitigate this problem. Thus, this will increase the soil's water holding capacity for agricultural purposes and decrease sediment pollution in Weany Creek and the Great Barrier Reef.

Acknowledgements

I thank my mentor Dr. Grace Chiu and Dr. Josh Bowden who contributed ideas, technical help, and advising through the duration of the project. I also thank the HPC staff for their efforts in resolving compilation errors. Thanks to Dr. Rochelle Seitz, Ms. Jenny Dreyer and Ms. Katherine Longmire for coordinating the REU program at VIMS. Program funding for the VIMS Research Experience for Undergraduates was made available through a grant awarded from the National Science Foundation (grant # NSF OCE 1659656) to Drs. Linda Schaffner and Rochelle Seitz.

Literature Cited

Bartley, R., Roth, C.H., Ludwig, J., McJannet, D., Liedloff, A., Corfield, J., Hawdon, A. and Abbott, B. (2006). Runoff and erosion from Australia's tropical semi-arid rangelands: influence of ground cover for differing space and time scales. *Hydrological Processes*, 20, 3317–3333.

Chiu, G.S., Sherman, B., Bowden, J.C. (2013). "Bayesian melding for the integrated revised universal soil loss equation applied to Australian subcatchments." CSIRO internal draft report.

Eddelbuettel, D., and Francois, R. (2011). Rcpp: Seamless R and C++ Integration. Journal of Statistical Software, 40(8), 1-18. URL http://www.jstatsoft.org/v40/i08/.

Liedloff, A.C., Ludwig, J.A., Bartley, R. and Coughenour, M.B. (2005). Modelling tropical landscapes for ecological management: what can we learn from preliminary Savanna.au simulations. *MODSIM 2005 International Congress on Modelling and Simulation.* Modelling and Simulation Society of Australia and New Zealand, Melbourne, 354 – 360.

Lu, H., Gallant, J., Prosser, I.P., Moran, C. and Priestley, G. (2001*). Prediction of Sheet and Rill Erosion Over the Australian Continent, Incorporating Monthly Soil Loss Distribution.* Technical Report 13/01. CSIRO Land and Water.

Poole, D., & Raftery, A.E. (2000). Inference for Deterministic Simulation Models: The Bayesian Melding Approach. *Journal of the American Statistical Association,* 95, 1244 – 1255.

Post, D.A., Bartley, R., Corfield, J., Nelson, B., Kinsey-Henderson, A., Hawdon, A., Gordon, I., Abbott, B., Berthelsen, S., Hodgen, M., Keen, R., Kemei, J., Vleeshouwer, J., MacLeod, N. and Webb, M. (2006a). *Sustainable Grazing for a Healthy Burdekin Catchment*. Meat and Livestock Australia Ltd.

R Core Team (2013). R: A language and environment for statistical computing. R Foundation for Statistical Computing, Vienna, Austria. URL http://www.R-project.org/.

Renard, K.G., Foster, G.A., Weesies, D.K., McCool, D.K. and Yoder, D.C. (1997). Predicting soil erosion by water: A guide to conservation planning with the Revised

Universal Soil Loss Equation. *Agriculture Handbook 703*. United States Department of Agriculture, Washington DC.

Van Dijk, A.I.J.M., Bruijnzeel, L.A. and Rosewell, C.J. (2002). Rainfall intensity–kinetic energy relationships: a critical literature appraisal. *Journal of Hydrology*, 261, 1–23.

Wilkinson, S. N., Kinsey‐Henderson, A. E., Hawdon, A. A., Hairsine, P. B., Bartley, R., and Baker, B. (2018) Grazing impacts on gully dynamics indicate approaches for gully erosion control in northeast Australia. *Earth Surf. Process. Landforms*, 43: 1711– 1725. doi: 10.1002/esp.4339.

Wischmeier, W.H. and Smith, D.D. (1958). Rainfall energy and its relationship to soil loss. *Transactions, American Geophysical Union*, 39, 285–291.

Yang, X., and Yu, B. (2015). Modelling and mapping rainfall erosivity in New South Wales, Australia. *Soil Research*. 53. 10.1071/SR14188.

Bottom Boundary Layer Dynamics Modelling in the Gulf of Mexico "Dead Zone"

Jacob Wacht
William & Mary

Mentor(s): Dr. Courtney Harris and Dr. Linlin Cui

2 August 2019

Synopsis

A one-D Regional Ocean Modeling System (ROMS) model was developed using August 2018 field study data courtesy of Dr. Kanchan Maiti (LSU). The model results followed the same bottom shear stress variability as the field data. However, more fine tuning is necessary before including sediment resuspension and biogeochemical equations to better understand the "Dead Zone" chemical, physical, and biological processes.

Abstract

The project included a 1-D (vertical) model developed from ROMS to represent a 20-m deep field site offshore of the Mississippi Delta in the Gulf of Mexico for 24 hours in August 2018 and for Hurricane Ike with the same water column initial conditions. The model input included time dependent waves with steady state temperature, salinity, density, and speed profiles. The model results were compared with field data taken in August 2018, which included taking conductivity, temperature, depth, and water column velocity measurements on the Louisiana shelf, and near-bed Acoustic Doppler Velocimeter (ADV) deployments at four sites. The bottom shear stress velocity was estimated using the Turbulent Kinetic

Energy (TKE) method. The model-derived bottom shear stress velocity was compared to that from the ADV to assess how well conditions were mimicked. In low energy environments, such as the field site, bottom currents during the deployment are not enough to resuspend materials. However, in high energy situations (e.g. Hurricane Ike), storm-induced resuspension is very likely, which would affect the Dissolved Oxygen and other chemical elements in the anoxic/hypoxic zone as un-respired dead cells are reintroduced from the bottom to the water column to be respired. The model was made with a focus on the bottom boundary layer to later be evolved into a fully coupled hydrodynamic, sediment transport, and biogeochemical model (HydroBioSed) to better understand the seasonally occurring "Dead Zone".

Introduction

Understanding the processes that impact ocean acidification on the Gulf of Mexico continental shelf requires study of ocean chemistry within the bottom boundary layer, and fluxes between the seafloor and water column. Specifically, quantifying bottom boundary layer turbulence in the Gulf of Mexico will help determine suspended sediment resuspension and Dissolved Inorganic Carbon (DIC) flux from seafloor sediments.

The study area is the Louisiana continental shelf, west of the Mississippi River Delta, and on the "Dead Zone['s]" northeast fringe (Fig.1). The "Dead Zone" is a volume of oxygen-depleted water (dissolved oxygen < 2 mg/l) that seasonally occurs in the bottom boundary layer; its extent peaks in the summer and fades as stratification breaks down during the winter (Fry et al., 2016). Oxygen depletion that forms the Dead Zone has been exacerbated by nutrient input overload due to fertilizer use, sewage treatment, and urban deforestation within the Mississippi River watershed (Rabalais et al., 2002).

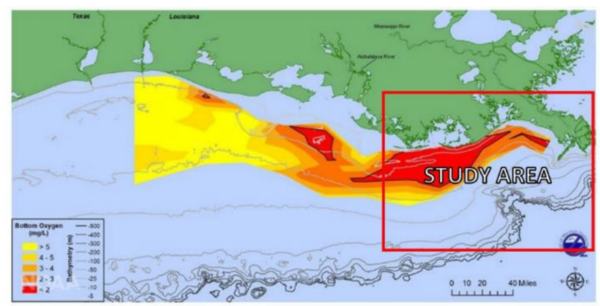

Figure 1: Overview map of the "Dead Zone's" footprint on with the study area on the northwest tip on the continental shelf (Rabalais, N., LSU/LUMCON, and Turner, G., LSU, 2018).

Once the water column is stratified during the spring, a warm nutrient-rich surface layer forms that creates conditions prime for massive algal blooms. The spring bloom produces detrital matter that sinks to the bottom of the water column, but stratification limits mixing between the surface and bottom waters. As bacteria respire the falling plankton oxygen levels within the bottom layer rapidly decrease. This creates zones where the oxygen is too low for benthic and pelagic organisms to survive, hence the name "Dead Zone". The "Dead Zone" alters organism diversity and livable ranges (Rabalais et al., 2002). The "Dead Zone" also has high DIC concentrations that acidify the bottom water (Feely et al. 2010; Cai et al., 2011). However, the notion that hypoxia and acidification solely develop from nutrient input and stratification is vastly oversimplified; bottom boundary layer interactions with the seabed greatly affect the water characteristics below the pycnocline (Rowe and Chapman, 2002). Hypoxia is a bottom boundary layer phenomenon in many systems, including the Gulf of Mexico (Moriarty et al., 2018; Zhang et al., 2015).

The bottom boundary layer is a distinct water volume that interacts with the bottom sediment (Grant and Madsen, 1986). It is defined as the near-bed portion of the water column within which bottom friction is important. The layer has a large impact on hypoxia as well as interior flow (Zhang et al., 2015). Through buoyancy advection-driven convergence at places where the pycnocline intersects with the bottom boundary layer low oxygen water in the bottom layer can move upward into the water column (Zhang et al., 2015). Oxygen levels within the "Dead Zone" are impacted by bottom sediment and bottom boundary layer processes (Moriarty, et al., 2018). The bed shear stress imposed by the bottom boundary layer flows on the seabed determine whether sediment will or will not be resuspended. Particulate resuspension reintroduces into the water column organic matter to be decomposed, decreasing oxygen levels there (Moriarty et al., 2018). A three-dimensional, coupled hydrodynamic model run for the Northern Gulf of Mexico showed that the bed shear stress frequently overcame the minimum amount needed to resuspend sediment and impact the bottom water (Moriarty et al., 2018). The model also found the largest fluxes lowering oxygen and increasing ammonium occurred during resuspension events (Moriarty, et al., 2018).

However, most models simplify or neglect the effect of resuspension on bottom boundary layers' physical and biogeochemical properties altogether (Fennel et al. 2011; Hetland and DiMarco 2008). By neglecting resuspension, the model results may overestimate the dissolved oxygen within the "Dead Zone" (Moriarty et al., 2018). A ROMS model run by Moriarty et al. (2018), incorporated a HydroBioSed model that included resuspension and the hydrodynamic role in regulating organic matter between the bottom water and sediment. At present, however, HydroBioSed has not attempted to resolve the carbon cycle.

Measuring the DIC flux due to bed layer interaction will improve our understanding of pH changes that have ecological impacts on the benthic and pelagic organisms within the layer. Limited research focuses on the role that bottom boundary layer processes and sediment interactions play in ocean acidification. Only one study has reported observed DIC fluxes from the benthos using box cores (Lehrter et al., 2012).

Obtaining measurements in the bottom boundary layer is difficult, especially when the near-bed region and sediment bed itself is to be sampled, and during energetic storm periods when resuspension events occur. However, measurements from the bottom boundary layer and sediment bed are needed to understand near-bed ocean acidification. To fill this gap, Dr. Kanchan Maiti (LSU) conducted a field cruise in summer, 2018. He deployed a bottom lander capable of measuring sediment bed chemistry and near-bed conditions, similar to previous work (Adhikari et al., 2015). Additionally, an Acoustic Doppler Velocimeter (ADV) was placed on the lander to measure near-bed velocity, including turbulent velocity fluctuations. The lander was deployed at four locations between August 14 and 27, 2018. Data from the field study will be useful for development of a coupled hydrodynamic – geochemistry - sediment transport model that can be used to assess the role of resuspension in oxygen dynamics and ocean acidification in the bottom boundary layer.

As a step toward developing a coupled HydroBioSed model, a 1-D (vertical) simulation was run to assess how well current models predict the bed stress at the study sites. After demonstrating that the model conforms to field conditions, it is useful to simulate an extreme event capable of significant sediment resuspension into the bottom boundary layer.

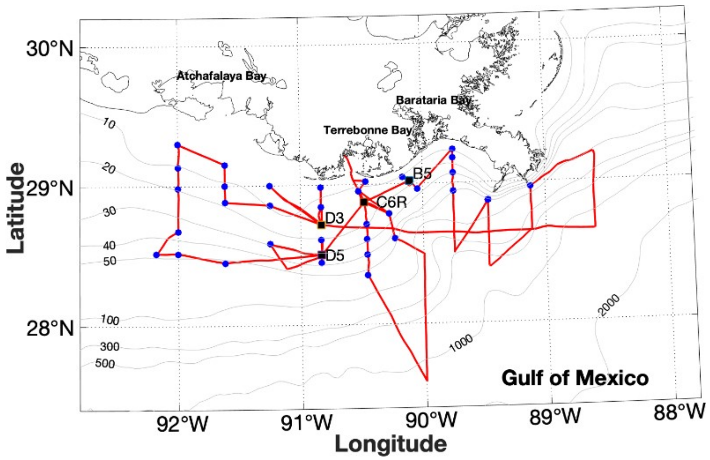

Figure 2: Site locations for the four ADV deployments (C6R,B5,D3 and D5), CTD drops (blue dots), and the shipboard ADCP track (red line). Contour lines represent bathymetry in meters. Locations provided by Dr. K. Maiti (LSU).

Table 1. Description of station locations, deployment time, and depth (information courtesy of Dr. K. Maiti, (LSU).

Station Name	Date	Lat (°)	Lon (°)	Depth (m)
C6R(b1)	8/14/2018	28.8716	-90.4811	20
B5(b2)	8/16/2018	29.0208	-90.1058	18
D3(b3)	8/19/2018	28.7167	-90.8333	18
D5(b4)	8/21/2018	28.5	-90.8333	32.88

Methods

The field locations included: the ADV dropped at 4 sites C6R, B3, D5, and D3; Conductivity Temperature Depth (CTD) measurements made around each drop site; additionally, an Acoustic Doppler Current Profiler (ADCP) was mounted to the boat hull to take current data while underway.

CTD Operation

The CTD was winched down, at specific latitude and longitude coordinates, into the water column and held at chosen depths where measurements are taken. The CTD records Depth (m), Pressure (db), Temp (degC), Density (kg/m^3), Turbidity [NTU], Conductivity (mS/cm), Conductivity 2 (mS/cm), Fluorescence, O_2 (mg/l), O_2 2 (mg/l), Salinity (PSU), PAR,, Scan Count, and Bottles Fired. Sampled sites included lowering depths from 16 to 40 meters.

ADV Operation

Fig. 3 displays the ADV sampling method. Each sample was saved to the data sheet for analysis. In the diagram the samples are represented by the vertical ticks. A sample represents the average over a 5-second period. The values being averaged to create each sample are identified as pings. The ping rate was 5 Hz, so that each 5-second sample represented an average of 50 pings. Each sample contains the average velocity ($\overline{u}, \overline{v}$ and $\overline{w}$); and standard deviation of u', v', and w'; where u' represents the residual between the instantaneous velocity u (for a single ping) and the sample-averaged velocity $\overline{u}$. The samples were collected in bursts. The ADV recorded 60 samples in a burst; then went into sleep mode for 25 minutes where no measurements were taken; after the 25-minute period another burst was recorded. The cycle was repeated continuously through each deployment.

The ADV for the August 2018 cruise was configured to run in burst mode while taking pings at a 10 Hz rate and recording a sample every 5 seconds. The burst duration was 180 seconds that resulted in 60 samples, separated by 5 seconds, every burst.

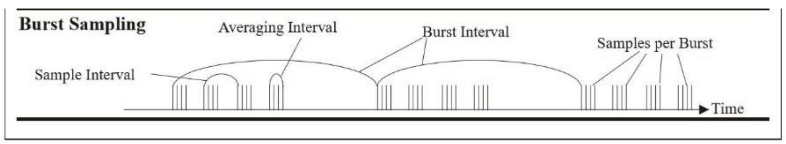

Figure 3: Illustration of Argonaut-ADV sampling strategies (Argonaut-ADV Operation Manual Firmware Version 11.2).

ADV Processing

Each bottom deployment velocity measured by the ADV in the horizontal (u and v) and vertical (w) directions were filtered to remove spikes from ADV operation using a kernel analytics program (Islam and Zhu, 2013). Each spike (extraneous sample) timestamp in the horizontal and vertical directions was recorded. Then, using the ADV derived standard error for each sample, the TKE method was completed to find the bottom shear stress velocity U_* (Kim et al., 2000). The shear stress velocity can be compared to model results to determine how well the model matched actual conditions.

ADCP Operation

The ADCP was mounted pointing downwards from the boat hull during the August 2018 cruise and configured to record velocity profiles to a maximum depth of 24 m split into 40 bins that were each about 1.67 m thick. During processing reflections were removed from the data as well as extraneous velocity spikes. The ADCP data was rotated from boat direction to align with the cardinal North, East, and Up.

Numerical Model Configuration

A 1-D (vertical) implementation of the ROMS was developed to represent 20 m depth deployment at site C6R (Fig. 2). The model was driven by observed salinity, temperature and velocity data. The closest CTD cast descent to the ADV data collection's start time was used to specify conductivity and temperature at depth. Vertical profiles of salinity and temperature show that the water column was very stratified, and the density was influenced more heavily by salinity than temperature (Fig. 4 a-d). The salinity influence is expected due to the site's proximity to the Mississippi River delta and its outflow. The ADCP velocity measurements made within an hour of the CTD deployment were time-averaged to provide water column velocities. Because the ADCP doesn't provide reliable near bottom velocity measurements, the ADV was used to specify the speed at 0.3 m above the seabed. At the seabed the velocity was assumed to approach zero. Fig. 4f shows the derived vertical velocity profile. These data were used to develop an input file for the 1-D model that specified the velocity, temperature, and salinity profiles. The model was configured to run at a steady state due to the highly stratified, stable nature of the site.

Waves were included into the model as a forcing file using significant wave height, surface period, and direction from the nearest NOAA buoy 42002 located on the Texas shelf in the Gulf of Mexico. Time series of wave parameters are shown in Fig. 5. Buoy 42002 was used since it was the closest wave monitoring device with data for the C6R station while the ADV was deployed. The bottom wave period, needed by the ROMS model, was calculated using code from Wiberg and Sherwood (2006).

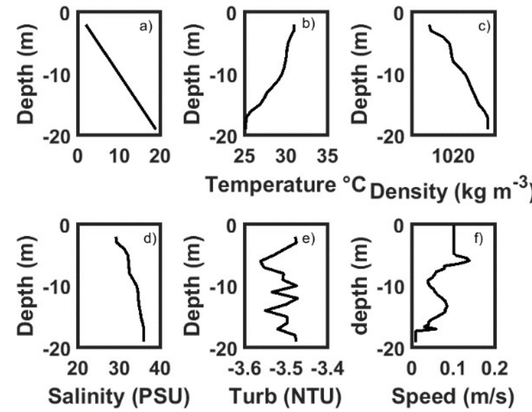

Figure 4: Vertical profiles of (a) the sample number, (b) temperature, (c) density, (d) salinity, (e) turbidity, (f) velocity. Panels (a)-(e) from CTD data at station C6R; Panel (f) is an average of the ADCP horizontal speeds measured within 40 minutes of the CTD cast instead of an hour due to boat movement.

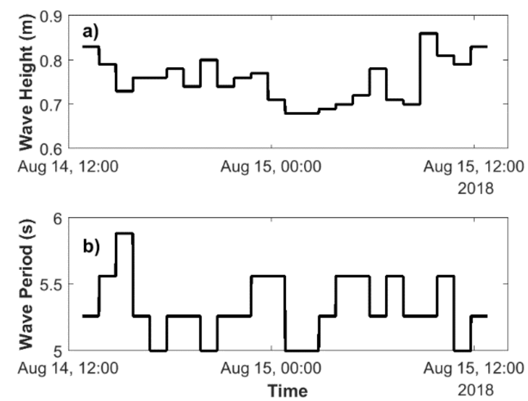

Figure 5: Time series of (a) wave height and (b) wave period for the C6R deployment. The data from the buoy 42002 was sampled hourly. Hence, a constant height and period for every hourly measurement was assumed to be inputted into the simulation.

Results

Field Data

Initial U_* calculations from the ADV data at each site were on the same order of magnitude as previous models run by Moriarty et al. (2018) in the Gulf of Mexico. The expected range was an order of magnitude around $10^{-1} cm\ s^{-1}$ for normal ocean conditions. The calculated U_* for each site remained in the expected range. Fig. 6 shows the time series of the calculated shear stress velocity at site C6R.

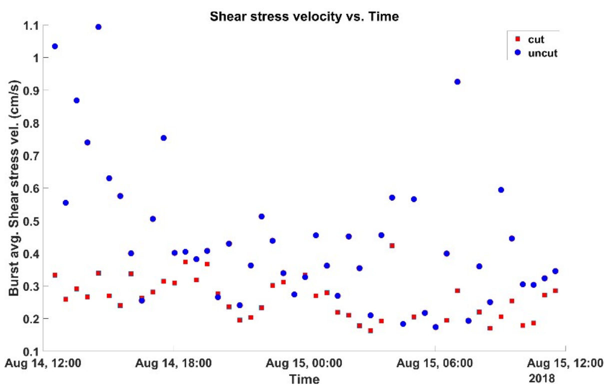

Figure 6: Time series burst-averaged U_* from uncut data (blue dots) and cut data (red squares) calculated at the C6R site using the TKE method. The burst averaged is within the expected shear velocity range.

One-D Hydrodynamic Model

A model was configured and run to simulate the shallow water conditions found in the first deployment site C6R for the 24-hour time period. This site (20 m) was selected as a focus because waves will have a bigger effect on resuspension here than at the deeper sites.

Data from Fig 4. was used for forcing conditions within the model. Wave data from Fig 5. was inputted for the model time. The vertical axis (depth) was split into 50 bins for calculation.

1-D hydrodynamic model results

The model was configured to run at steady state conditions and remains at this profile. Fig. 7 shows a comparison between model results and CTD field measurements. The model matched the field conditions as it is very stratified and remains stratified over the time range. The much less dense surface layer represents the freshwater outflow from the Mississippi River and denser, deeper layers are constituted by the colder, more saline Gulf of Mexico water (Fig. 7b-d). The model Density matches the CTD profile well (Fig. 7b-d).

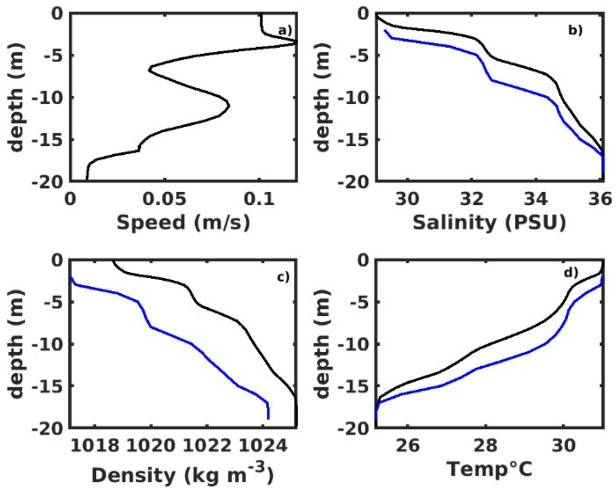

Figure 7: Model speed (black) (a), a comparison between modeled (black) and observed (blue) (b) salinity, (c) density, and (d) temperature.

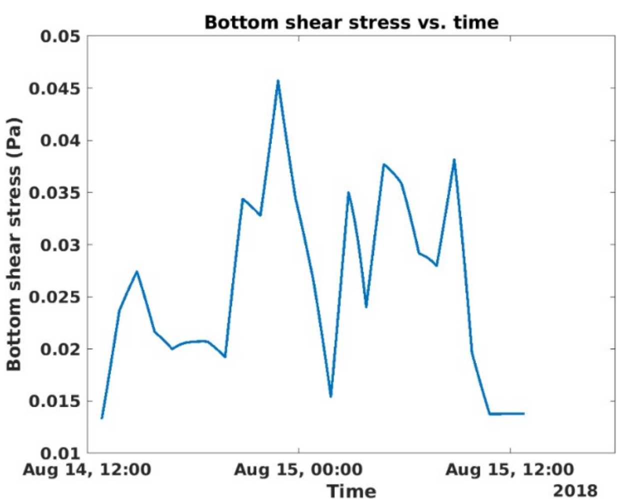

Figure 8: Time series of modeled bottom shear stress.

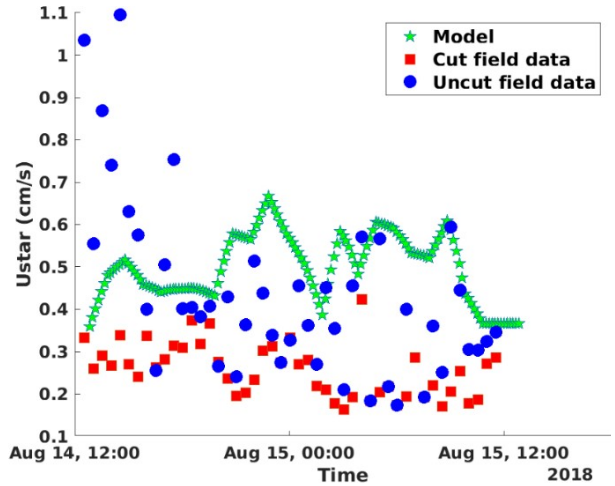

Figure 9: Time series of U_* derived from the field (blue dots), U_* calculated from the cut field data (red squares), and model outputted U^* (green stars).

<u>Model Validation</u>

The model predicts U_* to the same order of magnitude for the field site C6R (Fig. 9) as the experimental values but is slightly larger than the cut data and uncut data. Its variability matches the fluctuations seen in the cut data due to waves. The RMS difference between the model estimates and the cut data was 0.27, which shows the error within a reasonable range. For the uncut data the RMS difference was 0.25. Similarly, the bottom stress also matched expected values.

The stress for calm conditions falls within the same range (10^{-2} order of magnitude and less than 0.05) as measured by in calm summer conditions in the field by Wright et al. 1997 (Fig. 8). Because fine sediment typically requires critical bed stresses of about 0.1 Pa (Wright et al. 1997) for motion, the bottom stress is not enough to resuspend particles off the bottom, whether the observed or model values were considered.

Discussion

Since the model represented the field with some level of accuracy, a simulation was run to represent Hurricane Ike wave conditions using the same water column structure to see if hurricane conditions would be sufficient to suspend sediment. Hurricane Ike was a category 4 storm that passed across Cuba and through the Gulf of Mexico in a Northwest direction and reverted course northeastward after making land fall (Fig. 10) (Brown et al. 2010). The storm lasted from September 1, 2008 to September 16, 2008 (Brown et al. 2010).

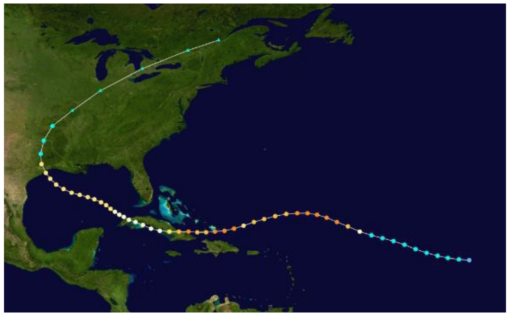

Figure 10: Track of Hurricane in 2008 (Hurricane Ike Track).

Wave height and period during Hurricane Ike's path were taken from the WaveWatch III simulated data base. Wave direction information was not available. The wave direction was assumed to be 315 degrees.

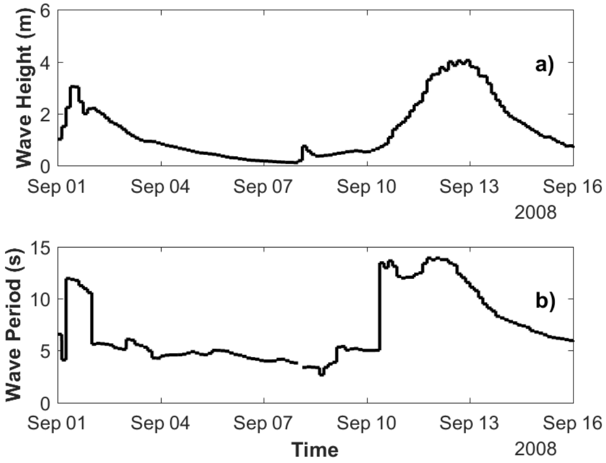

Figure 11: Time series of (a) wave height and (b) wave period for the Hurricane Ike duration at the C6R site from WaveWatch III. Wave heights were reported by the model every 3 hours. Therefore, the waves were assumed to be at a constant height and period over each that 3-hour reported timestep.

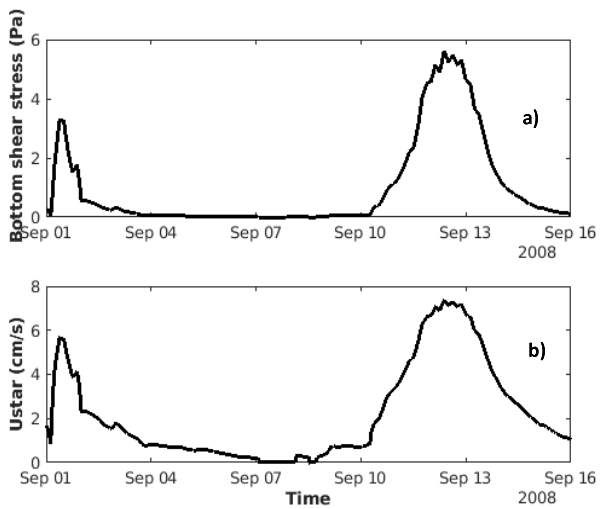

Figure 12: Modeled (a) combined wave and current bottom shear stress and (b) combined wave and current shear stress velocity for the Hurricane Ike simulation.

Hurricane Results

As expected, when Ike passed closest to the station and through the Gulf of Mexico the forces on the bottom and shear stress velocity increased tremendously. The shear was more than enough to resuspend sediment off the bottom. The forces acting on the bottom (Fig. 12a) during storm conditions were slightly lower (about 2 pascals on average) than that of Xu et al. (2017) model run in the Gulf of Mexico for the storm of the century that occurred in 1993.

Conclusions

The model run for both the calm conditions at C6R and high energy environment during Hurricane Ike needs further improvement. Adjusting the bottom roughness, ADV height, and turbulence closures all have an impact on the measured bottom shear stresses and velocities. Further work includes better refining and running the model to match the field conditions at each ADV site instead of just C6R, scaling to 1-D, including wind, chemical changes, and biological equations. The developed 1-D hydrodynamic model developed is the first step in evolving into a more complex HydroBioSed model for the Gulf of Mexico.

Acknowledgements

I thank everyone who contributed ideas, technical help, or equipment - from VIMS: Dr. Courtney Harris and Dr. Linlin Cui for constant support, guidance, technical help, and motivation; Matt Fair for always being available for coding help and model setup; Danielle Tarpley for general help and group meeting input; and Dr. Grace Massey for discussions about acoustic instrumentation. Also, Dr. Kanchan Maiti (Louisiana State University) provided the data collected in the Gulf of Mexico. Thanks to Jenny Dreyer and Katherine

Longmire for coordinating the REU program at VIMS. Program funding for the VIMS Research Experience for Undergraduates was made available through a grant awarded from the National Science Foundation (grant # NSF OCE 1659656) to Drs. Linda Schaffner and Rochelle Seitz.

Literature Cited

Adhikari, P.L., White, J.R., Maiti, K, and Nguyen, N., 2015. Phosphorus speciation and sedimentary phosphorus release from the Gulf of Mexico sediments: Implication for hypoxia. *Estuarine, Coastal and Shelf Science.* 164, 77-85. doi: https://doi.org/10.1016/j.ecss.2015.07.016.

Argonaut-ADV Operation Manual Firmware Version 11.2. *SonTek,* url: http://www.sontek.com

Brown, D.P., Beven J.L., Franklin, J.L., and Blake, E.S., 2010. Atlantic Hurricane Season of 2008. *Mon. Wea. Rev.* 138, 1975–2001. doi: https://doi.org/10.1175/2009MWR3174.1

Cai, W.J., 2011. Estuarine and Coastal Ocean Carbon Paradox: CO2 Sinks or Sites of Terrestrial Carbon Incineration? *Annual Review of Marine Science.* 3, 123-145.

Feely, R. A., Alin, S.R., Newton, J., Sabine, C.L., Warner, M., Devol, A., Krembs, C. and Maloy, C., 2010. The combined effects of ocean acidification, mixing, and respiration on pH and carbonate saturation in an urbanized estuary. *Estuarine Coastal and Shelf Science.* 88, 442-449.

Fry, B., Justić, D., Riekenberg, P. *et al*., 2015. Carbon Dynamics on the Louisiana Continental Shelf and Cross-Shelf Feeding of Hypoxia. *Estuaries and Coasts.* 38, 703-721. https://doi.org/10.1007/s12237-014-9863-9

Hurricane Ike Track. wikimedia.org/wikipedia/commons/5/5f/Ike_2008_track.png.(https://upload.wikimedia.org/wikipedia/commons/5/5f/Ike_2008_track.png)

Islam, M.R., and Zhu, D.Z., 2013. A Kernel Density Based Algorithm to Despike ADV Data. *Journal of Hydraulic Engineering*. 139(7), 785-793.

Kehui, X., Harris, C.K., Hetland, R.D., and Kaihatu, J.M., 2011. Dispersal of Mississippi and Atchafalaya sediment on the Texas–Louisiana shelf: Model estimates for the year 1993. *Continental Shelf*

Research. 31, 1558–1575. Doi:10.1016/j.csr.2011.05.008

Fennel, K., Hetland, R.D., and DiMarco, S.F., 2011. A coupled physical-biological model of the Northern Gulf of Mexico shelf: model description, validation and analysis of phytoplankton variability. *Biogeosciences.* 8 (7), 1881-1899. doi: https://doi.org/10.5194/bg-8-1881-2011

Hetland, R.D., and DiMarco, S.F., 2008. How does the character of oxygen demand control the structure of hypoxia on the Texas-Louisiana continental shelf? *Journal of Marine Systems*. 70, 49–62. doi:10.1016/j.jmarsys.2007.03.002.

Kim, S.-C., and Friedrichs, C. T., 2000. Estimating Bottom Stress in Tidal Boundary Layer from Acoustic Doppler Velocimeter Data. *Journal of Hydraulic Engineering*. *126*(6), 399. https://doi.org/10.1061/(ASCE)0733-9429(2000)126:6(399)

Lehrter, J. C., Beddick, D.L., Devereux, R., Yates, D.F., and Murrell, M.C., 2012. Sediment-water fluxes of dissolved inorganic carbon, O2, nutrients, and NO3- from the hypoxic region of the Louisiana continental shelf. *Biogeochemistry*. 109(1/3), 233-252.

Grant, W.D. and Madsen O.S., 1986. The Continental-Shelf Bottom Boundary Layer. *Annual Review of Fluid Mechanics.*18(1), 265-305, doi: https://doi.org/10.1146/annurev.fl.18.010186.001405.

Moriarty, J. M., Harris, C. K., Friedrichs, M. A. M., Fennel, K., and Xu, K., 2018. Impact of seabed resuspension on oxygen and nitrogen dynamics in the northern Gulf of Mexico: A numerical modeling study. *Journal of Geophysical Research: Oceans*. 123, 7237– 7263. https://doi.org/10.1029/2018JC013950

Rabalais, N.N., and Turner, R.E., 2018. Gulf of Mexico Dead Zone 2018. *LUMCON/LSU*.

Rabalais, N.N., Turner, R. E. , and Wiseman, W.J., 2002. Gulf of Mexico Hypoxia, A.k.a. "The Dead Zone". *Annual Review of Ecology and Systematics. 33*, 235-63. Doi: 10.1146/annurev.ecolsys.33.010802.150513

Rowe, G. T., and Chapman, P., 2002. Continental shelf hypoxia: Some nagging questions. *Gulf of Mexico Science*. 2, 155–160.

Wiberg, P.L., and Sherwood, C.R., 2006. Calculating wave-generated bottom orbital velocities from surface-wave parameters. *Computers & Geosciences.* 34, 1243-1262. doi: 10.1016/j.cageo.2008.02.010.

Wright, L.D., Sherwood, C.R., and Sternberg, R.W., 1997. Field measurements of fair weather bottom boundary layer processes and sediment suspension on the Louisiana inner continental shelf. *Marine Geology.* 140, 329-345, doi: https://doi.org/10.1016/S0025-3227(97)00032-7

Zhang, W., Hetland, R.D., DiMarco, S.F., and Fennel, K., 2015. Processes controlling mid-water column oxygen minima over the Texas-Louisiana shelf. *J. Geophys. Res: Oceans*. 120, 2800– 2812. doi:10.1002/2014JC010568.

Interactions between *Vibrio* Bacteria and Phytoplankton Species

Coral O'Brien

Virginia State University

Mentors: Dr. Corinne Audemard and Dr. Kimberly Reece

2 August 2019

Synopsis

Vibrio species associated with phytoplankton cultures were most closely related to *V. brasiliensis*. *Vibrio* were found much more abundant outside the *Akashiwo sanguinea* bloom than inside the bloom. Turbidity and chlorophytes potentially affect abundance of the *Vibrio* community in the York River.

Abstract

The objective of this study was to investigate the interactions between *Vibrio* bacteria and phytoplankton species. We analyzed the abundance and diversity of *Vibrio* species occurring in algal cultures and in water samples collected from the York River during the presence and absence of a phytoplankton bloom. Samples were plated on culture media and isolates were collected and analyzed by sequencing a fragment of the heat shock protein 60 gene (*hsp60*). Neighbor Joining phylogenetic trees were constructed to identify the isolates' closest relatives. All the *Vibrio* isolates associated with

phytoplankton cultures of the dinoflagellates *Alexandrium monilatum, Margalefidinium polykrikoides,* and *Chaetoceros neogracile* were identical to each other and closely related to *Vibrio brasiliensis* (97% sequence identity). This suggests that this species is particularly adapted to culture conditions. During a bloom of the dinoflagellate, *Akashiwo sanguinea, Vibrio* were found to be much more abundant outside than inside the bloom. This suggests *A. sanguinea* may be preying on or inhibiting growth of *Vibrio* communities in the York River. In contrast with the algal samples, York River water samples were associated with high *Vibrio* species diversity based on *hsp60* gene sequences. Additional samples and isolates would need to be analyzed to fully assess the effect of phytoplankton on *Vibrio* species composition. However, turbidity and chlorophytes seem to affect the abundance of *Vibrio* species in the York River. The effect of turbidity has been observed in previous studies but the impact of chlorophytes will need to be further investigated.

Introduction

In coastal environments, some bacteria from the genus *Vibrio* and certain species of phytoplankton can become harmful to marine organisms and humans. Factors influencing their abundance and distribution need to be identified to reduce the health risks associated with these organisms. Several studies have suggested that *Vibrio* and phytoplankton species may interact in various ways ranging from beneficial interaction for both organisms (mutualism) to prey-predator relationships depending on the species considered (Ramanan et al., 2016). With this in mind, the ecology of *Vibrio* species may be influenced by the phytoplankton species co-occurring in the environment, and vice versa. This study will contribute to a better understanding of the interactions between *Vibrio* species and phytoplankton species because both *in situ* and phytoplankton culture data were used.

Vibrio species are gram-negative bacteria that naturally occur in warm coastal and marine environments either associated with organisms, attached to inert particles or free-living in the water (Hunt et al., 2008). Some *Vibrio* species can cause harm to marine organisms such as shrimp, fish and shellfish but also to humans (CDC, 2019). Among the species affecting humans, the most well-known is *Vibrio cholerae*, which causes cholera, particularly under poor water quality conditions. In the US, the two species of primary concern are *Vibrio vulnificus* and *Vibrio parahaemolyticus*. Together these bacteria are responsible for an estimated 80,000 illnesses and 100 deaths per year, with infections associated with exposure of wounds to coastal waters or with consumption of raw or undercooked shellfish (CDC, 2019). In order to prevent illnesses associated with *Vibrio* species, it is critical to identify the environmental factors influencing the distribution and abundance of these bacteria. Within this context, several studies have suggested that the abundance and identity of the phytoplankton species in the natural waters may be an important factor to consider (Paranjpye et al., 2015; Maine et al., 2015).

Phytoplankton are photosynthetic plankton that naturally occur in the water. They are playing a key role as the basis for food web for many organisms. Under certain conditions, some phytoplankton species can form blooms, which are defined as a rapid increase in the number of phytoplankton cells in a body of water. While most blooms are not harmful, some species form blooms that can be harmful to marine animals and/or humans. As an example, Mulholland et al. (2009), reported that *Margalefidinium* (formerly *Cochlodinium*) *polykrikoides* blooms occurring in the Chesapeake Bay can caused "100% mortality of juvenile fish (*Cyprinodon variegates*) in less than 24 h and 20% mortality in juvenile American oysters (~21 mm; *Crassostrea virginica*) within 72 h". Gaining a better understanding of the ecology of phytoplankton species, in particular harmful algal bloom (HAB) species, is important in order to predict when and where these blooms may occur so mitigation strategies can be designed.

Vibrio and phytoplankton species co-occur within the coastal environment, especially during the warmer months. Studies have suggested that they may interact in ways depending on the species of *Vibrio* and the algae. For example, some *Vibrio* species attach to algae, and some are free-living (floating in water or in the culture medium) (Su et al., 2007). Despite earlier research, still little is known concerning individual species of *Vibrio* and phytoplankton interaction.

We chose to investigate these interactions using contrasting 'environments'. First, we use phytoplankton cultures because 1) previous studies conducted in our laboratory showed that *Vibrio* species occur in some of the algal cultures and 2) these cultures are from single phytoplankton species and are maintained under controlled conditions. Second, we intended to assess the impact of an algal bloom in the York River on the abundance and diversity of *Vibrio* species occurring in the water. The bloom occurs in the natural environment so under a much more complex set of environmental parameters than an algal culture, however, we hypothesized that a high density of phytoplankton cells may have a stronger -and measurable- impact on the *Vibrio* species community.

Methods

1. Algal cultures

Samples were obtained from cultured phytoplankton species maintained in the Reece laboratory and the Aquaculture Genetics and Breeding Technology Center (ABC) Hatchery to assess if *Vibrio* species are present in these cultures. *Alexandrium monilatum, Margalefidinium polykrikoides, Prorocentrum minimum,* and *Karlodinium venificum* cultures were collected from the Reece laboratory; *Pavlova pingus, Tahitian isochrysis, Tetraselmis chui, Prorocentrum minimum*, and *Chaetoceros neogracile* cultures were collected from ABC. Cultures from both locations were collected and plated on June 4th, 5th, and 11th, 2019.

2. Algal bloom in the York River

Water samples were collected from the York River on July 10th, 2019, during a bloom of the dinoflagellate species, *Akashiwo sanguinea*. Samples were collected 30 cm under the surface of the water outside and inside the bloom so the diversity and abundance of *Vibrio* species could be compared. Samples were plated and processed using a culture approach.

3. York River water samples

Duplicate water samples were collected from 5 sites located on the York River (Fig. 1) as part of an NSF funded project (LYRE project) on June 18th, 2019. Samples were collected 15 cm under the surface of the water. These sites were chosen based on their similar salinities (13.30–15.57 psu), so the potential influence of salinity was kept minimal. The choice of these sites was also guided by the chlorophyll levels measured at the time of sampling. Chlorophyll was considered as a proxy for phytoplankton abundance and we hypothesized that the wide range of values (5.9–20.8 µg/L) would allow to identify differences among the *Vibrio* species community collected under different chlorophyll levels. Temperature, dissolved oxygen, pH, and turbidity were also recorded at each site. Finally, each duplicate water sample was also analyzed microscopically to identify phytoplankton species.

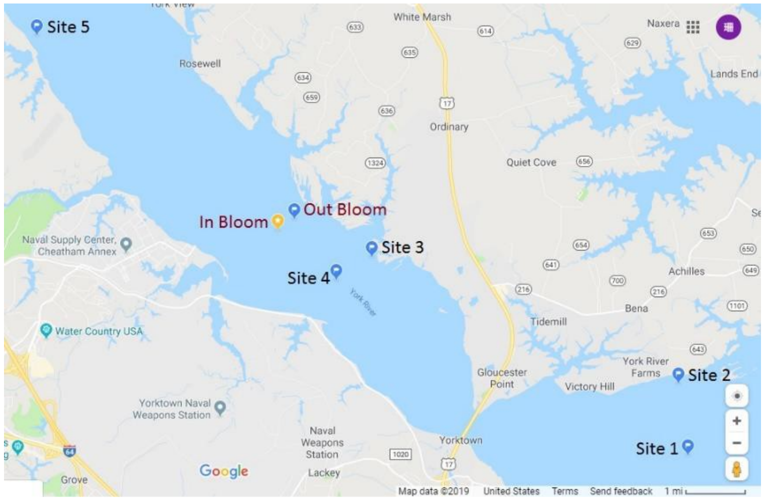

Figure 1: Map of sites where the bloom and York River water samples were collected.

4. *Vibrio* spp. abundance, isolation and identification

Abundance of *Vibrio* species in all the collected algal or York River samples were measured using a culture approach. Upon arrival at the laboratory, samples were plated on a *Vibrio*-selective medium, thiosulfate citrate bile salts sucrose (TCBS) agar. After incubation at 26˚C for 24 to 48 hours, the colonies on the plates were counted and the numbers of colony forming units (CFU) per mL of sample were calculated. For some of the samples, the total number of bacteria were estimated by plating additional sample aliquots on a medium designed for general marine bacteria (marine agar).

For each sample type, up to 16 individual colonies were grown in liquid medium (nutrient broth with 2% NaCl) and incubated at 26 ˚C for 24 to 48 hours. Turbid cultures were preserved in 20% glycerol at -80˚C and additional 50 µL aliquots were collected and placed at -20˚C for subsequent DNA sequencing.

a. PCR amplification of partial heat shock protein 60 gene (*hsp60*)

The enriched aliquots preserved for each isolate were placed at 100˚C for 10 min in a PCR machine to release the DNA from the bacteria cells. After centrifugation of the boiled suspension (~800 rcf for 1 min), the DNA of each isolate was amplified by polymerase chain reaction (PCR) using universal bacteria primers targeting a portion of the gene coding for the *hsp60* gene described by Goh et al. (1996).

Each PCR reaction contained 15.70 µl dH_2O, 0.40 µl of 10 mg/mL bovine serum albumin (BSA), 2 µl 10X buffer, 0.4 µl of 10 mM dNTPs, 0.2 µl of each primer at 100 µM, 0.1 µl of 5 units Taq polymerase and 1 µl of template DNA for a final volume of 20 µl. Positive and negative controls were included in each PCR run. The

PCR amplification conditions were as described by Bruto et al. (2017): 95 ˚C for 2 mins of initial denaturation, then 30 cycles consisting of 95 ˚C for 30 secs, 55 ˚C for 30 secs, and 72 ˚C for 30 secs, followed by a final extension at 72 ˚C for 6 mins.

PCR products were run on an agarose gel (2%) under electrophoresis to confirm amplification and size of the product (600 bp). The gel was treated with ethidium bromide and amplified PCR products were visualized under UV light. The isolates associated with PCR product of the correct size were purified as described below.

b. PCR product purification

The DNA Clean + Concentrator kit by Zymo Research was used to purify the PCR products. 10 µL of each PCR product was processed following the manufacturer's protocol and the purified product was eluted in 12 µL of dH_2O. The concentration and the purity of the obtained DNA (ng/µl) was measured on the Nanodrop.

c. DNA sequencing

Each direct sequencing reaction required 2.555 µL of dH_2O, 0.25 µL of Big Dye, 0.875 µL of 5X Buffer, 0.32 µL of the *hsp60* forward or reverse primer, and 0.25 µL of purified PCR product, yielding 5 µl of mixture. The PCR amplification conditions were: 96 ˚C for one min of initial denaturation, then 25 cycles of 96 ˚C for 10 secs, 50 ˚C for 5 secs, and 60 ˚C for 4 mins, ending with 4 ˚C forever. After resuspension in Hi-Di Formamide, and denaturation of the products, sequencing was performed on an ABI 3500 genetic analyzer according to the manufacturer's instructions.

Sequencher was used to pair up forward and reverse sequences and edit them. MacVector (version 17.0.5) was used to align obtained DNA sequences against DNA sequences from strains or species previously described (available in GenBank). MEGA7 was used to build a Neighbor Joining phylogenetic tree from the alignment prepared using MacVector.

Results

1. Algal cultures

After plating of algal species samples on TCBS, an absence of colonies was noted for *P. pingus, T. isochrysis, T. chui, P. minimum and K. venificum.* For *A. monilatum, M. polykrikoides,* and *C. neogracile*, colonies were observed on TCBS plates, and well isolated colonies were collected. Well isolated bacterial colonies were also collected from a *K. venificum* marine agar plate.

A total of 22 colonies were successfully sequenced and aligned against *hsp60* sequences from known *Vibrio* species. Sequencing data showed that all the isolates associated with *A. monilatum, M. polykrikoides and K. venificum* were identical to each other and were closely related to *V. brasiliensis* (97% identity) (Fig. 2). *Vibrio* colonies associated with the *C. neogracile* did not amplify correctly during PCR, so they could not be identified.

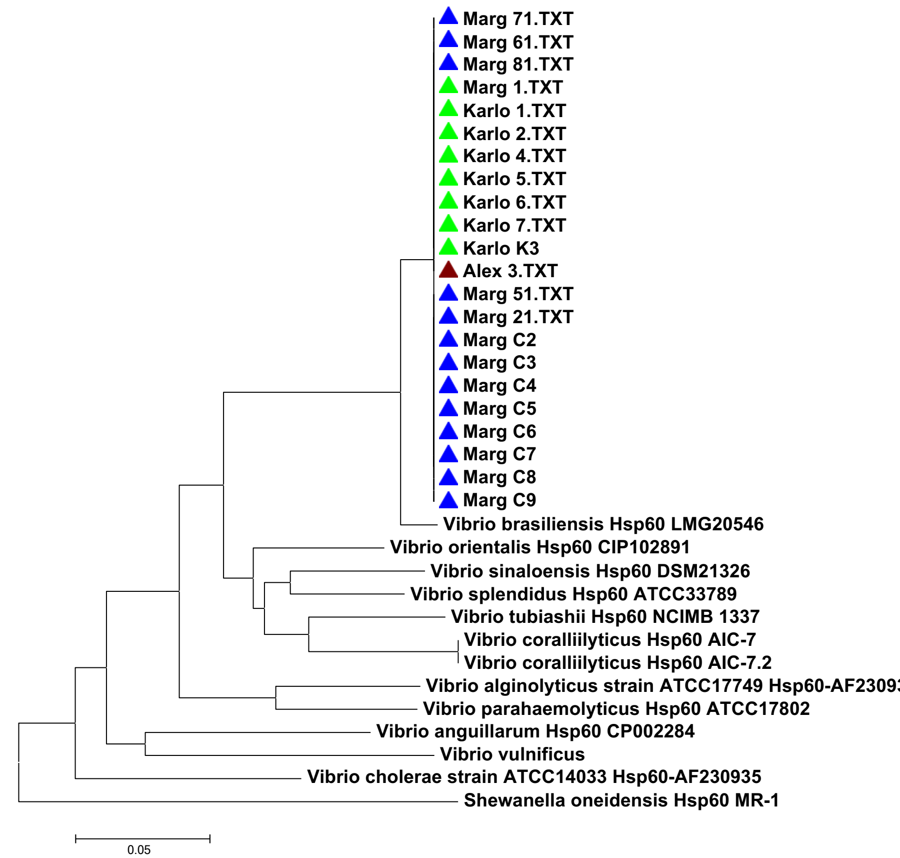

Figure 2: Neighbor Joining Phylogenetic tree of *Vibrio* isolates associated with phytoplankton cultures. All *hsp60* sequences are identical and are 97% similar to *V. brasiliensis*.

2. Algal bloom in the York River

A bloom of the dinoflagellate *Akashiwo sanguinea* occurred on July 10th, 2019 and “in bloom” and “out bloom” samples were plated on TCBS. After incubation, 9 colonies were observed on the in bloom plate, while a lawn of colonies were observed on the out bloom plate (Fig. 3). The event occurred late during this project, which hindered our ability to pursue identification of the isolates.

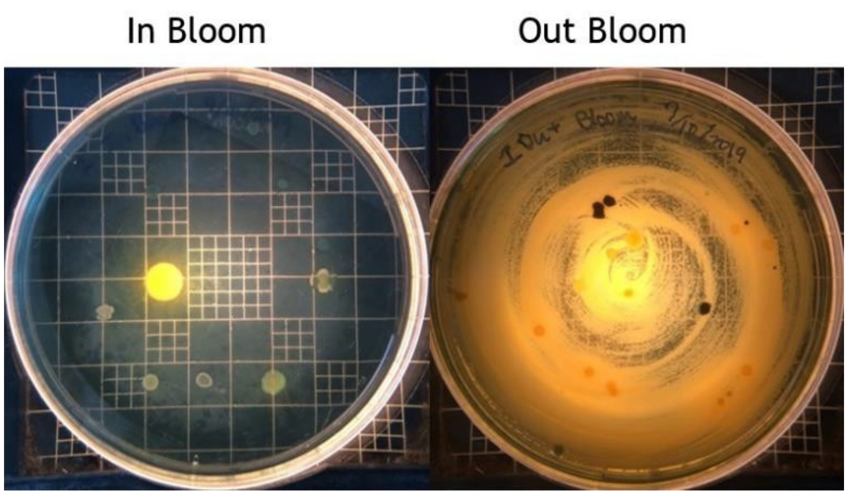

Figure 3: Pictures of in bloom and out bloom TCBS plates after 48 hours of incubation at 26˚C. A major difference in the density of colonies on the two plates was observed.

3. York River water samples

Environmental parameters recorded at time of sampling are shown in Figure 5. Both turbidity (1–47.8 mg/mL) and chlorophyll (5.9–20.8 µg/L) showed wide variability between sites. Values recorded for salinity (13.30–15.65 psu), dissolved oxygen (6.08–8.85 mg/L) and pH (7.67–8.15) were homogenous between sites. Interestingly, a similar trend was observed for turbidity measurements and *Vibrio* abundance (CFU/mL) with highest values for both parameters recorded at Site 3 and 5.

Based on phytoplankton analysis (Fig. 6), pennate diatoms (0–80 cell/mL) and chlorophytes (55–185 cells/mL) were the most commonly observed phytoplankton in the samples. These 2 groups also showed higher abundance than the filamentous diatoms (<15 cells/mL only at site 2), *K. venificum* (17.5/mL only at site 1) and the dinoflagellate, *Akashiwo sanguinea* (37.5/mL only at site 3). Plotting *Vibrio* abundance against the abundance of these species revealed a potential inverse relationship between *Vibrio* CFU/mL and chlorophytes levels.

From these York River water samples, a total of 58 isolates were analyzed, 33 were sequenced successfully and a Neighbor Joining phylogenetic tree was built (Fig. 4). Diversity of the sequences obtained from these isolates was large. 30 sequences were unique, and only three of the sequences were found at more than one site. Some isolates were closely related to *V. brasiliensis*, three isolates closely related to *V. aestuarianus* (99–100% similarity), one isolate had 100% similarity to *V. crassostreae*, one isolate had 100%

similarity with *V. harveyi* Other isolates shared less than 98% similarity with other *Vibrio* species (Fig. 4).

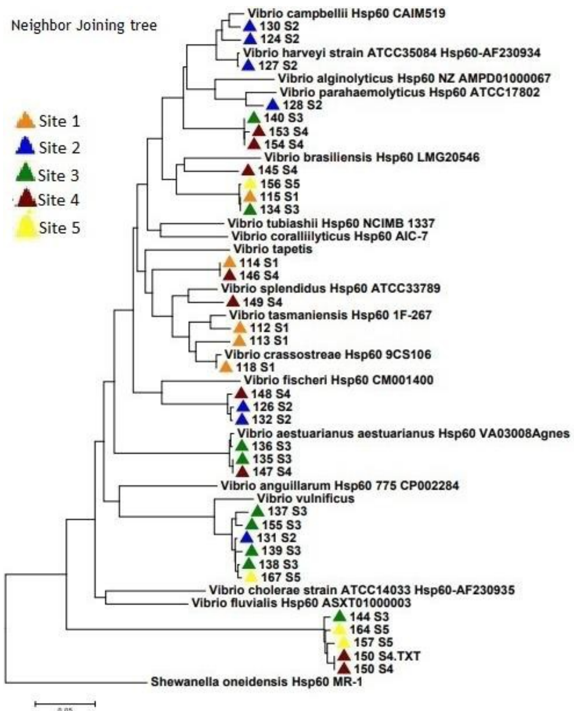

Figure 4: Neighbor Joining Phylogenetic tree of *Vibrio* species *hsp60* gene sequences associated with York River water samples. The collection sites are indicated by triangles of different colors. High diversity is seen in these isolates.

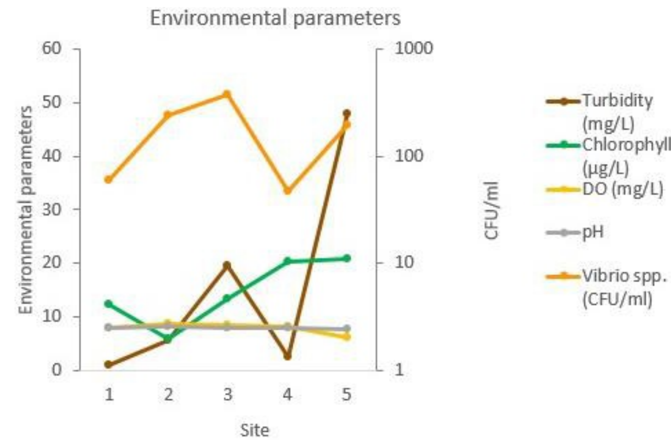

Figure 5: Environmental parameters measured at each York River site. Similar trend was observed between *Vibrio* CFU/mL and turbidity mg/L.

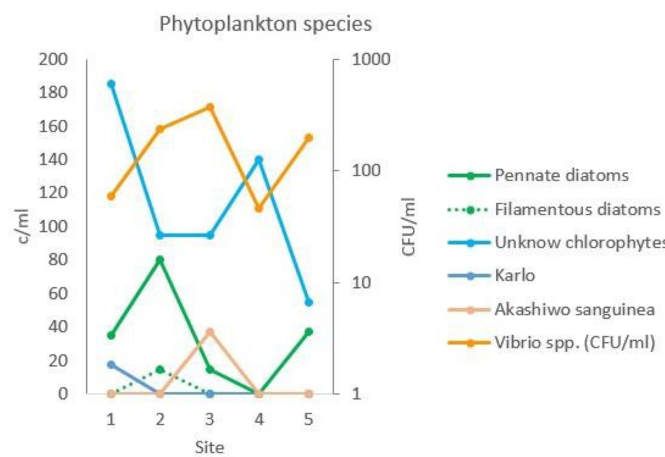

Fig. 6: Abundance of the phytoplankton groups identified at each York River site. Inverse relationship was observed between *Vibrio* CFU/mL and chlorophyte counts/mL.

Discussion

Vibrio spp. present in algal cultures

Colonies isolated from dinoflagellate algal cultures (*A. monilatum, M. polykrikoides*, and *K. venificum*), all shared an identical partial *hsp60* gene sequence that placed them as close relatives to *V. brasiliensis*. This species was first described by Thompson et al. (2003) in samples collected in marine aquaculture systems. In light of this paper, our data would again suggest that *V. brasiliensis* is well adapted to culture conditions. Since algal cultures are not axenic, one can hypothesize that other *Vibrio* species may have initially been present in these phytoplantkon cultures but that *V. brasiliensis* was the only one able to persist. While isolates associated with *A. monilatum* and *M. polykrikoides* were from TCBS plates, the isolates associated with *K. venificum* were from marine agar. This is very interesting because no *Vibrio* colonies formed on TCBS agar for *K. venificum*, yet the sequences of the colonies from the marine agar plates were identical to the ones obtained from *A. monilatum* and *M. polykrikoides.* We cannot exclude that this result may be the results of errors made throughout the process and further investigation will need to be conducted.

Vibrio spp. during an algal bloom in the York River

The major difference of *Vibrio* abundance between in bloom and out bloom (Fig. 3) was striking. Unfortunately, due to the time of the bloom, the identification of the *Vibrio* species could not be conducted. We hypothesize that *A. sanguinea* either inhibited growth or preyed on the *Vibrio* species. Future work will need to be conducted to investigate the specific interactions between *Akashiwo sanguinea* and different *Vibrio* species.

Vibrio spp. in York River water samples

The similar trend between *Vibrio* abundance and turbidity was very interesting since *Vibrio* species are known to attach to particles (inert or living organisms such as phytoplankton or zooplankton). *Vibrio* spp. abundance and chlorophyll levels did not show a significant trend (Fig. 5), however, based on the phytoplankton identification and counts, we observed an inverse relationship between *Vibrio* and chlorophyte abundance (Fig.6). This suggests there may be a negative effect of chlorophytes on *Vibrio* communities in the York River. More research needs to be done to see if similar trends would be observed with more samples and during different months of the year.

In terms of diversity, the high number of unique sequences suggests that the *Vibrio* community in the York River is very diverse and additional isolates would need to be analyzed to fully assess the species present and to determine if the species composition is affected by phytoplankton abundance and diversity. The isolates analyzed during this study were in some instances closely related to known oyster pathogens (*V. splendidus, V. crassostreae,* and *V. aestuarianus*), known shrimp pathogens (*V. harveyi*), and known human pathogens (*V. parahaemolyticus and V. vulnificus*).

Acknowledgements

I would like to thank the National Science Foundation for funding the VIMS Summer Research Experience for Undergraduates and the LYRE project. Rochelle Seitz, Program Director. Jennifer Dreyer, Program Coordinator. Kathrine Longmire, Program TA. Thanks to lab coworkers for helping me with the entire process: Alanna Macintyre, Gail Scott, Sam Fortin, William Jones, Victoria Simmons and Amanda Chesler.

Literature Cited

Center for Disease Control and Prevention. (2019). *Vibrio* species causing Vibriosis. https://www.cdc.gov/vibrio/index.html

Bruto, M., James, A., Petton, B., Labreuche, Y., Chenivesse, S., Alunno-Bruscia, M., et al. Roux, F. L. (2016). Vibrio crassostreae, a benign oyster colonizer turned into a pathogen after plasmid acquisition. The ISME Journal, 11(4), 1043-1052. doi:10.1038/ismej.2016.162

Goh S. H., Potter S., Wood J. O., Hemmingsen S. M., Reynolds R. P., Chow A. W. (1996) HSP60 gene sequences as universal targets for microbial species identification: studies with coagulase-negative staphylococci.J. Clin. Microbiol. **34**:818–823

Hunt, D. E., David, L. A., Gevers, D., Preheim, S. P., Alm, E. J., & Polz, M. F. (2008). Resource Partitioning and Sympatric Differentiation Among Closely Related Bacterioplankton. *Science,320*(5879), 1081-1085. doi:10.1126/science.1157890

Maine, C. R., Salvitti, L. R., Whereat, E. B., & Coyne, K. J. (2015). Community-Level and Species-Specific Associations between Phytoplankton and Particle-Associated Vibrio Species in Delawares Inland Bays. *Applied and Environmental Microbiology,81*(17), 5703-5713. doi:10.1128/aem.00580-15

Mulholland, M. R., Morse, R. E., Boneillo, G. E., Bernhardt, P. W., Filippino, K. C., Procise, L. A., et al. Gobler, C. J. (2009). Understanding Causes and Impacts of the Dinoflagellate, Cochlodinium polykrikoides, Blooms in the Chesapeake Bay. *Estuaries and Coasts,32*(4), 734-747. doi:10.1007/s12237-009-9169-5

Paranjpye, R. N., Nilsson, W. B., Liermann, M., Hilborn, E. D., George, B. J., Li, Q., et al. (2015). Environmental influences on the seasonal distribution of *Vibrio parahaemolyticus* in the Pacific Northwest of the USA. FEMS Microbiol Ecol. 2015 Dec;91(12).

Ramanan, R., Kim, B., Cho, D., Oh, H., & Kim, H. (2016). Algae–bacteria interactions: Evolution, ecology and emerging applications. *Biotechnology Advances,34*(1), 14-29. doi:10.1016/j.biotechadv.2015.12.003

Su, J., Yang, X., Zheng, T., & Hong, H. (2007). An efficient method to obtain axenic cultures of Alexandrium tamarense—a PSP-producing dinoflagellate. *Journal of Microbiological Methods,69*(3), 425-430. doi:10.1016/j.mimet.2006.07.005

Thompson F. L., Li, Y., Gomez-Gil B., Thompson C. C., Hoste B., Vandemeulebroecke K., Rupp G. S., Pereira A., De Bem P., Sorgeloos M. M., Swings J. (2003). *Vibrio neptunius* sp. nov., *Vibrio brasiliensis* sp. nov. and *Vibrio xuii* sp. nov., isolated from the marine aquaculture environment (bivalves, fish, rotifers and shrimps). In. J. Syst. Evol. Microbiol. 53: 245-252

Red Disease and Antibiotic Resistance of American Eels

Thalia Wallace

Community College of Philadelphia

Mentors: Amanpreet Kohli and Andrew Wargo

2 August 2019

Synopsis

Some significant findings of my research include isolating bacteria such as *Vibrio* and *Aeromonas species* from American eels with red disease. These bacteria are also known human pathogens. In addition, we also found different levels of susceptibility of these bacteria to various commonly used antibiotics. Lastly, a literature search provided some potential natural remedies effective against these bacteria.

Abstract

The objectives for this project were to identify potential pathogens associated with the red disease and test antibiotic sensitively of these pathogens. We accomplished these by isolating bacteria from the skin lesions and internal organs of the eels and identifying these bacteria by 16s rRNA gene sequencing. We found 15 different bacterial species and focused on the 4 dominant ones. We also tested the susceptibility of isolated bacteria to antibiotics. The 6 antibiotics that we tested sensitivity for were Sulfamethoxazole Trimethoprim (SXT), Imipenem (IPM), Ceftazidime (CAZ), Aztreonam (ATM), and Gentamicin (GM). Our results showed the 4 main bacteria isolated were susceptible to all antibiotics tested.

Introduction:

Infectious diseases are ubiquitous in all fish populations (NOAA Fisheries 2018) and can lead to population declines and extinctions in the wild (Harvell, et al 2002). In aquaculture, diseases can cause significant production losses (Assefa and Abunna 2018). This can affect the livelihoods of people dependent on these resources in multiple ways. For example, people may lose their jobs, have reduced income, and this may lead to food insecurity. (Assefa and Abunna 2018). Therefore, it is important that we find potential solutions to reduce losses associated with disease.

Introducing fish from one place to another can transmit nonnative pathogens and parasites resulting in novel disease epidemics (NOAA Fisheries 2018). This is particularly problematic in aquatic environments because water, and thus pathogens, move freely between the wild fish environment and aquaculture (NOAA Fisheries 2018). In addition to these potential impacts on aquaculture, and fisheries, some fish pathogens can also pose as health risks to humans (Novotny et al. 2004). Humans may come in contact with pathogens by either direct consumption of seafood or handling fish during recreational activities (Novotny et al. 2004). Some bacteria that can transfer from fish to humans are *mycobacterium marinum*, *streptococcus iniae*, and *vibrio cholera.* But some bacteria that affect aquaculture and wild fish are Vibriosis, Aeromonasis, Streptococcosis, and Pseudomonasis (Haenen 2016). Many of these bacteria are opportunistic in nature and disease is typically stress associated.

A variety of antibiotics are used worldwide in aquaculture species (Alderman and Hastings 1998). Effective antibiotics against bacterial diseases include Ampicillin, Penicillin, Streptomycin, and Tetracycline (Alderman and Hastings 1998). Although antibiotics and vaccines exist for some fish pathogens, antibiotic resistance is common (Alderman and Hastings 1998). Antibiotic resistance is when thepathogens become resistant to the antibiotics designed to kill or cure them. (CDC 2018). This can greatly hinder the management of the pathogen (CDC 2017). Antibiotic resistance has become particularly problematic in aquaculture as use of antibiotics over time in aquaculture has promoted the evolution of antibiotic resistance (CDC 2017).

Resistance to many antibiotics has been detected in fish (Done et al. 2015). So, we need to either develop new antibiotics or find other alternatives to treat fish diseases. A potential solution to antibiotic resistant bacteria can be herbal remedies. Herbal drugs are medicines made from the plants and they are important in disease control because they have antioxidant and antimicrobiological properties (Citaratus 2009). It is believed that many herbal remedies effective in humans, may also be effective for fish diseases (Pandey et al. 2014). Herbal remedies are less susceptible to the evolution of drug resistance because they contain multiple antibiotic compounds (Reverter et al. 2017). On the contrary, commercial antibiotics often only contain one compound, which is easier for the pathogen to evolve around (Reverter et al. 2017). Herbal remedies such as pomegranategarlic, ginger, and honey have been shown to be effective at reducing stress, promoting growth, and preventing infections (Reverter et al. 2017).

An important aquaculture species affected by disease is the American eel (*Anguilla rostrata*). The American eel is an ecologically and economically important finfish that lives along the East Coast of North America, including Chesapeake Bay. They are ecologically important because they serve as prey and predators. They are economically important because they are used as bait for recreational fishing, and internationally they are used as a food source, especially in Asia and Europe. International Union for the Conservation of Nature (IUCN), listed American eels as endangered in 2013 (Jacoby et al. 2017). Reasons for their declining population in the wild include diseases (Atlantic State Marine Fisheries Commission 2019). Also, according to ASMFC 2017 stock assessment American eels remain depleted in U.S waters since 2014. An emerging disease in American eels is “red disease”. Clinical signs of this disease are skin ulcers, lesions and mortality (Fig. 1).

Fig. 1: Clinical signs of the red disease of American eels.

Little research has been conducted on the red disease in North America, but studies were currently funded by the National Oceanic and Atmospheric Administration (NOAA) under the direction of Aman Kohli at VIMS to investigate its etiology and epidemiology.

My project was focused on providing aquaculture with variety of treatment options, that differ in their efficiency and cost, for the red disease of American eels. This could facilitate disease management in aquaculture. The specific objectives for my project are:

1) Identify potential pathogens associated with red disease
2) Test antibiotic sensitivity of these pathogens
3) Test effectiveness of natural remedies against these pathogens

Methods:

Eel collection

We collected 21American eels (*Anguilla rostrata*) from an aquaculture/holding facility in Whitestone, VA. The fish collected included 18 fish that showed a variety of clinical signs of the red disease including skin ulcers, lesions, and redness. In addition, 3 fish that did not show any clinical signs of the red disease were also collected to serve as a control. All eels were euthanized with MS222 and packed in Ziploc bags to bring back to VIMS over ice.

Bacterial isolation

In the biological safety level 2 (BSL-2) lab at VIMS, microbial samples were obtained from the external skin lesions and internal organs (spleen and liver) of the fish to isolate potential pathogens. The samples were placed on two types of bacterial media – Thiosulfate-citrate-bile-salts-sucrose agar (TCBS), which is a vibrio-specific media and Tryptic soy agar (TSA), which is a general media that supports growth of all bacteria. Multiple rounds of sub-culturing were performed until individual and isolated colonies were obtained.

Bacterial identification

Different bacteria isolated from the fish were identified by sequencing the 16s ribosomal ribonucleic acid (rRNA) gene. 16s rRNA gene sequencing is a standard method for identification and bacterial taxonomy (Clarridge 2004). For this process, isolated individual bacterial colonies underwent a boil preparation in 100ul of 0.1X Tris EDTA buffer (pH 8.0). This DNA obtained from the boil prep served as template for the next PCR step.

A PCR requires *taq* polymerase-0.125ul, reverse and forward primers-0.25ul, DNA template-2.000ul, nucleotides-0.5ul, 10x buffer +MgCl2 from the taq PCR core kit. The DNA goes through 3 steps which are denaturation, annealing, and extension. The PCR products were run on a 1.5% agarose gel by electrophoresis and seen under UV light to confirm presence of 500bp DNA fragments. Successfully amplified samples were cleaned using the column-clean method and quantified using a nanodrop. Appropriate sequencing reactions were then set-up using these concentrations. The sequencing PCR conditions were to use big dye reagent, 5x buffer, primers, template, and water. After sequencing on an ABI 3500 genetic analyzer, we used BLAST search from National Center Biotechnology Information (NCBI) to identify the bacteria.

Antibiotic sensitivity

The Kirby-Bauer method (disc diffusion test) method was used for testing antibiotic sensitivity of potential pathogens associated with the red disease. The Kirby-Bauer method is a standard method used to test antibiotic sensitivity or resistance against bacteria (Hudzicki 2009). Fresh bacterial cultures were used, and isolated colonies were added to saline until turbidity matched 0.5 McFarland standard (approx. 1.5×10^8 bacterial colonies) A bacterial lawn was plated on Mueller-Hinton media and 3 antibiotic discs and 1 control (paper disc) were put on each plate. After overnight incubation, the zone of inhibition surrounding the antibiotic was measured in mm. These zones were compared to disk diffusion breakpoints, published by (CLSI (2018), to determine the level of susceptibility. Antibiotics tested were Levofloxacin (LVX)-5ug, Sulfamethoxazole Trimethoprim (SXT)-23.75-1.25ug, Imipenem (IPM)-10ug, Ceftazidime (CAZ)-30ug, Aztreonam (ATM)-30ug, and Gentamicin (GM)-10ug. Table 1 is showing diameter of the zone of inhibitions measured. For example, If I measured the zone of inhibition for CAZ for the bacteria *Vibrio cholerae* and if it was greater than 21mm then the bacteria will be susceptible against this antibiotic. But if it was in between 18-20mm or less than 17mm then it would have been intermediate or resistant.

Table 1

Bacteria	Isolates	Antibiotics											
		CAZ		IPM		GM		SXT		LVX		ATM	
Aeromonas veronii	1C	32	S	22	I	24	S	35	S	40	S	44	S
Aeromonas veronii	1C	36	S	24	S	30	S	35	S	40	S	50	S
Aeromonas veronii	1C	34	S	24	S	24	S	36	S	38	S	42	S
Aeromonas veronii	10B	36	S	22	I	21	S	35	S	42	S	44	S
Aeromonas veronii	10B	32	S	23	S	24	S	35	S	40	S	38	S
Aeromonas veronii	10B	35	S	25	S	25	S	40	S	42	S	40	S
Aeromonas veronii	17B (A)	31	S	20	I	26	S	37	S	40	S	44	S
Aeromonas veronii	17B (A)	36	S	22	I	26	S	36	S	44	S	44	S
Aeromonas veronii	17B (A)	34	S	26	S	25	S	38	S	40	S	44	S
Aeromonas hydrophila	12A	31	S	24	S	26	S	36	S	42	S	46	S
Aeromonas hydrophila	12A	26	S	25	S	28	S	36	S	42	S	44	S
Aeromonas hydrophila	12A	31	S	24	S	27	S	33	S	42	S	40	S
Aeromonas hydrophila	17A	26	S	26	S	30	S	40	S	44	S	44	S
Aeromonas hydrophila	17A	25	S	24	S	30	S	35	S	40	S	40	S
Aeromonas hydrophila	17A	35	S	28	S	30	S	39	S	40	S	44	S
Aeromonas hydrophila	20B (A)	24	S	30	S	34	S	44	S	44	S	50	S
Aeromonas hydrophila	20B (A)	26	S	30	S	32	S	40	S	48	S	48	S
Aeromonas hydrophila	20B (A)	34	S	27	S	32	S	40	S	45	S	48	S
Aeromonas salmonicida	12B	34	S	23	S	22	S	36	S	44	S	30	S
Aeromonas salmonicida	12B	36	S	20	I	24	S	36	S	48	S	44	S
Aeromonas salmonicida	12B	35	S	25	S	24	S	34	S	48	S	44	S
Vibrio cholerae	4B	34	S	30	S	26	S	34	S	40	S	34	S
Vibrio cholerae	4B	34	S	30	S	26	S	34	S	44	S	34	S
Vibrio cholerae	4B	24	S	20	I	21	S	31	S	43	S	25	S
Vibrio cholerae	17B (B)	32	S	30	S	25	S	39	S	42	S	36	S
Vibrio cholerae	17B (B)	34	S	29	S	26	S	38	S	40	S	26	S
Vibrio cholerae	17B (B)	34	S	30	S	23	S	35	S	40	S	34	S
Vibrio cholerae	20B (B)	36	S	30	S	26	S	40	S	46	S	34	S
Vibrio cholerae	20B (B)	30	S	28	S	24	S	39	S	44	S	42	S

Vibrio cholerae	20B (B)	34	S	30	S	24	S	34	S	44	S	32	S

Results:

We isolated 15 different bacteria from the 18 eels that showed the clinic signs of red disease. The bacterial species that we identified were *Aeromonas cavaie, Aeromonas hydrophila, Aeromonas salmonicida, Aeromonas veronii, Aeromonas allosaccharophila,, Vibrio cholerae, Acidovorax sp., Acinetobacter johnsonii, Chryseobacterium sp, Flavobacterium granuli, Morganella morganii, Serratia marcescens, Shewanella putrefaciens, and Shewanella xiamenesis* (Fig. 2).

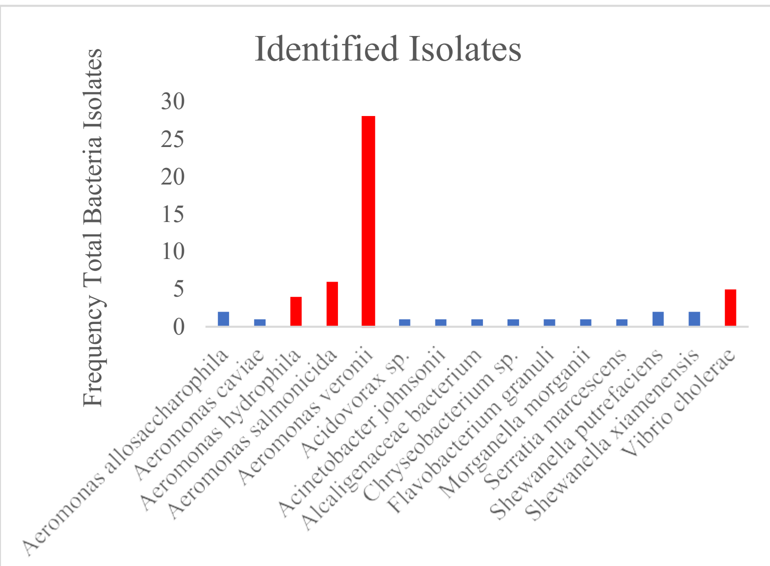

Fig. 2

The most dominant bacteria species were *Aermonas hydrophila, Aeromonas Salmonicida, Aermonas veronii, and Vibrio cholerae* (Fig. 3.). When examining the distribution of bacteria across the organs, spleen, liver, and skin lesion, we found that *Aeromonas veronii* was dominant in all 3 organs (Fig. 4,5,6). The different antibiotics tested showed different levels of bacteria are susceptible, and antibiotics are effective against the 4 bacterial diseases. All 4 of the bacteria were susceptible to all 6 antibiotics (Figs. 5-8). However, *Aeromonas veronii* and *Aeromonas salmonicida* showed intermediate levels of resistance against IPM. My natural remedy research revealed that ginger and honey are effective against the bacteria *Aeromonas hydrophila*.

Natural Remedy	Bacteria	Reference
Garlic	*Escherichia coli* *Pseudomonas aeruginosa*	Betoni et al. 2006 Chikwem et al. 2008
Pomegranate	*Salmonella typhimurium*	Negi et al. 2002
Honey	*Aeromonas hydrophila*	Ramalivhana 2013
Ginger	*Aeromonas hydrophila*	Pandey et al. 2012

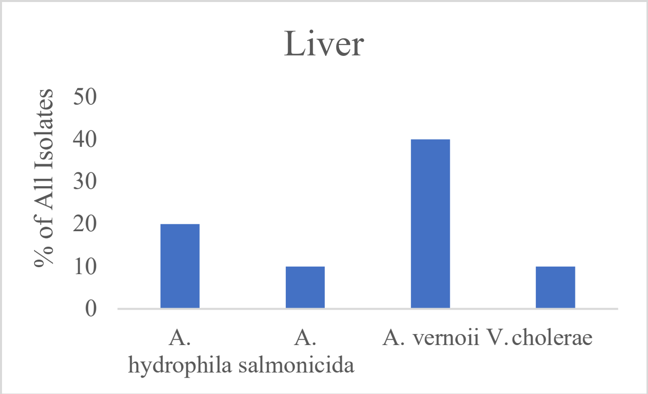

Fig. 3

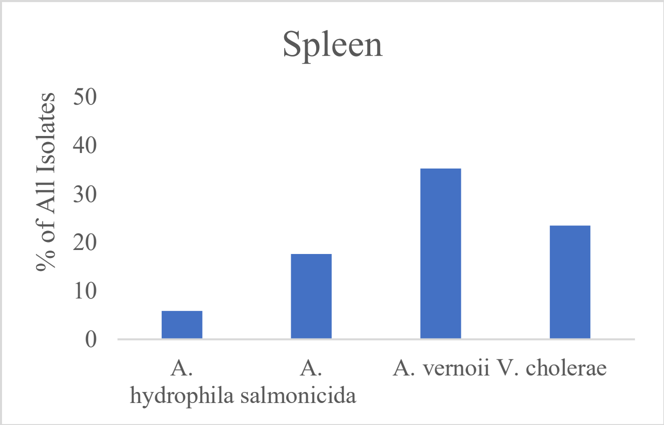

Fig. 4

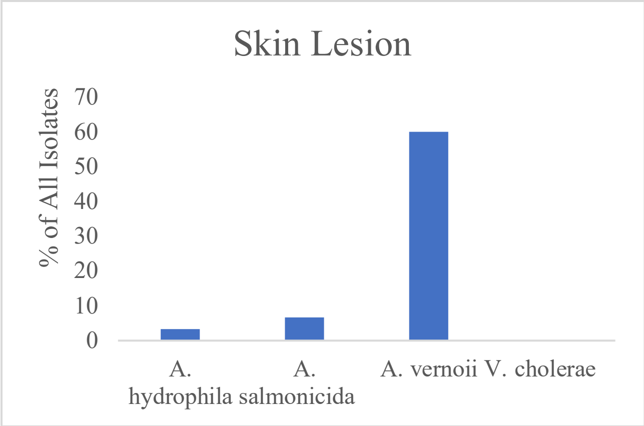

Fig. 5

Significance:

Overall this work is important because some identified pathogens are also human pathogens which puts humans at risk. Many of the pathogens are opportunistic and are associated with stress. This is important for the eel industry because there is fish mortality associated with red-disease that can cause economic losses to the low-income communities which depend on this resource. Red disease may also be contributing to the declining wild population of American eel. Our work sheds light on potential causative agents of red disease and the efficacy of antibiotics as a management tool and managing stress by improving holding conditions. Lastly, future research for natural remedies is warranted.

Acknowledgements:

I would like to thank my mentors Aman Kohli and Andrew Wargo for making this project possible. I would like to thank Wargo lab members such as Barbara Rutan, Paula Dye, and Hannah Brown for contributing ideas and giving me the extra hand. I also will like to thank Jenny Dreyer and Katherine Longmire for coordinating the REU program at VIMS, and program funding from NSF. Lastly, I would like to thank my interns for such a great experience.

Literature Cited:

"About Antimicrobial Resistance | Antibiotic/Antimicrobial Resistance | CDC." *Centers for Disease Control and Prevention*, Centers for Disease Control and Prevention, 10 Sept. 2018, www.cdc.gov/drugresistance/about.html

Alderman, D. J., and T. S. Hastings. "Antibiotic Use in Aquaculture: Development of Antibiotic Resistance – Potential for Consumer Health Risks* - Alderman - 1998 - International Journal of Food Science & Technology - Wiley Online Library." *International Journal of Food Science & Technology*, John Wiley & Sons, Ltd (10.1111), 4 Feb. 2003, onlinelibrary.wiley.com/doi/epdf/10.1046/j.1365-2621.1998.3320139. x.

"Antibiotic Resistance Questions and Answers | Community | Antibiotic Use | CDC." *Centers for Disease Control and Prevention*, Centers for Disease Control and Prevention, 25 Sept. 2017, www.cdc.gov/antibiotic-use/community/about/antibiotic-resistance-faqs.html

Assefa, et al. "Maintenance of Fish Health in Aquaculture: Review of Epidemiological Approaches for Prevention and Control of Infectious Disease of Fish." *Veterinary Medicine International*, Hindawi, 26 Feb. 2018, www.hindawi.com/journals/vmi/2018/5432497/abs/

"Atlantic States Marine Fisheries Commission." *Species - Atlantic States Marine Fisheries Commission*, Oct. 2017, www.asmfc.org/species/american-eel.

Citarasu, Thavasimuthu. "Herbal Biomedicines: A New Opportunity for Aquaculture Industry." *SpringerLink*, Springer Netherlands, 22 Mar. 2009, link.springer.com/article/10.1007/s10499-009-9253-7.

Done, Hansa Y, et al. "Does the Recent Growth of Aquaculture Create Antibiotic Resistance Threats Different from

Those Associated with Land Animal Production in Agriculture?” *The AAPS Journal*, Springer US, 21 Feb. 2015, www.ncbi.nlm.nih.gov/pmc/articles/PMC4406955/.

Harvell, C. Drew, et al. “Climate Warming and Disease Risks for Terrestrial and Marine Biota.” *Science*, American Association for the Advancement of Science, 21 June 2002, science.sciencemag.org/content/296/5576/2158/tab-pdf.

Jacoby, D., Casselman, J., DeLucia, M. & Gollock, M. 2017. *Anguilla rostrata* (amended version of 2014 assessment). *The IUCN Red List of Threatened Species* 2017: e.T191108A121739077. http://dx.doi.org/10.2305/IUCN.UK.2017-3.RLTS.T191108A121739077.en. Downloaded on 21 June 2019.

Noaa. “Aquaculture Fish Health.” *NOAA Fisheries*, NOAA Fisheries, 12 Jan. 2018, www.fisheries.noaa.gov/content/aquaculture-fish-health

Novotny, L., et al. "Fish: a potential source of bacterial pathogens for human beings. A review." Veterinarni Medicina-UZPI (Czech Republic) (2004).

Pandey, Govind & Sharma, Madhuri & K Mandloi, A. (2014). Medicinal plants useful in fish diseases. Plant Archives.

Reverter, Miriam, et al. “Use of Medicinal Plants in Aquaculture - Reverter - 2017 - Wiley Online Books.” *Wiley Online Library*, John Wiley & Sons, Ltd, 7 Apr. 2017, onlinelibrary.wiley.com/doi/10.1002/9781119152125.ch9#.

Understanding the feeding ecology of the Atlantic deep-sea scallop *Placopecten magellanicus* using DNA barcoding

Brittany Baker
Oakland University

Mentors: Dr. Jan McDowell, Dr. David Rudders, and Ellen Biesack

2 August 2019

Synopsis

The key goal of my research was to establish a molecular based approach to identify diatoms, to the lowest taxonomic level possible, present in the gut contents of Atlantic deep-sea scallops, *Placopecten magellanicus*, and compare the molecular identifications to identifications to those from previous microscopy-based identification surveys. I compared two different markers, COI and *rbcL-3P* (which I will refer to as *rbcL* for the remained of the paper) previously used in identification of diatoms. The marker *rbcL-3P* was more successful since diatom sequences generated using this marker had a higher percent identity to marine diatom species using BLAST searches. Three orders of diatoms were found in gut contents based on *rbcL*. The findings of this study prove the feasibility of using molecular markers to identify diatoms present in the guts of scallops. Understanding the diet is important for sustainable management since it directly relates to growth.

Abstract

It has been observed that the rate of growth of offshore, Atlantic deep-sea scallops is lower than that of the inshore,

shallow water scallops and it has been hypothesized that this may be due to a difference in food availability. Previous microscopy-based studies have found that in offshore scallops, the pelagic diatom species *Eucampia zoodiacus, Ditylum brightwelii,* and *Coscinodiscus* spp. were the principal components of the diet in the early fall, which coincides with the period of greatest water column mixing and the bloom period for these species. Additionally, another diatom genus, *Thalassiosira,* was found to supply a substantial portion of the energy consumed by inshore *P. magellanicus* during the spring bloom. The results of this study established a molecular based approach to identify diatoms present in the gut contents of samples of Atlantic deep-sea scallops. Results are compare dto previous findings based on microscopy. The development of these methods will be important because the mechanics of sea scallop feeding (mortar and pestle type grinding by a crystalline style) makes visual identification of diatoms to be difficult. In my research, I extracted diatom DNA from scallop digestive glands, amplified fragments of the COI and *rbcL* genes, cloned and finally sequenced. I identified 35 diatom sequences belonging to several orders within the gut contents of sea scallops using BLAST searches and phylogenetic trees. I would recommend using the marker *rbcL* as a barcode for identifying diatoms in gut contents. The results of this study provide additional insight on a scalable method to assess the diet of sea scallops, which impacts its growth, and thus contributes to our ability to sustainably manage it as a resource.

<u>Introduction</u>

As Virginia's most valuable fishery, Atlantic deep-sea scallops, *Placopecten magellanicus*, brought in $32.6 million at dockside in 2013 and is of interest to researchers because the feeding ecology of this species across its range is not well-understood. Previous studies have analyzed gut contents using microscopy. My work will establish a molecular based approach to identify diatoms present in the gut contents of a sample of sea scallops.

Ecological Background

Atlantic deep-sea scallops are found from the Gulf of St. Lawrence (Canada) to North Carolina. Feeding ecology is not well-understood but visual surveys have found that the Atlantic deep-sea scallop is opportunistically feeding on pollen grains, algae, and diatoms. This finding is logical, because they are filter-feeders, however, grinding of food particles by a crystalline style in the gut sometimes causes visual identification of diatoms to be difficult, because the grinding process destroys the diatom's valve which is necessary for identification (Shumway et al. 1987, Fisher 2000). Diatoms are suspected to be an important food source, but uncertainty exists with respect to the exact species and relative composition of the diet and how diet varies across time and space.

Growth rate in sea scallops depends on many environmental factors including food availability (Shumway & Parsons 2016). It is interesting to note that the rate of growth of offshore, deep water scallops was found to be less than that of the inshore, shallow water scallop. It has been hypothesized that this is likely due to a difference in food availability in these areas. Given the importance of understanding the ecological basis for the observed differences in growth rate, I hope to add molecular methods and results that provide information about the feeding ecology of the Atlantic deep-sea scallop to the existing body of research (Schick et al. 1988).

Research Goals

In the short-term, the preliminary data I collect will contribute to the proof of concept supporting the method of DNA barcoding to examine the feeding ecology of bivalves. DNA barcoding is founded on the principle that the divergence of a DNA fragment corresponds to biological division of species (Moniz & Kaczmarska 2009). The specific results of this research will form a methodological basis to identify food resources important to sea scallops and provide an approach to assess how these food resources vary across time and space.

Methods

Data Collection

Sea scallop digestive glands were collected 50 miles east of Ocean City, MD by the Sea Scallop Research Program using a dredge at 27-28 meters depth during February of 2019 (Figure 1). From the sampled scallops, digestive glands were removed, fixed in 95% ethanol and stored at 4°C.

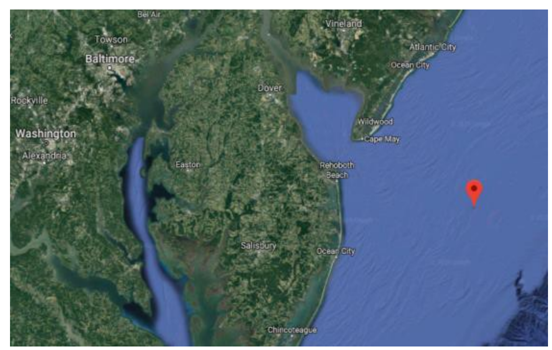

Figure 1: This map shows the field collection site 50 miles east of Ocean City, Maryland.

DNA Extraction

I subsampled eight scallop digestive glands. In order to subsample scallop gut contents, I used scissors and tweezers to extract material from within the gut (about 200 milligrams) and avoid scallop tissue that could result in contamination in subsequent steps in my process. Four methods of DNA extraction were tested to see which would provide the greatest amount of DNA as measured on a Qubit Fluorometer (Thermo Fisher Scientific, Waltham, MA), and resulted in the largest intact DNA fragments determined by gel electrophoresis. The four extraction methods tested included: QiaAmp DNA Stool kit (Qiagen, Hilden, Germany), carboxylated magnetic beads, SA-Gen (Vasselon 2017), and MP Bio FastDNA Spin Kit for Feces (MP Biomedicals, Santa Ana, CA). The reason we want high molecular weight DNA is it is difficult to amplify degraded DNA.

PCR

I performed various PCR protocols based on the literature using different primer sets, markers, and temperature gradients (Table 1). The objective was to find a primer set that was effective for diatoms while not amplifying scallop DNA. A range of temperature gradients were tested to optimize annealing temperature, and were determined to be 5°C above and below published temperatures for the primer sets. In order to make sure my primer sets did not amplify scallop DNA, I extracted (using the DNeasy Blood and Tissue kit following the manufacturer's published protocol) scallop muscle tissue from samples collected during the June 2019 cruise conducted by the Sea Scallop Research Program and attempted amplification of these samples alongside my gut material.

Table 1: This table shows all the primer sets and PCR protocols I tested based on prior literature. Highlighted and bolded rows are primer sets and protocols that I found to amplify diatom DNA without amplifying scallop DNA.

Locus	Source	Genome	Results
rbcL	Vasselon et al. 2017	Chloroplast	No amplification
rbcL-3P	**Hamsher et al. 2011; Levialdi Ghiron 2006**	**Chloroplast**	**Successful**
ITS-2	White et al. 1990	Nuclear	Amplified scallop DNA
COI-5P	Evans et al. 2007	Mitochondrial	No amplification
COI-5P	Hamsher et al. 2011	Mitochondrial	Amplified scallop DNA
CoxI	**Iwatani et al. 2005**	**Mitochondrial**	**Successful**
CoxI	Ehara et al. 2000	Mitochondrial	No amplification
COI	Guo et al. 2015	Mitochondrial	No amplification
ITS	Guo et al. 2015	Nuclear	No amplification

Cloning and Sequencing

Cloning is used to address the issue that results from the presence of multiple species in my digestive gland samples. Cloning is effective for these DNA samples of mixed origin because each colony incorporates a unique sequence or single cell. I followed the Invitrogen TOPO TA Cloning Kit for Sequencing using their published protocols. The procedure starts with the creation of LB agar plates to which ampicillin was added to a final concentration of 50µg/ml as a final concentration. Ampicillin is added to the plates in order to kill the competent cells that did not take up my vector. I included the control which came with the kit to gauge how successful my cloning was and that all the reagents were reacting properly. Then, I added 3' A-Overhangs Post-Amplification following that protocol to the PCR products that were amplified more than two days prior to the cloning reaction using *Taq* polymerase. Afterwards, I performed the TOPO Cloning Reaction using 2µl of PCR product, 1µl of salt solution, 2µl of water, and 1µl of TOPO vector. I used 2µl of the final cloning reaction for transformation into One Shot TOP10 chemically competent cells using the published protocol and spread 50 and 75 µl of the cells onto plates which were incubated overnight at 37°C. I picked the colonies and restreaked them onto new plates and incubated again overnight at 37°C. I finally executed a boil prep on a subset of restreaked colonies to release the DNA within the cells. I then performed PCR using the M13 primers. I used the Qiagen Taq Core PCR kit with the following recipe amounts for each of the reagents 20.375 µl of PCR water, 2.50 µl of 10X buffer and $MgCl_2$, 0.5 µl of dNTPs (10mM each), 0.25 µl of forward primer (10 µM), 0.25 µl of reverse primer (10 µM), and 0.125 µl of Taq polymerase (50U/ µl). I used the following cycling protocol: 94°C for 2 minutes, 29 cycles of 94°C for 30 seconds, 54°C for 30 seconds, 72°C for 1 minute, and 72°C for 5 minutes. I visualized the products by running gel electrophoresis to look for the correct fragment size (expected 760 bp for COI and 991 bp for *rbcL*) and performed PCR Purification QIAquick on the samples that were of the expected size.

Next, I used the Nanodrop to get input amounts for BigDye reactions. I was aiming for samples between 5-20 ng/µl because that is what is required for BigDye Sequencing reaction for a fragment from 500-1000 bp. Finally, a Cycle Sequencing PCR was performed using 5-20 ng of template, 0.25 µl of BigDye reagent, 0.875 µl of 5X buffer, 0.32 µl of forward M13 primer, and filled to 5 µl with DI water. The protocol for this reaction is denaturation at 96°C for 1 minute and 25 cycles of 96°C denature for 10 seconds, 50°C annealing for 5 seconds, and 60°C extension for 4 minutes. Then, I used the ABI Ethanol/Sodium Acetate Precipitation Big Dye PCR Cleanup before rehydrating with HiDi Formamide, denaturing for two minutes and putting the final products into the sequencing machine.

I used an ABI 3500 Genetic Analyzer (Applied Biosystems) with a 50cm array for direct sequencing using the Z dye set.

Blast Searches and Phylogenetic Trees

Before BLAST searching and constructing trees I also cleaned up the sequences by reviewing the chromatograms in Sequencher and cutting the primers for my markers. Once the genetic material is sequenced, I did a BLAST (Basic Local Alignment Search Tool) search to identify diatoms to the lowest taxonomic level possible. GenBank is a reference for genetic sequences (to look up the identity of sequences where anyone can put in the identity of sequences). My criteria for finding a match was to use the highest percent coverage and identity either the top one or if there were similar results the first three. It returns a measure of how similar my sequence is to the database's sequence on a list of top hits.

In creating my phylogenetic trees, I first collapsed unique sequences. Next, I created neighbor-joining phylogenetic trees using the program PAUP*. In neighbor-joining trees the branch lengths represent evolutionary time. I populated the phylogenetic trees with my own unique sequences as well as GenBank sequences from species from the literature and I had as hits for BLAST searches. All sequences were aligned for each tree in MacVector and trimmed to equal lengths.

Results

DNA Extraction

I successfully extracted DNA from eight of the February cruise scallops using the QiaAmp DNA Stool kit (Qiagen, Hilden, Germany) following the pathogen steps of the published protocol. The Qubit Fluorometer data demonstrated that the QiaAmp DNA Stool kit (Qiagen, Hilden, Germany) provided the greatest amount of high molecular weight DNA of the four extraction methods tested. I wanted high quality high-molecular weight DNA which was determined by use of a Nanodrop and gel electrophoresis.

PCR

The primer sets and protocols I found to work were based on Iwatani et al. (2005) and used COI as a marker and Hamsher et al. (2011) and Levialdi Ghiron (2006) and used *rbcL*-3P as a marker. I used the Qiagen Taq Core PCR kit with the following reaction protocol: 17.625 µl of PCR water, 1.250 µl of BSA (1mg/mL), 2.50 µl of PCR buffer (10X), 0.5 µl of dNTP (10mM each), 1 µl of forward primer (10 µM), 1 µl of reverse primer (10 µM), and 0.125 µl of Taq (50U/ µl). For *rbcL*, I used the same Qiagen Taq Core PCR kit recipe except I used 1.25 mL of each primer. I used the cycling protocols from Iwatani et al. (2005) and Hamsher et al. (2011) for COI and *rbcL* respectively.

Some of the primer sets I tested had amplification at the correct length for diatom DNA, while other primer sets had amplification at the correct length for scallop DNA as well as diatom or amplified nothing (Table 1). The primer sets and protocols I found to reliably work were ones that amplified diatoms while not amplifying scallops since that would confound my cloning and sequencing results.

Cloning and Sequencing

I successfully cloned PCR products from each of my eight sample at each locus (COI and *rbcL*). Then, I picked 280 colonies to amplify the DNA from using the M13 PCR. Of those, 50 colonies were the correct size for the maker *rbcL* and 31 colonies were the correct size for the marker COI. I sequenced 81 colonies and had 52 successful sequences.

BLAST Searches and Phylogenetic Trees

For COI, my fragments were from 517 to 532 bp between the forward and reverse primers. For *rbcL* my fragments were around 760 between the forward and reverse primers. There were 35 diatom sequences found between my two markers using BLAST searches. The percent identity range for the maker COI was 81%-91% identity with an average of 85.8%. The percent identity range for *rbcL* was 91%-100% with an average of 97.1%. For *rbcL*, my BLAST search identified 8 diatom species in my cloned samples, 1 diatom order in my cloned samples, and were unable to identify 7 diatoms to an order (Table 2). Thirteen samples matched the order Coscinodiscales which was our most abundant order. For COI, my BLAST search identified 10 diatom species, 3 diatom orders and were unable to identify 3 diatoms to an order. The marker COI returned matches for freshwater diatom species, bacteria such as *Candidatus Pelagibacter ubique* and *Pythium* sp., and fungi such as *Phytophthora colocasiae*.

Table 2: This table includes the diatoms I found to the lowest taxonomic level possible for the two markers (COI and *rbcL*). Columns are sample identifications and rows are diatom genera or species. It is a tally of diatom genera or species identified in my cloning samples using the two markers (COI and *rbcL*) and BLAST searches.

	004		034		045		042		041		037		019	
Classification	COI	rbcL	COI	rbcL	COI	rbcL	COI	rbcL	COI	rbcL	COI	rbcL	COI	rbcL
Actinocyclus sp.				1										
Coscinodiscus radiatus				1										
Coscinodiscus sp.						2				2				
Coscinodiscus wailessi				4						2		1		
Pseudo-nitzschia pungens	1		1											
Pseudo-nitzschia sp.													2	
Sellaphora pupula					3		4							
Skeletonema menzellii			1											
Other diatoms				5			3					2		

For the creation of a phylogenetic tree for the marker COI, my sequences were all trimmed to a length of 348 base pairs to incorporate as many sequences as possible (Figure 2). The COI dataset had 6 unique sequences after discarding 9 identical sequences. Four of my cloned samples into two diatom orders based on the COI phylogenetic tree. Three of my samples were close to species of *Coscinodiscus*. Another one of my samples was close to species of *Skeletonema.* Two of my sequences are in white because they did not have anything similar enough to them (Figure 2).

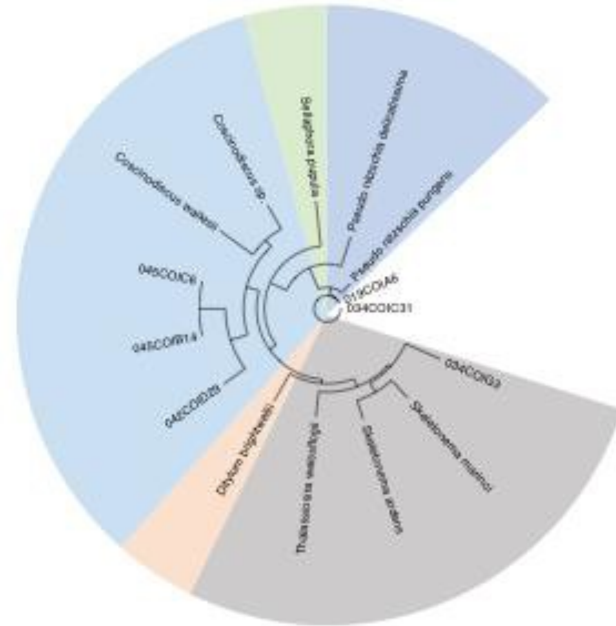

Figure 2: This figure depicts a circular phylogenetic tree for the marker COI. The diatom orders represented include: Coscinodiscales (light blue), Navicuales (green), Bacillariales (dark blue), Thalassiosirales (gray), and Lithodesmiales (orange). My cloning samples are the ones labeled with a number, the marker, and another number. Published GenBank sequences are presented as the genus or species of diatom they represent. The scale bar for the branch lengths is included.

For the creation of a phylogenetic tree for the marker *rbcL*, my sequences were all trimmed to a length of 644 base pairs to incorporate as many sequences as possible (Figure 3). The *rbcL* dataset had 11 unique sequences after discarding 8 identical sequences. Eleven of my cloned samples fit into three diatom orders based on the *rbcL* phylogenetic tree. Two of my samples were close to species of *Pleurosigma*. Two of my samples were close to species of *Actinocyclus*. Five of my samples were close to species of *Coscinodiscus.* Two of my samples were close to species of *Stephanodiscus.*

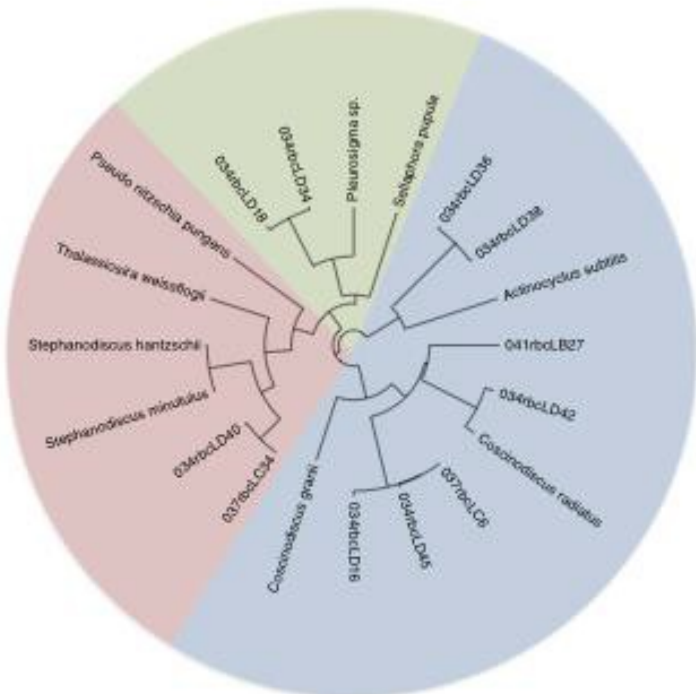

Figure 3: This figure depicts a circular phylogenetic tree for the marker *rbcL*. The diatom orders represented include: Navicuales (green), Coscinodiscales (blue), and Thalassosirales (red). My cloning samples are the ones labeled with a number, the marker, and another number. Published GenBank sequences are presented as the genera or species of diatom they represent. The scale bar for the branch lengths is included.

Discussion

COI

BLAST results for COI had low identity to sequences available in GenBank. Three of my unique sequences returned BLAST results matching *Sellaphora pupula* with 81-83% identity, whereas these same samples appeared in my phylogenetic tree close to *Coscinodiscus* spp. which is likely the correct result since it is a marine diatom and *Sellaphora pupula* is a freshwater diatom. Another one of my unique sequences returned a BLAST result matching *Skeletonema menzellii* at 86% identity and this same sample appeared in my phylogenetic tree close to *Skeletonema* spp. There were few matches between BLAST results and what I discovered it matched on the phylogenetic tree because top hits for BLAST results were based on both percent coverage and identity, so some sequences on BLAST may have had fewer base pairs percent off. An example is that it would report *Coscinodiscus* with BLAST which I could compare to what the phylogenetic tree reported it being close to. Additionally, the marker COI had a lot of mismatches or base pairs that do not match because of percent identity. For the phylogenetic tree, all the diatom orders represented in my samples are found in North America which makes sense because we sampled from North America. The BLAST sequences *Sellaphora* and *Ditylum* did not have any of my samples close to them or they were further away on the branch. I expected to find these diatoms since they were reported in BLAST results. The reason why two of my COI samples were in white and nothing was close to them between my BLAST search results and phylogenetic trees with no branch occurring including those two samples was BLAST was not clear what goes with what and my samples could perhaps be related to *Pseudo-nitzschia* based on BLAST results but BLAST is a basal group on the tree.

rbcL

All my samples matched for the maker *rbcL* between BLAST and phylogenetic trees. There is a monophyletic clade with 034*rbcL*D42 and *Coscinodiscus radiatus*. Results from BLAST searches may not be included in the phylogenetic trees because the BLAST sequence was too short, or the sequence was long and slightly off from my sample (half the sequence was on mine, but the other half was off). *Gyrosigma* was found in BLAST results but was too short of a sequence to incorporate in the phylogenetic tree. All these diatom orders are found in North America which makes sense because we sampled from North America. The diatom orders I found in my phylogenetic trees that have been identified before in the literature include Coscinodiscales and Thalassiosirales (Shumway et al. 1987, Malviya et al. 2016), whereas the diatom order Naviculales had not.

Comparison of Marker Success

The marker *rbcL* worked a lot better since it had a higher percent matching than the marker COI. The marker COI was an overall less successful marker for marine diatoms. It did not have close enough matches on BLAST (the average percent identity for the marker COI was 85.8%). The marker COI returned matches for freshwater diatoms (*Sellaphora pupula* 81-83 % identity). Additionally, the phylogenetic tree for COI showed my sequences being more closely related to different species than the BLAST search results.

The marker *rbcL* was a more successful marker for marine diatoms. It had very close matches on BLAST (average percent identity of 97.1%). All the results made sense geographically (all North American marine diatoms including *Coscinodiscus* spp.). Additionally, the phylogenetic tree for the marker *rbcL* showed my sequences being closely related to the same species as the BLAST search results.

I would recommend using *rbcL* as a barcode in the future for identifying diatoms in gut contents. Molecular techniques have potential to improve the base of knowledge of what scallops are feeding on because some diatom species present in scallop gut contents can not be identified visually due to the grinding of the diatom valve in the scallop gut (Fisher 2000). Grinding in the gut is unfavorable because it causes visual identification of diatoms to be difficult, thus I got back more diatoms species by using molecular methods. There were diatoms found through both visual surveys (Shumway et al. 1987, Malviya et al. 2016) and this study using molecular methods including *Coscinodiscus* spp. and *Thalassiosira* spp. However, I did find new diatom species that were not present in visual surveys including: *Skeletonema* spp., *Pleurosigma* spp., *Actinocyclus* spp., and *Stephanodiscus* spp.

Future work could identify a dietary basis for geographic difference in growth that have been observed in past visual surveys (Schick et al. 1988) and is important for the management of the fishery. There are many other options for future work. Verifying my primers work for specific cultured diatom species would further prove my primers work for diatoms. Sequencing diatom species present in the environment would allow for a good comparison with scallop gut contents. Additionally, matching diatoms sequenced with diatoms found through visual identification would provide a ground truth to molecular methods. Another potential molecular method to try would be next-generation sequencing. This study was an important first step to confirm diatoms were present in scallop guts and to test primers work for a wide range of diatom species which can be adapted for next-generation sequencing.

Acknowledgements

I would like to thank everyone who contributed ideas, technical help, samples, or equipment including: my mentors Dr. Jan McDowell and Dr. David Rudders, my lab manager Ellen Biesack, Jackson Martinez, Sally Roman, and Erin Mohr. Thanks to Jenny Dreyer and Katherine Longmire for coordinating the REU program at VIMS. Program funding for the VIMS Research Experience for Undergraduates was made available through a grant awarded from the National Science

Foundation (grant # NSF OCE 1659656) to Drs. Linda Schaffner and Rochelle Seitz.

Literature Cited

Ehara, M., Inagaki, Y., Watanabe, K.I., Ohama, T. 2000. Phylogenetic analysis of diatom *coxI* genes and implications of a fluctuating GC content on mitochondrial genetic code evolution. Curr Genet. 37, 29-33.

Evans, K.M., Wortley, A.H., Mann, D.G. 2007. An assessment of potential diatom "barcode" genes (*cox*1, *rbc*L, 18S, and ITS rDNA) and their effectiveness in determining relationships in *Sellaphora* (Bacillariophyta). Protist. 158(3), 349-364.

Fisher, R.A. 2000. Biology of Certain Commercial Mollusk Species: Scallops *In* Marine and Freshwater Products Handbook (eds. Martin, R.E., Carter, E.P., Flick, G.J., Davis, L.M.) Technomic, Lancaster, PA, USA. 83-109.

Guo, L., Sui, Z., Zhang, S., Ren, Y., Liu, Y. 2015. Comparison of potential diatom 'barcode' genes (the 18S rRNA gene and ITS, COI, *rbcL*) and their effectiveness in discriminating and determining species taxonomy in the Bacillariophyta. INT J SYS EVOL MICR. 65, 1369-1380.

Hamsher, S.E., Evans, K.M., Mann, D.G., A.and Saunders G.W. 2011. Barcoding diatoms: exploring alternatives to COI-5P. Protist. 162, 405-422.

Iwatani, N., Murakami, S., Suzuki, Y. 2005. A sequencing protocol of some DNA regions in nuclear, chloroplastic and mitochondrial genomes with an individual colony of *Thalassiosira nordenskioeldii* Cleve (Bacillariophyceae). Polar Biosci. 18. 35-45.

Levialdi, G. 2006. Plastid phylogeny and chloroplast inheritance in the planktonic pennate diatom *Pseudo-nitzschia* (Bacillariophyceae). Doctoral Thesis, Universita Degli Studi Di Messina.

Malviya, S., Scalco, E., Audic, S., Vincent, F., Veluchamy, A., Poulain, J., Wincker, P., Iudicone, D., Vargas, C., Bittner, L., Zingone, A., Bowler, C. 2016. Insights into global diatom distribution and diversity in the world's ocean. P. Natl. A. Sci. Plus 113(11), E1516-E1525.

Moniz, M.B.J., Kaczmarska, I. 2009. Barcoding diatoms: is there a good marker? Mol. Ecol. Resourc. 9, 65-74.

Schick, D.F., Shumway S.E., and Hunter M.A. 1988. A comparison of growth rate between shallow water and deep water populations of scallops, *Placopecten magellanicus* (Gmelin, 1791), in the Gulf of Maine. Am. Malacol. Bull. 6(1), 1-8.

Shumway, S.E., Selvin, R., Schick, D.F. 1987. Food resources related to habitat in the scallop *Placopecten magellanicus* (Gmelin, 1791): a qualitative study. J. Shellfish Res. 6(2), 89-95.

Shumway, S.E., Parsons, G.J. 2016. Scallops: biology, ecology, aquaculture, and fisheries. Dev. Aquacult. Fish. Sci. 40(3), 1196 pp.

Vasselon, V., Domaizon, I., Rimet, F., Kahlert, M., Bouchez A. 2017. Application of high-throughput sequencing (HTS) metabarcoding to diatom biomonitoring: Do DNA extraction methods matter? Freshw. Sci. 36(1), 162-177.

Using Macroinvertebrate Assemblages to Assess Nursery Habitat Quality for Juvenile Black Sea Bass and Summer Flounder

Nicholas Coleman

Coastal Carolina University

Mentors: Shannon Smith, Dr. Troy Tuckey, and Dr. Mary Fabrizo

2 August 2019

Abstract

Macroinvertebrate assemblages among four habitats of varying structural complexity were sampled with standardized monitoring units for reef fishes (SMURFS) in the Piankatank River to assess nursery habitat quality for juvenile black sea bass (*Centropristis striata*) and summer flounder (*Paralichthys dentatus*). Habitats were sampled in triplicate during three biweekly sampling events in May 2019. Simpson's diversity, richness, evenness, and abundance were used to compare macroinvertebrate assemblages among the four habitats. Non-metric multidimensional scaling (nMDS) was applied to data on relative abundance of taxa in the four habitats, and water quality was overlaid on this ordination. There was a significant difference ($p=0.022$) in the macroinvertebrate assemblages among the four sampled habitats. Sampled water quality parameters (depth (m), water temperature (ºC), salinity (ppt), conductivity (mS/cm), dissolved oxygen (mg/L), turbidity (FNU), and pH) did not have a significant influence on the distribution of macroinvertebrates. Seagrass habitats supported the highest abundance of potential prey (amphipods, isopods, and polychaetes) and exhibited water quality factors that differed from those observed in all other habitats. Observed

differences in macroinvertebrate assemblages are likely driven by habitat complexity or some other factor that was not analyzed. Beginning to identify the characteristics of four common habitats of varying structural complexity can increase the understanding of how they might be used by juvenile black sea bass and summer flounder in the Chesapeake Bay, and ultimately assist in focusing management and conservation efforts.

Introduction

Coastal ecosystems provide many valuable functions, but their role in the development of juvenile fish is among the most important. A proper understanding of the habitat characteristics that support juvenile fish is essential to develop appropriate fisheries management and conservation goals. The term most often used to refer to areas used by fish during their early life (eggs, larvae, and juveniles) is 'nursery'. Previously, entire estuarine systems were designated as nurseries, making effective and focused fisheries management difficult (Beck. et al. 2001). Several papers have offered improved definitions of nurseries and their contribution to adult populations. For example, Beck et al. (2001) defined nurseries as areas that contribute a disproportionate biomass of juveniles per unit area. Similarly, Dahl et al. (2006) offered that nurseries should be identified based on their contributions to adult populations. While these definitions have improved the understanding of the relationship between nurseries and offshore populations, they may fail to recognize the geographic connectivity among habitats utilized by juvenile fishes. Because of the dynamic processes associated with fish development and because different life stages exploit a diversity of habitats, successful delineation of nursery habitats has proven difficult (Nagelkerken et al. 2015). Nagelkerken et al. (2015) proposed a new approach termed 'dynamic seascape', which accounts for the various habitats used by juvenile fish.

Black sea bass *Centropristis striata* and summer flounder *Paralichthys dentatus* are two economically and ecologically important species that use Chesapeake Bay, Virginia and its tributaries as nurseries; these species have life history strategies that are best studied using the dynamic seascape concept. Although previous studies revealed the use of estuaries as nurseries for black sea bass and summer flounder, limited information exist on the conditions that make such areas advantageous for juvenile development. Based on fisheries-independent surveys, juvenile black sea bass enter the

Chesapeake Bay in spring (Apr); they exploit estuarine habitats until late fall (Oct-Nov) when they emigrate offshore (Moser & Shepherd 2009, Tuckey & Fabrizio 2010). Similarly, juvenile summer flounder are found in the Chesapeake Bay in spring (late Mar); this species utilizes saltmarsh lagoons and other habitats until individuals emigrate from coastal areas in December (Rountree & Able 1992, Caposssela et al. 2013, and Tuckey and Fabrizio 2013).

Provision of food is one of the many services offered by nurseries, yet little is known about the diet of most juvenile fishes (Nagelkerken et al. 2015). Prey abundance is strongly influenced by habitat type, and prey selection can vary through ontogeny (Nunn et al. 2011). The limited research on the feeding habits of juvenile black sea bass and summer flounder indicates dietary overlap, with both species feeding on macroinvertebrates such as amphipods, polychaetes, and isopods (Orth and Heck 1980, Burke 1995). In North Carolina, summer flounder from salt marsh habitats fed predominantly on polychaetes (Burke 1995), possibly because polychaetes are abundant in these areas (Cammen 1979). These results suggest that juvenile summer flounder use habitats where prey is plentiful (Burke 1995). Furthermore, salt marsh habitats are structurally complex, and such complexity is known to support high diversity and abundance of fish (Orth and Heck 1980) and macroinvertebrate assemblages (Lubbers et al. 1990).

Factors that influence macroinvertebrate assemblages differ among habitats, which ultimately results in macroinvertebrate assemblages that vary by habitat type (Nunn et al. 2011). Thus, habitat used by juvenile summer flounder and black sea bass may be influenced by macroinvertebrate assemblages and the conditions that support them in the Chesapeake Bay. My study, as part of a larger project to delineate habitats that support these two species (Fabrizio et al. 2018), focused on assessing the abundance and diversity of macroinvertebrate assemblages among four potential nursery habitats of distinct structural complexity: seagrass, oyster reefs, marsh, and soft bottom. To my knowledge, this is the first project to conduct a fine scale delineation of nursery habitats of varying structural complexity in the Chesapeake Bay for these species.

I hypothesize that the four habitats analyzed in this project will have dissimilar macroinvertebrate assemblages, therefore influencing the value of each habitat for black sea bass and summer flounder. The composition of macroinvertebrate assemblages will be compared with reported dietary analysis of juvenile black sea bass and summer flounder to assess the prey resources at each habitat. This study expands on previous studies of juvenile fish and potential prey abundances in habitats that focus on vegetated and non-vegetated habitats by examining prey assemblages for juvenile fishes in four distinct habitats. The results of this study can contribute to understanding the value of estuarine habitats that may be used by juvenile black sea bass and summer flounder, and ultimately assist fisheries managers in making focusing conservation efforts.

Methods

Study Area

The 39.3-km long Piankatank River is located in Middlesex County. The river is fed by the Dragon Run swamp, one of the most pristine watersheds in Virginia, and empties into Chesapeake Bay. Sample sites were located near Gwynn Island at the interface of the Piankatank River and the Chesapeake Bay (Figure 1).

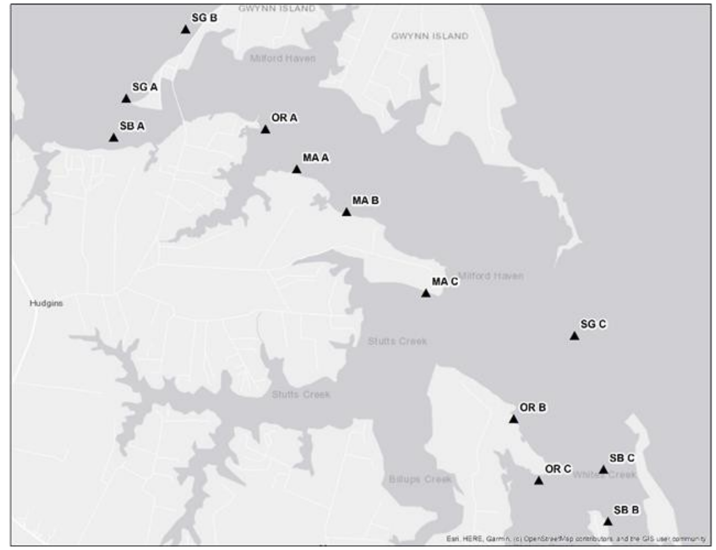

Figure 1: Map of the lower Piankatank River sampling sites in Middlesex County, Virginia. Sites include marsh habitat (MA A, MA B, MA C), oyster reef habitat (OR A, OR B, OR C), soft-bottom habitat (SB A, SB B, SB C), and seagrass habitat (SG A, SG B, SG C).

Macroinvertebrate Collection

Four habitat types (seagrass, oyster reefs, marsh creek, and soft bottom) in the Piankatank River, Virginia, were sampled in May 2019, using standardized monitoring units for reef fishes (SMURF). SMURFs, which are a passive fishing gear, were deployed in shallow water for 48 hours during three biweekly sampling events to collect juvenile fishes; because the outer mesh of the collection device is 1mm, this gear also captures mobile invertebrates. Each habitat was sampled in triplicate, and two SMURFs were deployed at each triplicate site per sampling event for a total of 72 samples. Water quality (such as habitat depth (m), water temperature (ºC), salinity (ppt), conductivity (mS/cm), dissolved oxygen (mg/L), turbidity (FNU), and pH) was recorded at each site using a YSI Pro DSS. SMURF contents were rinsed down into a washtub and the SMURF was visually inspected to ensure all invertebrates were removed. Washtub contents were poured into a 1 mm mesh collection bag that retained invertebrates but allowed water to drain. Mesh bag contents were then transferred and rinsed in a sieve, and organisms were transferred to plastic bags and preserved using 70% ethanol.

SMURF contents were subsequently analyzed in the laboratory. Information on the date, location, habitat type, site, and replicate were recorded for each sample. A dissecting microscope was used to identify and count invertebrates; identifications were conducted to the lowest possible taxonomic level, except amphipods which were identified to order (Amphipoda) and grouped together. Invertebrates were identified using dichotomous keys (VIMS 1960; Bartholomew 2004; and VIMS 2013). The abundance and weights of each taxon were recorded.

Macroinvertebrate Assemblage Analysis

Macroinvertebrate count data were converted into relative abundance data prior to non-metric multidimensional scaling (nMDS) ordination implemented in R (R version 3.5.1) to remove potential issues caused by higher numbers of some taxa. Ordinations were used to explore relationships between habitat type and assemblage composition of macroinvertebrates. The nMDS ordinations used the Bray-Curtis similarity index applied to data on the relative abundance of taxa in the four observed habitats. The function *envfit* in the R package vegan was used to assess differences in macroinvertebrate assemblages among habitats and determine if water quality factors had a significant influence on macroinvertebrate assemblages. Significant differences in macroinvertebrate assemblages among habitat were assessed using the *envfit* function, which fits vectors to the nMDS ordination and tests for statistical significance with 999 permutation tests. Simpson's diversity index, richness, and evenness were calculated for assemblages at each site within each habitat; to do this I combined macroinvertebrate counts across sampling events. Differences in water quality parameters among habitats were assessed with ANOVA. To further investigate specific differences in these parameters, means and 95% confidence intervals were calculated for each habitat and compared.

Results

Macroinvertebrate Assemblages

A total of 6,836 invertebrates representing 19 species and 7 orders was sampled during May 2019. Total invertebrate abundance was highest in seagrass habitats (n= 3,870) and lowest in marsh habitats (n=610). Species richness exhibited little variation among habitats. Mean invertebrate richness ranged from 7.7 (standard error [SE]=0.33) at seagrass habitats to 9.7 at oyster reef habitats (SE=1.00). Simpson's diversity ranged from 1.4 (SE=0.05) at marsh habitats to 2.1 (SE=0.19) at seagrass habitats. Similarly, evenness ranged from 0.12 (SE=0.01) at marsh habitats to 0.23 (SE=0.02) at seagrass habitats. The four most abundant taxa were amphipods (Amphipoda), grass shrimp (*Palaemonetes* spp.), mottled dog whelk (*Phrontis vibex*), and common clam worm (*Alitta succinea*), representing 98% of all observed invertebrates. Amphipods were the most abundant taxon in all sampled habitats. Amphipods, polychaetes, and isopods were most abundant at seagrass habitats while grass shrimp were most abundant in oyster reefs.

Macroinvertebrate assemblages were grouped by species, although overlap among assemblages was also observed. When species were overlaid with habitat sites in the nMDS ordination space (Figure 2, Table 1), I observed a significant difference (p=0.02) in macroinvertebrate assemblages among sites. For example, two oyster reef sites, and one marsh site were grouped closely, suggest similar macroinvertebrate assemblage occurred at these sites, even though habitat type varied. All seagrass sites were grouped closely and associated with amphipods. Another grouping was observed for the following isopods: *Sphaeroma quadridentatum*, *Erichsonella attenuata*, *Idotea metallica*, and an unidentified isopod. One soft-bottom site was not grouped closely to any other sites.

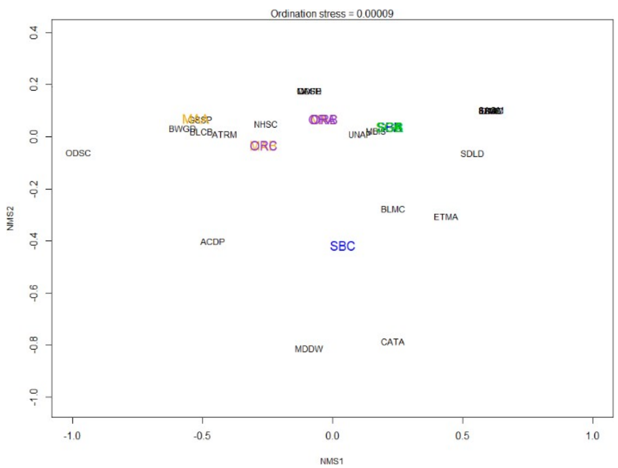

Figure 2: A non-metric multidimensional scaling (nMDS) ordination for the macroinvertebrate assemblages of 12 sampled sites Species and orders are represented by a four-letter code. Sites are represented by a four-letter code and color coordinated by habitat.

Table 1: Abbreviation, common name, and species name of taxa described in Figure 2. Taxa without widely accepted common names are listed by their genus then family in parentheses.

Abbreviation	Common Name	Species Name/ Taxonomic Group
MDDW	Mottled Dog Welk	*Phrontis vibex*
ACDP	Thorn Isopod	*Ancinus depressus*
MDFE	Midge Fly Larvae	*Chironomidae*
CACD	Calanoid Copepod	*Calanoida*
SAQM	Sea Pill Bug	*Sphaeroma quadridentatum*
BLMC	Baltic Macoma Clam	*Macoma balthica*
BCSU	Blue Crab	*Callinectes sapidus*
GSSP	Grass Shrimp	*Palaemonetes*
UNIS	Unidentified Isopod	*Isopoda*
DLSP	(Driloneris polychaete)	*Driloneresis*
ETMA	(Edotia isopod)	*Edotia montosa*
UNPY	Unidentified Polychaete	*Polychaeta*
UNAP	Unidentified Amphipod	*Amphipoda*
ECAT	Seagrass Isopod	*Erichsonella attenuata*
CATA	Common Atlantic Abra	*Abra aequalis*
MLMA	Mitchell's Macoma	*Macoma mitchelli*
SDLD	(Synidotea isopod)	*Synidotea laevidorsalis*
ITML	Idotea (isopod)	*Idotea metallica*
NHSC	Clam Worm	*Alitta succinea*
MBIS	Mound Back Isopod	*Edotia triloba*
ATRM	Atlantic Ribbed Mussel	*Geukensia demissa*
ODSC	Oceanobdella (leech)	*Oceanobdella sexoculata*
BWGD	Bhawania (polychaete)	*Bhawania goodei*
FBMC	Flat Back Mud Crab	*Eurypanopeus depressus*
SMCB	Say Mud Crab	*Dyspanopeus sayi*

Table 2: Mean water quality conditions for the four sampled habitat types. Confidence intervals (95%) are shown in parenthesis below the mean.

	Marsh	Oyster reef	Soft bottom	Seagrass	F	p
Temperature (ºC)	24.98 (22.75-27.20)	24.49 (22.65-26.33)	23.47 (21.70-25.24)	23.02 (23.39-24.66)	0.88	0.46
Salinity (ppt)	10.70 (10.61-10.78)	10.80 (10.68-10.94)	10.80 (10.64-10.95)	10.60 (10.47-10.72)	2.39	0.09
Conductivity (mS/cm)	18.12 (18.0-18.3)	18.27 (18.1-18.5)	18.25 (18.0-18.5)	17.92 (17.7-18.1)	2.87	0.05
DO (mg/L)	9.18 (8.59-9.76)	8.42 (7.82-9.04)	8.48 (7.92-9.03)	9.89 (9.33-10.45)	5.43	<0.01
Turbidity (FNU)	6.92 (4.40-9.44)	8.92 (5.54-12.3)	7.09 (3.98-10.20)	2.77 (2.18-3.35)	3.75	0.03
pH	8.28 (8.24-8.31)	8.12 (8.00-8.24)	8.19 (8.10-8.26)	8.40 (8.37-8.43)	8.74	<0.01
Depth (m)	0.40 (0.36-0.45)	0.81 (0.72-0.91)	0.67 (0.63-0.70)	0.83 (0.76-0.89)	2.76	<0.01

Water Quality

Water quality factors were overlaid on the nMDS plot of macroinvertebrate assemblages, but none of the sampled water quality factors had a significant influence ($p>0.05$) on the composition of macroinvertebrate assemblages. There was no significant difference in mean temperature ($F=0.88$, $p=0.46$) or salinity ($F=2.39$, $p=0.09$) among the sampled habitats. There was a significant difference in the mean conductivity ($F=2.87$, $p=0.05$) among habitats, however a comparison of the means indicated no significant difference in conductivity among habitat pairs. Mean dissolved oxygen was significantly higher in seagrass habitats than in oyster reefs and soft-bottom habitats (Table 2). Mean turbidity was significantly lower in seagrass habitats compared with all other habitats (Table 2). Mean pH was significantly higher at seagrass habitats compared with marsh and oyster reefs (Table 2). Mean depth was significantly lower in marsh habitats compared with all other habitats and mean soft-bottom depth was significantly lower than seagrass habitats (Table 2).

Discussion

Macroinvertebrate Assemblages

Seagrass habitats had the highest macroinvertebrate abundance, but the lowest diversity. In contrast, marsh habitats had the lowest macroinvertebrate abundance but the highest diversity. Given the abundance of amphipods in seagrass habitats, the consideration of further species designation for this group would likely increase diversity. Given the structural complexity of oyster reefs, they were expected to have macroinvertebrate abundances comparable to seagrass habitats, however I observed a relatively low abundance of macroinvertebrates in oyster reefs. In this study, aquaculture oyster cages or deposited oyster shells served as oyster reef habitat and it may be that these less established habitats do not function as “true” oyster reefs. Additionally, anthropogenic influence via manipulation and proximity to shoreline along working water fronts may have influenced the macroinvertebrate assemblages that recruited to our sampled oyster reef sites.

Amphipods, polychaetas, and isopods were taxa of interest because they are consumed by juvenile black sea bass and summer flounder (Orth and Heck 1980, Burke 1995). Amphipods, polychaetes, and isopods were most abundant in seagrass, and I hypothesize that seagrasse habitats may provide enhanced feeding opportunities for juvenile black sea bass and summer flounder.

Oyster reefs shared similar invertebrate assemblages with marsh habitats, whereas seagrass habitats shared similar invertebrate assemblages with soft-bottom habitats. Seagrass habitats were grouped closely with one another, suggesting that macroinvertebrate assemblages were less variable among seagrass sites than at all other habitat types. Amphipods were closely associated with seagrass habitats, which is reflected in their high abundance at seagrass habitats. Amphipods and isopods are herbivores that consume epiphytic algae on seagrasses (Zimmerman and Harrington 1979, Williams and Ruckelshaus 1993), and this trophic relationship could explain the association between these invertebrates and seagrasses. Grass shrimp were most abundant in oyster reef and marsh habitats, but least abundant in soft-bottom habitats, suggesting habitat preference for structural complexity. One soft-bottom site was isolated from all other sites and further analysis indicated that this site exhibited the greatest species diversity, possibly because of its proximity to the Chesapeake Bay.

Water Quality

Water quality factors had no significant influence on the composition of macroinvertebrate assemblages, suggesting that habitat type or other factors that were not analyzed in this study drive the composition of macroinvertebrate assemblages in the lower Piankatank River. Significantly shallower depths observed in marsh habitats were attributed to the proximity of these sites to shore. The absence of a significant difference in the mean salinity and temperature among habitats was not surprising, because sites occurred within 6 km of each other. Although conductivity is positively influenced by salinity, I expected to find no significant difference in mean conductivity among habitats given that I observed no significant difference in mean salinity among habitats. This expectation was confirmed when I examined confidence intervals for mean conductivity among habitat types.

Water quality in seagrass habitats appeared to differ from that observed in all other habitats. Significantly higher mean dissolved oxygen concentrations observed in seagrass habitats are most likely attributed to oxygen production by seagrasses via photosynthesis. Primary production in seagrass habitats can also explain observed increases in mean pH. In densely vegetated shallow water habitats containing *Posidonia* *oceanica*, seagrass can consume CO_2 at a rate that can cause a significant increase in the pH of the surrounding waters (Frankignoulle and Distéche 1984). Although the species of seagrass sampled in this study was not determined, the elevated pH values observed in seagrass habitats suggest that a similar phenomenon may be occurring in the shallow areas of the Piankatank. Additionally, seagrasses have been reported as sinks for suspended inorganic matter in the Chesapeake Bay in the spring (Moore 2004), effectively collecting and removing suspended particles from the water column. It is likely that the significantly lower mean turbidity observed in seagrass habitats is attributed to the ability of seagrass to remove suspended particles. Furthermore, low turbidity water confers a growth advantage for seagrasses (Orth et al. 2006).

Conclusion

Macroinvertebrate assemblages were significantly different among the four sampled habitats in the lower Piankatank River. Water quality conditions did not have a significant influence on the distribution of macroinvertebrates among habitats, and I hypothesize that differences in assemblages among habitats are driven by structural complexity or other factors that were not analyzed in this study. Relatively high amphipod, polychaete, and isopod abundances in seagrass habitats suggest that these habitats may provide enhanced feeding opportunities for juvenile black sea bass and summer flounder. Results of my research can be used to begin to understand the unique characteristics of four common habitats in the Chesapeake Bay. Future studies should expand habitat assessment to multiple Chesapeake Bay tributaries and further characterize habitat types.

Acknowledgments

I thank Shannon Smith, Dr. Troy Tuckey, and Dr. Mary Fabrizio for their contribution to this project, without their assistance this would not have been possible. I also thank Dr. Rochelle Seitz, Jenny Dreyer, and Katherine Longmire for coordinating the REU program. Lastly, I am grateful to the Chesapeake Research Consortium for providing funds for my internship, and the NOAA Chesapeake Bay office for providing funds for this project (grant # NA18NMF4570254).

References

Bartholomew, A. (2004). Key to the polychaetes of Chesapeake Bay and coastal Virginia online: http://www.vims.edu/bio/benthic/polychaete.html

Beck, M.W., Heck, K.L., Able, K.W., Childers, D.L., Eggleston, D.B., Gillanders, B.M., Halpern, B., Hays, C.G., Hoshino, K., Minello, T.J. and Orth, R.J. (2001). The identification, conservation, and management of estuarine and marine nurseries for fish and invertebrates: a better understanding of the habitats that serve as nurseries for marine species and the factors that create site-specific variability in nursery quality will improve conservation and management of these areas. *Bioscience*, *51*(8), 633-641.

Burke, J. S. (1995). Role of feeding and prey distribution of summer and southern flounder in selection of estuarine nursery habitats. *Journal of Fish Biology*, *47*(3), 355-366.

Cammen, L. M. (1979). The macro-infauna of a North Carolina salt marsh. *American Midland Naturalist*, 244-253.

Capossela, K. M., Fabrizio, M. C., & Brill, R. (2013). Migratory and within-estuary behaviors of adult Summer Flounder (Paralichthys dentatus) in a lagoon system of the southern mid-Atlantic Bight. *Fishery Bulletin*, *111*(2), 189.

Fabrizio, M.C. Tuckey, T.D., Ross, P.G., Jr, and Snyder, R.A. (2018). Characterization of nursery habitats used by black sea bass and summer flounder in Chesapeake Bay and the coastal lagoons. *Proposal funded by NOAA Chesapeake Bay Office, Annapolis, MD.*

Frankignoulle, M., & Distèche, A. (1984). CO2 chemistry in the water column LS TTT. *Oceanologica acta*, *7*(2), 209-219.

Heck Jr, K. L., and Orth, R. J. (1980). Seagrass habitats: the roles of habitat complexity, competition and predation in structuring associated fish and motile macroinvertebrate assemblages. In *Estuarine perspectives* (pp. 449-464). Academic Press.

Lubbers, L., Boynton, W. R., and Kemp, W. M. (1990). Variations in structure of estuarine fish communities in relation to abundance of submersed vascular plants. *Marine Ecology Progress Series*, 1-14.

Moore, K. A. (2004). Influence of seagrasses on water quality in shallow regions of the lower Chesapeake Bay. *Journal of Coastal Research*, 162-178.

Moser, J., & Shepherd, G. R. (2009). Seasonal distribution and movement of black sea bass (*Centropristis striata*) in the Northwest Atlantic as determined from a mark-recapture experiment. *Journal of Northwest Atlantic Fishery Science*, *40*, 17-28.

Nagelkerken, I., Sheaves, M., Baker, R., and Connolly, R. M. (2015). The seascape nursery: a novel spatial approach to identify and manage nurseries for coastal marine fauna. *Fish and Fisheries*, *16*(2), 362-371.

Nunn, A. D., Tewson, L. H., & Cowx, I. G. (2012). The foraging ecology of larval and juvenile fishes. *Reviews in Fish Biology and Fisheries*, *22*(2), 377-408.

Orth, R.J., Carruthers, T.J., Dennison, W.C., Duarte, C.M., Fourqurean, J.W., Heck, K.L., Hughes, A.R., Kendrick, G.A., Kenworthy, W.J., Olyarnik, S. and Short, F.T. (2006). A global crisis for seagrass ecosystems. *Bioscience*, *56*(12), 987-996.

Rountree, R. A., and Able, K. W. (1992). Foraging habits, growth, and temporal patterns of salt-marsh creek habitat use by young-of-year summer flounder in New Jersey. *Transactions of the American Fisheries Society*, *121*(6), 765-776.

Tuckey, T. D., & Fabrizio, M. C. (2010). Estimating relative juvenile abundance of ecologically important finfish in the Virginia portion of Chesapeake Bay. *Project# F-104-R-14. Annual Report to Virginia Marine Resources Commission. Virginia Institute of Marine Science, Gloucester Point*.

Tuckey, T. D., & Fabrizio, M. C. (2013). Influence of survey design on fish assemblages: implications from a study in Chesapeake Bay tributaries. *Transactions of the American Fisheries Society*, *142*(4), 957-973.

Virginia Institute of Marine Science. Invertebrate Identification Guide (2013). Virginia Institute of Marine Science, College of William and Mary. https://www.vims.edu/research/departments/fisheries/programs/multispecies_fisheries_research/laboratory_methods/diet_analysis/invertebrate_id_guide/Invertebrate%20ID%20Guide.pdf

Virginia Institute of Marine Science. Keys to Virginia Invertebrates. (1960). Virginia Institute of Marine Science, College of William and Mary. https://doi.org/10.21220/V5030D

Williams, S. L., & Ruckelshaus, M. H. (1993). Effects of nitrogen availability and herbivory on eelgrass (Zostera marina) and epiphytes. *Ecology*, *74*(3), 904-918.

Zimmerman, R., Gibson, R., & Harrington, J. (1979). Herbivory and detritivory among gammaridean amphipods from a Florida seagrass community. *Marine Biology*, *54*(1), 41-47.

Characterizing York River Estuary Benthic Metabolism

Mary McGuinness
New Jersey Institute of Technology

Mentors: Dr. Iris Anderson, Graduate Students: Derek Detweiler and Michelle Woods

2 August 2019

Synopsis

The benthic metabolism of the York River Estuary (YRE) was classified as heterotrophic along the entire sampling transect. Chlorophyll-*a* was at the highest concentration in down-estuary sediment, where benthic microalgae competed with denitrifying bacteria for NO_x. Data analysis revealed that gross primary production (GPP) promoted respiration (R), and increased DOC uptake enhanced NH_4^+ remineralization.

Abstract

Spatial variation of benthic net ecosystem metabolism (NEM) and nutrient cycling of the York River Estuary (YRE), Virginia, USA was classified from rates of DO, DIC, DOC, and DIN fluxes observed during sediment core incubations. The entire estuary was classified as net heterotrophic. Additionally, data analysis showed that chlorophyll-*a* (chl-*a*) decreased up the estuarine gradient. Further analysis revealed that gross primary production (GPP) and respiration (R) were coupled, with GPP promoting R. We also observed that increased rates of NO_x uptake resulted in decreased denitrification rates. Lastly, a trend was detected between DOC

uptake and NH_4^+, indicating DOC respiration stimulated NH_4^+ production.

Introduction

NEM of benthic estuarine systems describes the relationship between primary production and respiration occurring in sediments. Systems with high inputs of nutrients, increased light, and low turbidity will favor primary production and can be classified as autotrophic, while systems with high concentrations of organic matter (OM) will favor respiration and promote heterotrophy (Kemp and Testa, 2011). NEM corresponds to carbon exchanges between the water column and the atmosphere, with autotrophic systems acting as a net sink for the greenhouse gas, CO_2, and heterotrophic systems acting as a net source of CO_2. (Borges et al 2005; Cai 2011). The NEM of estuaries can be altered from eutrophication, defined as the excess production of organic matter, including macro and microalgae and harmful algal blooms (HAB), resulting from high inputs of nutrients (Lemley and Adams 2019). During bloom conditions, cells deposit in the benthos and ae respired promoting heterotrophy. (Raymond and Bauer 2001; Cloern et al 2014).

Eutrophication in the YRE is often caused by runoff from the York River watershed, and this has the potential to trigger phytoplankton blooms, typically comprised of dinoflagellate species. Booms typically occur seasonally. During the winter, blooms of *Heterocapsa triquetra* are common. During the summer, intense blooms of *Margalefidinium polykrikoides* are regularly followed by blooms of *Alexandrium monilatum* (Reece 2015). During intensive bloom conditions, excess biomass accumulates in the benthos and is recycled which releases nutrients such as NH_4^+ and NO_x ($NO_2^- + NO_3^-$) into the benthos and water column. In estuarine system nitrogen limits primary production, increased production of nitrogen from remineralization can exacerbate blooms by providing bioavailable nutrients. Typically, remineralized nitrogen is assimilated by benthic microalgae, but increased turbidly and shading during HABs decreases benthic primary production. (Figure 1: Amber Hardison). Additionally, decomposition of deposited particulate organic matter (POM) from blooms release dissolved organic matter (DOM) and dissolved inorganic carbon (DIC) (Anderson 2017).

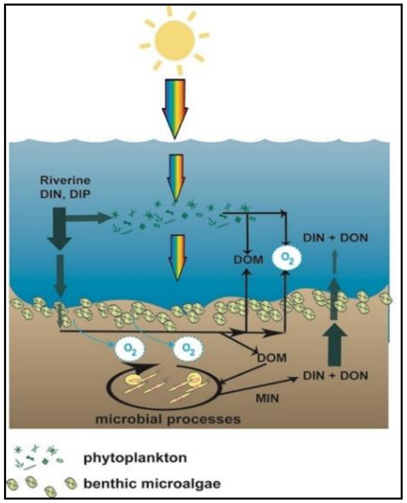

Figure 1: Diagram of Nutrient and carbon fluxes in autotrophic system.

The objective of this study was to classify the spatial variability in benthic metabolic parameters in the YRE using fluxes of dissolved oxygen (DO) and DIC. Additionally, DOC, DIN, and N_2 concentrations were measured to better understand the remineralization processes occurring in the benthos. Lastly, sediment samples were characterized based on their Chlorophyll-*a* concentrations. This project was part of larger study to characterize the YRE over a four-year period and study the effects of HABs on the overall carbon cycle (Anderson 2017).

Methods

Study Site

Our study was conducted in the YRE, which is a tributary of the Chesapeake Bay and is classified as a micro tidal mid-Atlantic estuary (Shen and Haas 2004). The YRE is subject to annual seasonal harmful algal blooms (HABs). The red tide blooms consisting of the dinoflagellates *Margalefidinium polykrikoides* and *Alexandrium monilatum*, typically occur in succession in late July through early September and have been observed almost annually for the last fifty and ten years respectively (Anderson, 2017).

Sample Collection

Our team conducted bimonthly cruises during spring tides, for consistency and accessibility of sample sites, in June in the YRE during pre-bloom conditions. During these cruises, a Dataflow system using a YSI 6600 datasonde, WET Labs CDOM sensor, Garmin global positioning system, and data acquisition system measured pH, dissolved oxygen (DO), salinity, and temperature every two seconds in the upper half meter of the water column (Figure 2: Woods). Triplicate sediment core samples were also taken at five sites (2, 3, 5, 8, and 9) in the YRE for our flux study along with grab samples for analyses of nutrients and DOM fluxes (Figure 3: Woods).

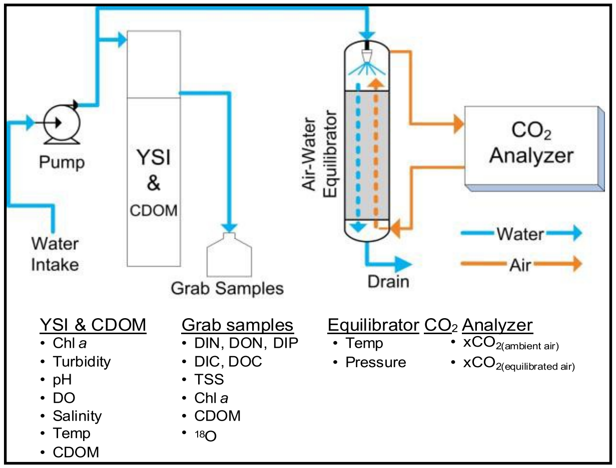

Figure 2: YSI instrumental design Schematic.

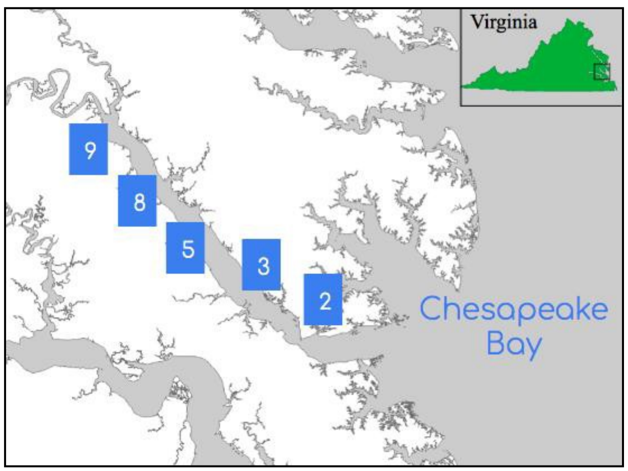

Figure 3: Map of shoal sample sites in YRE used for sediment core extraction.

Experimental Design

After collection, the sediment cores were placed in an environmental chamber under *in situ* conditions and placed in water baths filled with ambient York River water. The cores were left in the dark overnight to equilibrate and were subsequently capped and incubated for six hours (three hours in the dark and three hours in the light) the following day. Light conditions were simulated through the use of high intensity UV/PAR lamps to mimic natural sunlight. DIC, DOC, DIN, and DO samples were collected every 45 minutes throughout the six-hour incubation. Sample water was simultaneously replaced with filter-sterilized (0.2um) site water to avoid having any headspace in the cores. DIC samples were collected in gas tight exetainer tubes poisoned with HgCl2. DOC, DIN, and DON samples were filtered through a 0.45 µm filter and frozen until further analysis. DO was constantly monitored using a PreSens optical oxygen sensor. N_2 samples were taken at the beginning and end of the three-hour dark incubation and stored in exetainer vials laced with $ZnCl_2$ preservative. After all time-sets were complete, sediment samples were extracted at shallow (0-2) cm and moderate depths (2-5) cm for benthic Chl-*a* analysis.

Sample Analysis

DIN were measured using a Lachat QuickChem 8000 Auto analyzer. N_2 produced by denitrification and the conservative tracer Ar was measured using a membrane inlet mass spectrometer (MIMS). The ratio of N_2: Ar allowed us to correct for any contamination by N_2 from the atmosphere. DOC and DIC concentrations were measured using a Shimadzu TOC-V 5000 and Apollo SciTech DIC Analyzer, respectively. Changes in DOC and DO concentrations gave insight into the benthic metabolism of the system, while fluxes of DIN and DOC revealed remineralization processes in the benthic layer. Core extractions helped characterized the Chl-*a* concentrations of the sediment.

The difference between light and dark fluxes of DO were used to calculate respiration (R), gross primary production (GPP), and net ecosystem metabolism (NEM). NH_4^+ production and NO_x uptake was determined from DIN fluxes. Calculations for NEM (DO-based; micromoles per Liter per day) and nutrient fluxes (micromoles per Liter per hour) are shown below.

Calculations

[1] $R = F_D$

[2] $NCP = F_L$

[3] $NEM = (NCP * T_L) + (R * T_D)$

[4] $GPP = [NEM – (R * 24hr)] * (r^2 * h * \pi * 10^{-3})$

[5] NH_4^+ Flux $= F_D$

[6] NO_X Flux $= F_D$

where FD is hourly flux in dark conditions and FL is hourly flux in light conditions (micromole per Liter per hour). NEM (Eq. 3) is positive when Net Community Production (NCP) is greater than R and signifies net autotrophy and oxygen production, whereas a negative NEM signifies net heterotrophy and oxygen uptake.

Results

Site Characterization

All samples sites had a negative oxygen flux based NEM, indicating net heterotrophy along the estuary (Figure 4). Benthic Chl-*a* (milligram per square meter) concentrations decreased up-estuary with the highest concentrations at sites 2 and 3 (84.01 and 27.86 mg/m^2, respectively) and lowest concentrations at sites 8 and 9 (10.77 and 11.24 mg/m^2, respectively) (Figure 5).

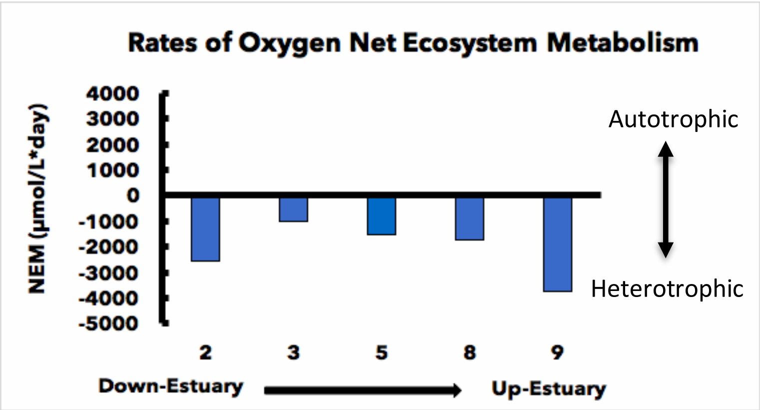

Figure 4: Plot displays NEM across the estuarine gradient. All sites have a net heterotrophic NEM.

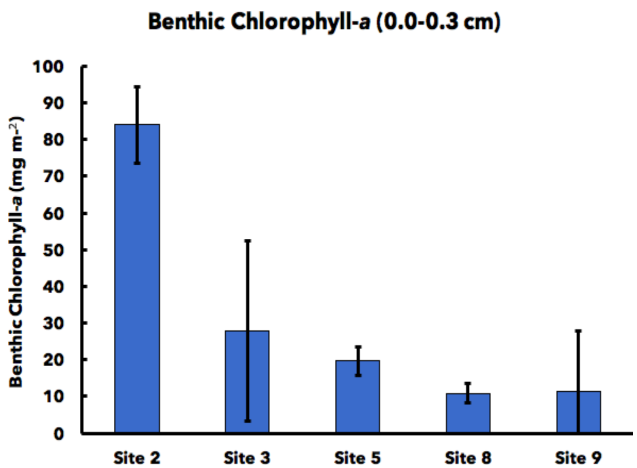

Figure 5: Graph shows chlorophyll-a concentrations across all sites. Highest concentrations observed down estuary.

Gross Primary Production and Respiration

The highest GPP was observed at sites 2 and 9 (86.25 and 144.38 µmole/day respectively) (Figure 6). Additionally, GPP and R were related. The oxygen uptake from respiration increased as oxygen production from GPP increased (Figure 7).

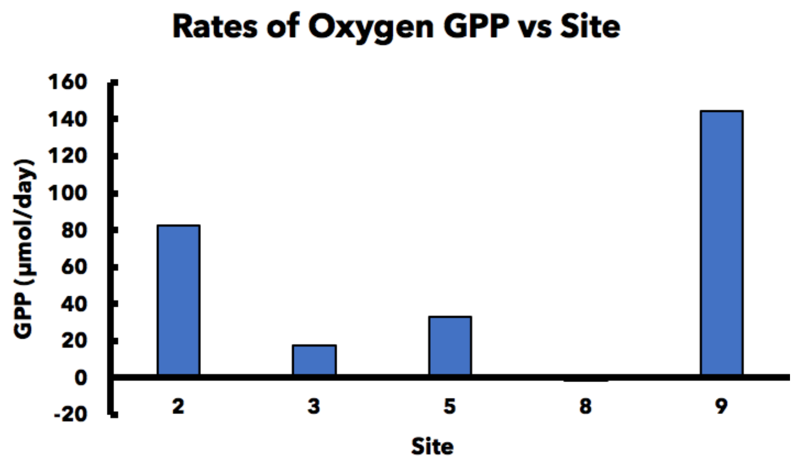

Figure 6: Displays gross primary production at different sample sites. Highest GPP rates occurred at sites 2 and 9.

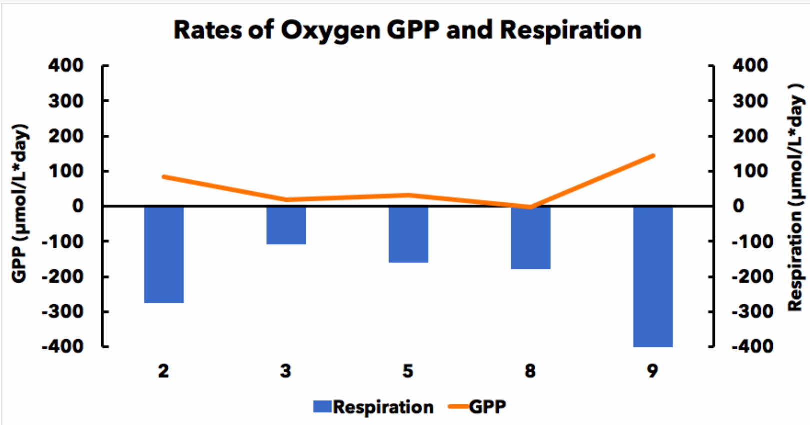

Figure 7: This plot shows the positive correlation between respiration and gross primary production.

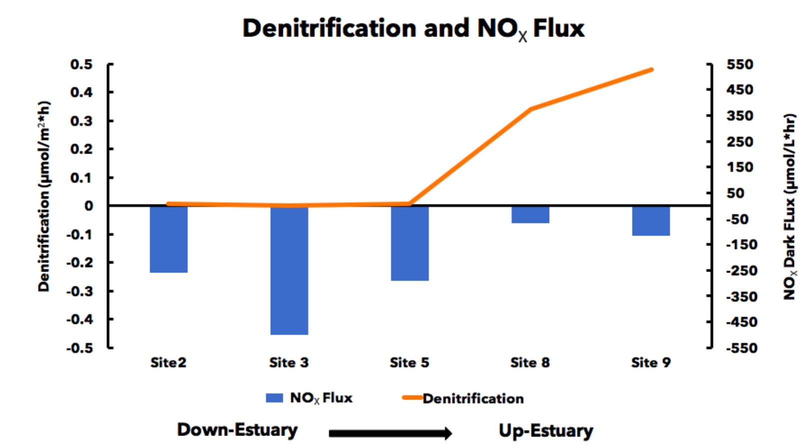

Figure 8: Plot reveals negative relationship between NO_x uptake and denitrification.

Nutrient Processes

Denitrification rates increased up the estuarine gradient, with the highest rates at sites 8 and 9 (375.7 and 527.0 μmole/m^2*hour, respectively). Denitrification occurring at the highest rates where NO_x uptake was the lowest (Figure 8). NH_4^+ and DOC were also coupled with NH_4^+ production increasing with increased DOC uptake (Figure 9).

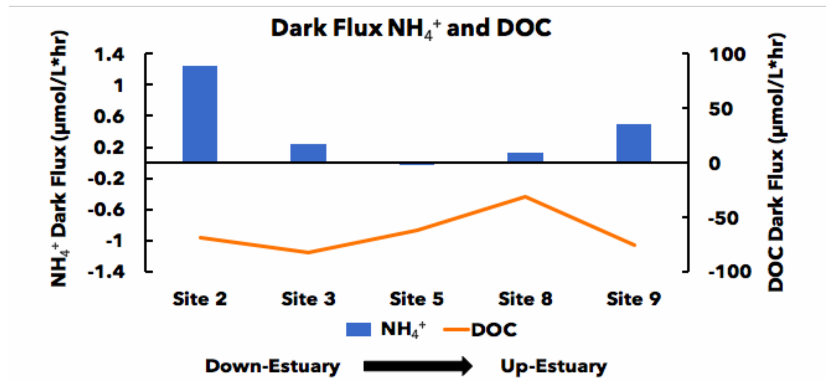

Figure 9: Conveys the positive association between DOC uptake and NH_4^+ production.

Discussion

This study of spatial variation in of benthic metabolism and carbon and nutrient fluxes in the YRE characterized the ecosystem and improved the understanding of the relationships between processes occurring in the benthos.

Net heterotrophic metabolism was observed across all sample sites. Up-estuary, high turbidity and decreased light attenuation could account for the increased respiration compared to GPP. Down-estuary, Chl-*a* concentrations were highest due to increased light and primary production. The heterotrophy observed in these sites is most likely a result of increased availability of organic matter from the long lasting *Heterocapsa* bloom that was observed during the winter and spring throughout the YRE. (Reece Unpublished).

Results show that GPP and R were correlated. As GPP increased, labile dissolved organic matter (DOM) was released into the benthos promoting respiration. Relationships were also observed between NO_X and denitrification as well as between DOC and NH_4^+. Denitrification rates were highest where NO_x uptake was lowest due to greater availability of NO_x for denitrifying bacteria. NO_x uptake was highest down-estuary where Chl-*a* concentrations were highest. This indicates benthic microalgae is competing with denitrifiers and decreases N_2 production. Lastly, NH_4^+ production was related to DOC uptake; as DOC is respired, DIN is demineralized and NH_4^+ is produced.

This study revealed the relationships between benthic processes and characterized the NEM and sediment throughout the YRE. In the future, this data can be used as a baseline for comparison when studying the effects of various factors (temperature, HABs, storms, etc.) on the NEM of the YRE.

Acknowledgments

Thanks to Jenny Dreyer, Rochelle Seitz, and Katherine Longmire for coordinating the REU program at VIMS. Funding for this project was provided by the National Science Foundation OCE #1737258. Special thanks to Michelle Woods, Derek Detweiler, and Dr. Iris Anderson for their mentorship and support throughout this project. As well as Evan Lawrence and Hunter Walker for their assistance with lab work and data processing.

Literature Cited

Anderson, I.C., Brush, M.J., Song, B., Reece, K.S. 2017. Alteration of carbon fluxes by intense phytoplankton blooms in a micro-tidal estuary. Proposal submitted to the National Science Foundation.

Anderson, Iris C., et al. "Impacts of Climate-Related Drivers on the Benthic Nutrient Filter in a Shallow Photic Estuary." *Estuaries and Coasts*, vol. 37, no. S1, 2014, pp. 46–62., doi:10.1007/s12237-013-9665-5.

Kemp, W.M. and J.M. Testa. 2011. Metabolic balance between ecosystem production and consumption. In: Wolanski E. and D.S. McLusky (eds.), *Treatise on Estuarine and Coastal Science* 7:83−118. Waltham: Academic Press.

Borges, A.V., Delille, B. and M. Frankignoulle 2005. Budgeting sinks and sources of CO2 in the coastal ocean: Diversity of Ecosystem counts. *Geophysical research letters* 32(14).

Cloern, J.E., Foster, S.Q. and A.E. Kleckner. 2014. Phytoplankton primary production in the world's estuarine-coastal ecosystems. *Biogeosciences* 11(9):2477-2501.

Cai, W.J. 2011. Estuarine and coastal ocean carbon paradox: CO2 sinks or sites of terrestrial carbon incineration? *Annu. Rev. Mar. Sci.* 3:123–145.

Crosswell, J.R., M.S. Wetz, B. Hales, and H.W. Paerl. 2012. Air–water CO_2 fluxes in the microtidal Neuse River Estuary, North Carolina. *Journal of Geophysical Research* 117:C08017.

Raymond, P.A., and J.E. Bauer. 2001. Use of 14 C and 13 C natural abundances for evaluating riverine, estuarine, and coastal DOC and POC sources and cycling: a review and synthesis. *Organic Geochemistry*, 32(4), 469-485

Daniel A. Lemley, Janine B. Adams, in Encyclopedia of Ecology (Second Edition), 2019

Reece, K.S. 2015. Monitoring for HAB species in VA waters of Chesapeake Bay during 2015: emerging HAB species in Chesapeake Bay. Annual report submitted to Virginia Department of Health (#VIMSHAB617FY16), Richmond, Va

Reese, unpublished Data citation.

Effects of pH and Temperature on the Growth, Development, and Metabolic Rate of the Pediveliger Larvae of the Eastern Oyster, *Crassostrea virginica*

Magaleate Kostelnik
University of Tampa

Mentors: Dr. Emily Rivest & Annie Schatz

2 August 2019

<u>Synopsis</u>

Temperature and pH had a significant effect on the growth and development of *Crassostrea virginica.* The effects of pH and temperature changed during the growth of the larvae, but an overall trend of development and growth decreased with decreased pH.

<u>Abstract</u>

This study aims to understand how pH and temperature effects the growth, development, and metabolic rates of the pediveliger of *Crassostrea virginica.* Embryos were grown in 4 treatments with 3 replicates: 29°C and pH 7.8 (temperature stressor); 29°C and pH 7.2 (multi stressor); 25°C and pH 7.2 (pH stressor); and 25°C and pH 7.8 (control). Growth was analyzed by measuring the area and longest length of at least 50 live larvae from each replicate at 24 hours, 6 days, and 11 days post fertilization. This was measured in ImageJ and the developmental stage of each those were larvae were recorded to analyzed how development changed over time in each treatment. Larvae that survived up to the pediveliger stage was used to perform respirometry at 20 days post fertilization to get oxygen consumption. The effects of pH and temperature

changed between additive and interactive during the growth of larvae. Overall, the development and growth of the larvae at 24 hours and 6 days decreased with decreased pH, while day 11 growth showed no significant effects. Not enough data was collected to suggest any significance effects of pH or temperature on the oxygen consumption of pediveligers. The data suggested pH may counter the effects of growth and development that higher temperatures promote.

Introduction

As atmospheric carbon dioxide (CO_2) concentrations rise due to increased combustion of fossil fuels, the consequences of global warming and ocean acidification are research topics of high priority. Some of the anthropogenic CO_2 is absorbed by the ocean and causes a change in the carbonate chemistry of the water. CO_2 combines with water to form carbonic acid (H_2CO_3), which dissociates into protons and bicarbonate ions. Bicarbonate dissociates again into carbonate ions and more protons. Carbonate ions combine with calcium ions to form calcium carbonate which is used to build calcium carbonate shells that many invertebrates rely on. If more protons are present due an increase in CO_2 absorption by the ocean, protons begin to compete with calcium to react with the available carbonate ions. The result is lower rates of calcium carbonate formation and higher rates of formation of bicarbonate, which is not a usable building block for shell formation (Solan and Whiteley, 2016). The increase in proton abundance also decreases the pH of the ocean, causing it to be more acidic. The acidity induces stress responses that disturb the metabolism of calcifiers, therefore disrupting the allocation of energy into processes like growth. If energy is getting allocated to maintain homeostasis as a stress response, then energy and materials are not getting used to build proteins to grow tissue and gain mass. Therefore, increased CO_2 has not only been shown to decrease the ability for an organism to make shells, but also decrease total protein of the organism (Pörtner, 2008).

The eastern oyster, *Crassostrea virginica*, is an ideal species for studying the effects of ocean acidification due to their importance as filter feeders that improve water quality, habitat builders, storm protectors, and significance in the seafood industry. *C. virginica* provides 19.7 million US dollars in revenue to Virginia while also providing hundreds of jobs to Virginia residents (Murry and Hudson, 2013). The dependence of Virginia's oyster aquaculture industry on the local water quality leads to sense of urgency to understand how potential changes in water conditions may affect oysters. The larvae of oysters are typically more sensitive to water conditions, so an emphasis should be focused on their early life stages (Kennedy et al., 1996). Oysters undergo multiple early developmental stages starting from the fertilized egg. *C. virginica* then develops into a trochophore after about 12 hours and then into the D-stage around 24 hours post-fertilization. The last developmental stage before settlement is the pediveliger, which takes around 2 weeks to reach and features a characteristic eyespot (Kennedy et al., 1996). As larvae, oysters can be more susceptible to ocean acidification than their adult counterparts. Increased partial pressure of carbon dioxide (pCO_2) can affect multiple stages of development, starting at fertilization and affecting survival of D-stage larvae (Parker et al., 2010). Veliger larvae of *C. virginica* raised in higher pCO_2 conditions had an overall smaller shell area when compared to larvae raised in preindustrial pCO_2 conditions. The low pH seawater provokes a stress response in the organism which is identified by the decrease in oyster shell thickness and is associated with overall declined health (Miller et al., 2009). Juvenile oyster responded with higher metabolic rates with elevated pCO_2. Older adult oysters also responded with increased metabolism when exposed to elevated pCO_2 (Parker et. al, 2012). The stress that the oysters go through are thought to be the reason why oxygen consumption raises and so does metabolism. These previous studies of effects of pCO_2 on young oysters indicate that acidity affects the entire life cycle of oysters, suggesting an arising cascade of detrimental effects as oysters grow.

Besides the decrease in ocean pH, other oceanic conditions are also being indirectly affected by rising atmospheric pCO_2. As a greenhouse gas, CO_2 adds to the warming of the atmosphere and concurrently the warming of the ocean. For ectothermic organisms, like oysters, temperature can influence the functionality of macromolecules. Higher temperatures tend to increase the rate of chemical reactions and resulting physiological processes up to a threshold temperature. Once over the threshold, proteins begin to degrade, and energy gets allocated away from processes like growth and reproduction. Instead, the energy goes into maintaining homoeostasis and repairing any further damage ensuing from rising temperatures (Solan and Whiteley, 2016). Small increases in temperature can lead to increased oxygen consumption and metabolism for *Crassostrea gigas* (Bougrier et al., 1995). This would support faster growth as long as sufficient food is available to meet energy requirements. Generally, as temperatures increased, time spent as larvae decreased for *C. virginica* (Kennedy et al., 2009). In order to accurately predict how organisms are affected by future conditions, experiments must be comprehensive and include the combined effects of like temperature and pCO_2 (Pörtner, 2008). When these parameters are combined, high temperatures and high pCO_2 increase the metabolism of adult *C. gigas* and lower their temperature tolerance (Lanning et al., 2010). Therefore, investigating the effects of temperature and pH on the larvae of *C. virginica* could be crucial to help understand potential effects of ocean acidification on the oyster industry.

This study aims to find how pH and temperature affect oyster larvae by measuring their development, growth, and metabolic rate. In addition, the study intends to understand if pH and temperature affect the time that larvae eye up and if the aerobic metabolism differ between larvae that eye up earlier than those that eye up later.

Methods

Tank Set Up

Acrylic tanks encased in a water jacket were filled with 1-um filtered sea water and brought to the following treatment conditions: 29°C and pH 7.8 (temperature stressor treatment); 29°C and pH 7.2 (multi stressor treatment); 25°C and pH 7.2 (pH stressor); and 25°C and pH 7.8 (control). Each treatment had 3 replicate tanks, resulting in a total of 12 tanks being used. Temperature of the larval culture was controlled using water jackets where water with specified temperatures circulated the larval tanks. Salinity, pH, and temperature conditions of the larval cultures were monitored and maintained every hour via a probe located inside each larval tank that is connected and communicates with a computer-based control system. To maintain desired pH levels for each treatment, the control system read current pH levels and dosed pure carbon dioxide gas to bring down pH and dosed CO_2 free air to raise pH through air stones accordingly.

Fertilization

Brood stock (line LILY15) was used from VIMS Aquaculture Genetics and Breeding Technology Center (ABC). Fertilization occurred at ABC, where 80 million eggs from 25 female oysters were artificially fertilized using sperm from 10 male oysters. Oysters were strip spawned to collect sperm and eggs. Eggs were rinsed before counting, sperm was added to fertilize eggs, and then embryos were rinsed through a 20-micron sieve. Eggs were fertilized at 2 pm, and at two hours post fertilization, embryos were separated evenly into jars assigned with each treatment and replicate number. Each jar was filled with the assigned water at each pH for each treatment and had approximately 3 million embryos. The jars were immediately transported and emptied into their assigned treatment tank.

Husbandry

100% water changes were performed three days per week for two weeks. Water changes were done using siphons that allowed water to flow through a sieve with mesh starting at 20 micrometers. The size of the mesh increased by 10 micrometers with each water change day, depending on monitored growth, in order to separate living larvae from dead larvae or detritus, which would flow through and be discarded. Filtered larvae were then poured into designated beakers using treatment water for immediate sampling. Once larvae were removed, the aquaria were cleaned using 0.2% bleach and 5% solution of thiosulfate. Tanks were then filled with 1um-filtered seawater, and the seawater was adjusted to treatment levels.

Sampling of larvae in the beakers was done by stirring beakers and placing 3-5 aliquots of 20-50 microliters onto a microscope slide. The larvae were counted in each drop until a coefficient of variance less than or equal to 10% was reached. Using the volume of aliquots for counts and volume of concentration of the larvae culture, calculations were made to estimate how many live larvae were in the tank. During counts, pictures of at least 50 live larvae where taken using glasX software via Leica MC170 HD camera for analysis using ImageJ.

Once estimates of live larvae were done, the larvae were returned to associated treatments. During the drops, water samples from each tank were collected for spectrophotometric pH. Two TA samples were collected from mixing tank that supplies all the water to the larvae tanks every single drop day and put into freezer for later analysis. One sample was taken from the first batch of mixing tank and the second was taken after the tanks were filled up. After larvae were returned to the assigned tanks, they were fed with *Isochrysis* algae according to feeding volumes from ABC.

Image Analysis

Photos of larvae from 24 hours post fertilization, 6- and 11-days post fertilization were analyzed for area and longest length through ImageJ. For calibration of larval images, a photo was taken of a micrometer using the same scope settings as were used when imaging the larvae each day. Using ImageJ, each photo was converted to a 16-bit type image, and the threshold was adjusted so that each larva was highlighted. The highlighted particles were analyzed to estimate area and maximum length of each larva. In addition to each measurement, the number of eggs, trochophores, veligers and pediveliger larvae in each photo were counted.

Respirometry

On 20 days post fertilization, pediveliger larvae from two replicate tanks of the multi-stressor treatment and one replicate tank of the pH treatment were loaded into jars filled with assigned treatment water. The jars were left in the treatment tanks to maintain temperatures and to starve larvae for 24 hours in order to prevent digestion from introduction bias into the oxygen consumption data. After 24 hours, larvae were collected using an 80-micrometer sieve and put in 5-10 ml of treatment water in assigned 50 mL tubes. Three counts of 20-50 uL aliquots from each tube were used for larval density estimates. One hundred larvae were taken from each tube and transferred to microcentrifuge tubes. The tubes were placed on ice for 3 minutes for larvae to settle to bottom. Water was then removed from tubes via micropipette and replaced with 0.2um-filtered treatment seawater. Transfer pipettes were used to move larvae and water from microcentrifuge tubes to glass Biological Oxygen Demand (BOD) vials. The vials were then filled the rest of the way with the 0.2-um filtered water. Vials were set on ice for another 3 minutes before capping to ensure no larvae were lost and no air bubbles were inside. Vials were incubated at assigned treatment temperatures for 2-3 hours. Then, individual vials were set on ice for 3 minutes before 500 uL water was immediately extracted through a medical grade gas-tight syringe and injected into a glass, water-jacketed respirometry cell. A Presens Microx4 meter was used with a needle-type oxygen microsensor (NTH-PSt7) to measure the dissolved oxygen concentration of each sample. Glass vials were also loaded with filtered seawater but no larvae to serve as blanks. Before reading samples, the oxygen microsensor was calibrated at 25 ºC first with a 0% dissolved oxygen solution (0.1 grams of sodium sulfate in 10 mL water), followed by

100% dissolved oxygen concentration of filtered seawater. Following respirometry of each vial, eyed larvae inside the vial were counted.

Statistical Analysis

Analysis was done in R software. Tests of normality and homogeneity of variance were done for each data set. The data was analyzed as two-way ANOVAs with pH and temperature as fixed factors and tank as a random factor.

Results

Development

After 24 hours, the high temperature treatment had the highest percent of D-stage larvae at 99% when compared to all other treatments in the same day. The low pH treatment had the fewest percent of D-stage larvae at 80% when compared to other treatments in the same day (Figure 1). Temperature and pH had a significant additive effect on percent D-stage, where the variables affected the stage independently (Two-way ANOVA, Table 1).

After 6 days post fertilization, only D-stage and veliger larvae were found in the samples. The high temperature treatment had the highest percent of veliger larvae with a total of 83%, when compared to the other treatments. The multiple stressor treatment had the lowest percent of veligers at 70% (Figure 2). Temperature and pH at day 6 had a significant interactive effect on percent veligers, which suggests that the effect of temperature varied depending on the pH level (Two-way ANOVA, Table 1).

On 11 days post fertilization, only temperature had a significant effect on percent veligers (Two-way ANOVA, Table 1). Temperature and the multi-stressor treatments both had the highest percentage of veligers, with both at 96% (Figure 3).

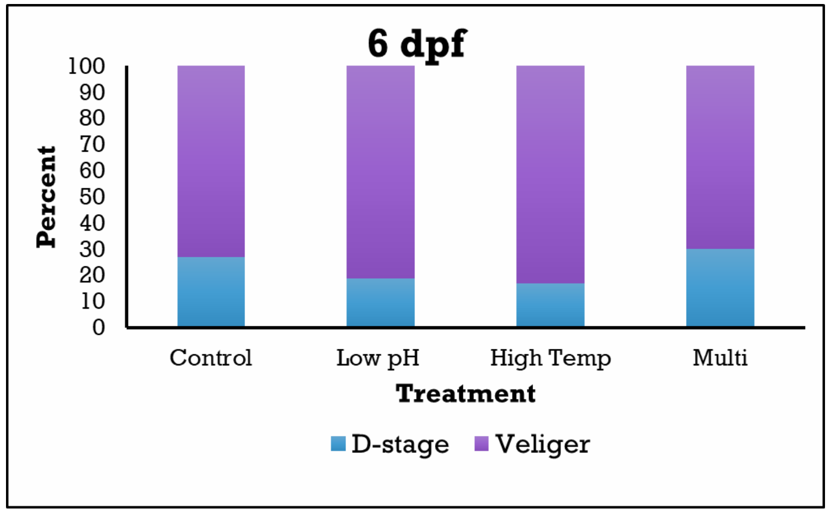

Figure 1: Percentage of eggs, trochophores, and D-stage larvae in each treatment after 24 hours post fertilization. Statistical comparison of pH and temperature by D-stage two-way ANOVA using type III sum of squares.

Table 1: Statistical comparison of pH and temperature by area, length, and larvae stage using type III sum of squares. Chi-squared, degrees of freedom, and p-values (p) were reported for these tests. Values that were significant are bolded.

DPF	*Response variable*	*Fixed Factors*	X^2	*df*	p
24 hours	Area	pH	399.52	1	**< 0.001**
		Temperature	171.16	1	**< 0.001**
		pH & Temp	0.3264	1	0.568
	Length	pH	150.2753	1	**< 0.001**
		Temperature	47.6736	1	**< 0.001**
		pH & Temp	3.6883	1	0.0548.
	% D-stage	pH	34.530	1	**< 0.001**
		Temperature	79.409	1	**< 0.001**
		pH & Temp	1.4243	1	0.2327
6	Area	pH	0.0584	1	0.8090
		Temperature	31.1839	1	**< 0.001**
		pH & Temp	8.8659	1	**0.002905**
	Length	pH	0.0865	1	0.7687
		Temperature	30.0502	1	**< 0.001**
		pH & Temp	9.3202	1	**0.002266**
	% Veliger	pH	2.1006	1	0.1472
		Temperature	2.8063	1	0.09389
		pH & Temp	6.5066	1	**0.01075**
11	Area	pH	0.0005	1	0.9822
		Temperature	1.6733	1	0.1958
		pH & Temp	0.0179	1	0.8937
	Length	pH	0.0134	1	0.9078
		Temperature	2.0339	1	0.1538
		pH & Temp	0.0708	1	0.7902
	% Veliger	pH	0.5291	1	0.4669724
		Temperature	11.3593	1	**< 0.001**
		pH & Temp	0.3696	1	0.54324

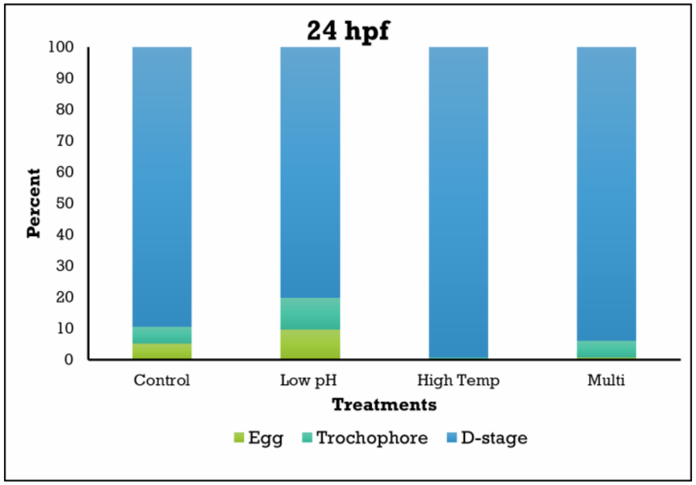

Figure 2: Percentage of D-stage and veliger larvae in each treatment at 6 days poster fertilization. Statistical comparison of pH and temperature by veliger two-way ANOVA using type III sum of squares.

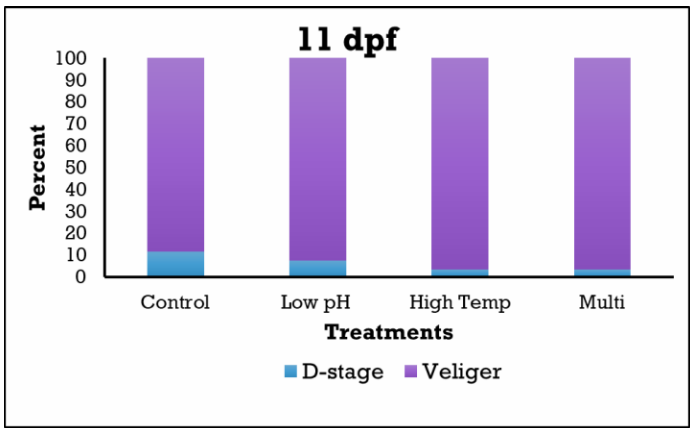

Figure 3: Percentage of D-stage and veliger larvae in each treatment at 11 days poster fertilization. Statistical comparison of pH and temperature by veliger two-way ANOVA using type III sum of squares.

Size

At 24 hours, the high temperature treatment had the largest average area and length at 3249 um^2 and 69.00 um, respectively, when compared to the other treatments (Figures 4, 5). Larval area at 24 hours showed significant additive effects of temperature and pH, such that the independent variables acted independently of each other (Two-way ANOVA, Table 1). The low pH treatment at ambient temperatures had the lowest average area and length at 2710 um^2 and 63.69 um larvae when compared to other treatments (Figure 4, Figure 5). Temperature and pH had significantly additive effects on length (Two-way ANOVA, Table 1). The effect of temperature on length at a lower pH is greater than the effect of temperature at a higher pH.

The size of larvae at 6 days post-fertilization showed significant interactive effects of pH and temperature on area and length (Two-way ANOVA, Table 1). The effect of temperature on area and length was greater at a higher pH than the effect of temperature on area and length at a lower pH. Again, the high temperature treatment had the largest area and lengths when compared to the other treatments at day 6 with an average area of 8063 um^2 and an average length of 104.6 um

(Figure 6, Figure 7). The pH treatment had the smallest area of all the treatments at day 6 with an area of 5990 um^2 (Figure 6). The area and length at day 11 suggested no significant effects induced on them by temperature or pH (Two-way ANOVA, Table 1).

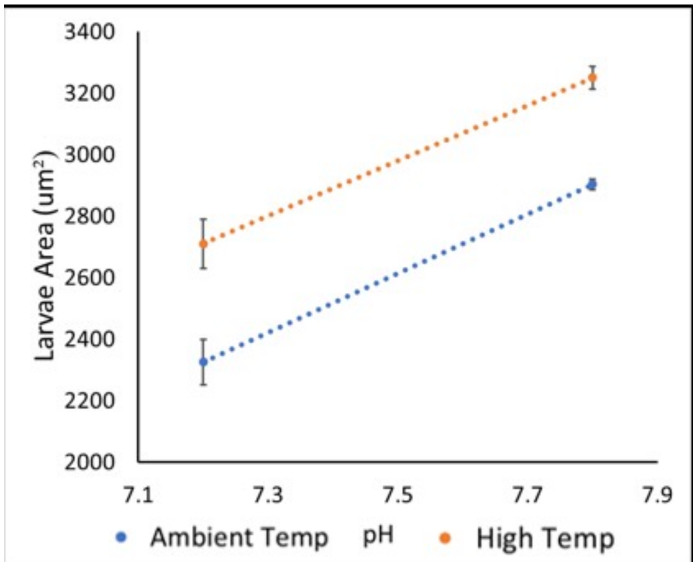

Figure 4: Comparing larvae area (um^2) by pH at 24 hours post fertilization. Blue line refers to the ambient temperature treatments (25°C) and the orange line refers to the high temperature treatments (29°C). Statistical comparison of pH and temperature by area with a two-way ANOVA using type III sum of squares. ANOVA suggested significant additive effects of temperature and pH on area.

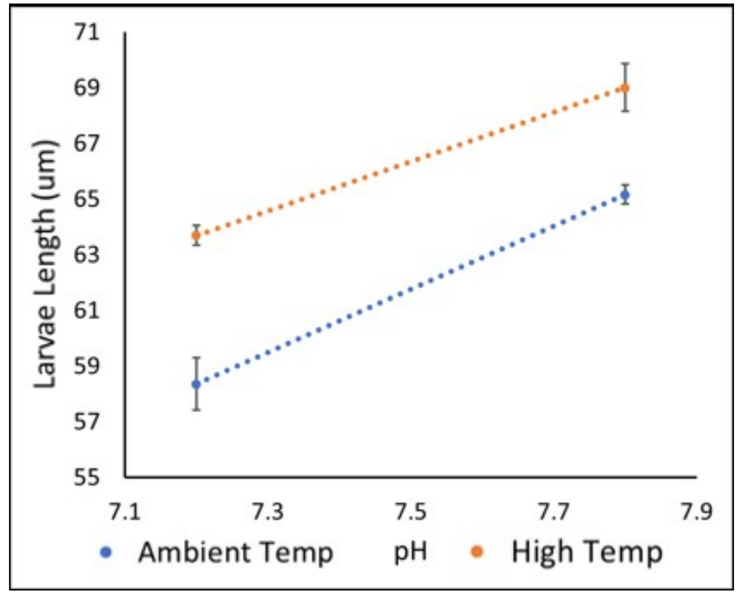

Figure 5: Comparing larvae length (um) by pH at 24 hours post fertilization. Blue line refers to the ambient temperature treatments (25°C) and the orange line refers to the high temperature treatments (29°C). Statistical comparison of pH and temperature by area with a two-way ANOVA using type III sum of squares. ANOVA suggested significant interactive effects of temperature and pH on length.

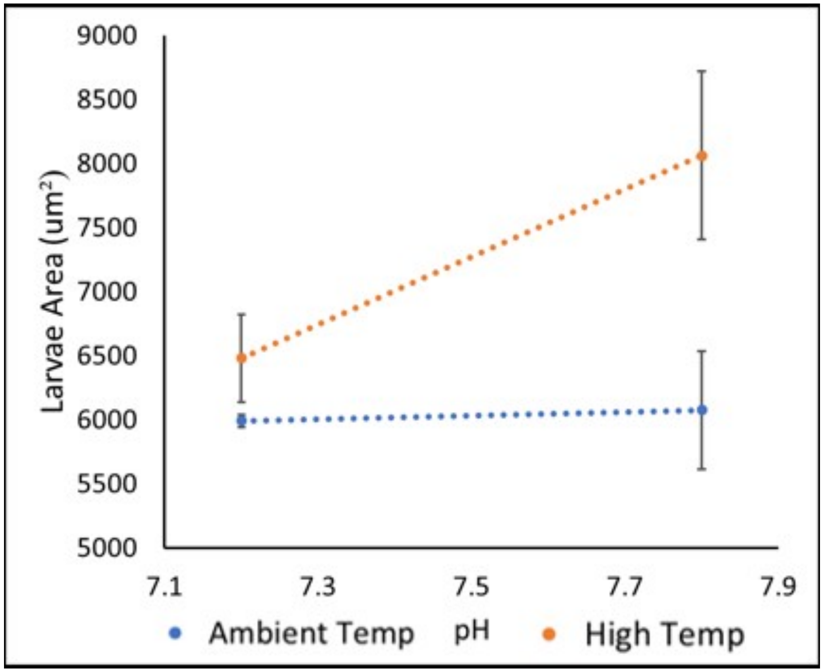

Figure 6: Comparing larvae area (um^2) by pH at 6 days post fertilization. Blue line refers to the ambient temperature treatments (25°C) and the orange line refers to the high temperature treatments (29°C). Error bars refer to standard deviations of the averages. Statistical comparison of pH and temperature by area with a two-way ANOVA using type III sum of squares. ANOVA suggested significant interactive effects of temperature and pH on area.

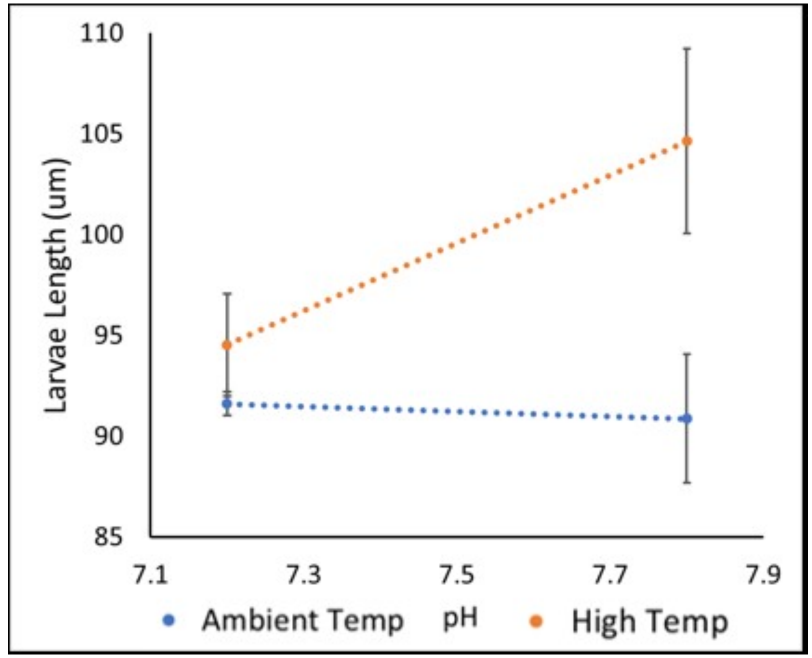

Figure 7: Comparing larvae length (um) by pH at 6 days post fertilization. Blue line refers to the ambient temperature treatments (25°C) and the orange line refers to the high temperature treatments (29°C). Error bars refer to standard deviations of the averages. Statistical comparison of pH and temperature by area with a two-way ANOVA using type III sum of squares. ANOVA suggested significant interactive effects of temperature and pH on length.

Metabolism

Oxygen consumption was standardized by size and the multi-stressor had an average of 1.563 pmol larva^{-1} hour^{-1} um^{-1} (Figure 8). This was less than the oxygen consumption rate of larvae in the pH treatment, which had 1.930 pmol larva^{-1} hour^{-1} um^{-1} (Figure 8). Due to lack of sufficient replication, no statistical analysis was run to detect significant effects imposed by temperature or pH.

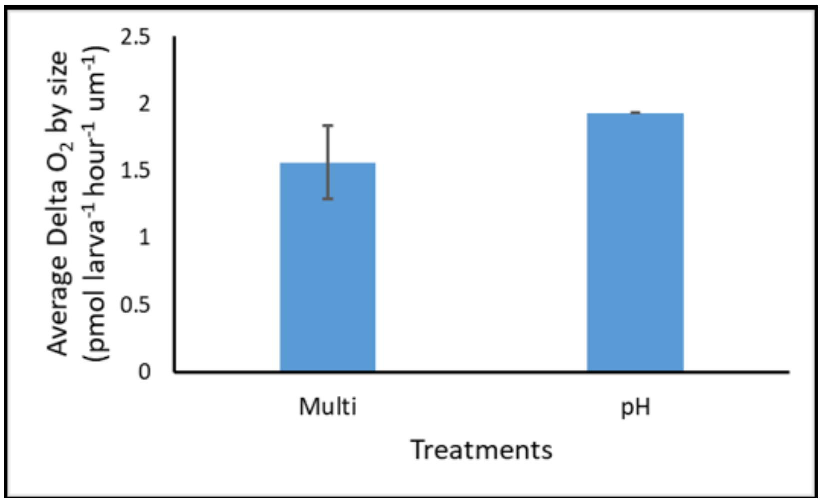

Figure 8: Average delta of oxygen standardized by size by treatments. Only multi-stressor and low pH treatments were tested, so no statistics comparisons were performed. Error bars refer to standard deviations of the averages.

Discussion

As increased CO_2 emissions provoke the threat of global warming, the expectation of raising ocean temperatures and acidity will become a reality, where organisms will have either have to adapt or suffer. From the results in this experiment, the larvae that grew in these OA conditions display overall slower development and growth. This was shown in 24 hours and in 6 dpf, which development, area, and length decreased as pH decreased (Figures 1, 2, 4, 5, 6, 7). In another study, *C. virginica* also had slower growth suggested by a decrease in area when put in more acidic conditions, but this study focused on changing the pCO_2 and did not look at length (Miller et al., 2009). The results of my study suggest that more acidic seawater counteracts growth, counteracting positive effects that higher temperatures would have had on the larvae. Although, not all effects were interactive, and the effects of pH and temperature on their development and growth often changed during the growth period of the larvae. Parker et al. (2010) found overall interactive effects of temperature and pH on development on D-stage larvae in *Saccostrea glomerate* and *Crassostrea gigas*, but this interaction also included fertilization type and species. For my experiment, temperature and pH showed additive effects on both development and size during the first 24 hours post fertilization, then switched to being interactive in later days. There is perhaps a process where the larvae are able to withstand OA conditions without significant effects on their need for growth within the first 24 hours. 24-hour larvae appeared to only be affected significantly if faced with conditions independently. They were able to take advantage of warmer waters or in low pH levels, appeared to suffer from struggling to build shells. After 24 hours, larvae weren't able to withstand OA without it significantly affecting their growth.

Pörtner and Farrell (2008) discuss and provide similar data to suggest that induced OA conditions on marine exothermic organism narrows their thermal tolerance scale for metabolism and growth. My experiment supports this theory in *Crassostrea virginica*, as shown by larvae grown in the multi-stressor, who had a smaller length even if grown in warmer conditions (Figure 5, 7). Since this study was not able to grow enough pediveligers to test metabolism in all four treatments and find any significant correlations, these data can only be used for preliminary interpretation. The results suggest that larvae in the multi-stressor treatment were under less stress because they consumed less oxygen than the larvae grown in low pH (Figure 8). If the study assumes that pH and temperature had interactive effects on their oxygen consumption like they had in their growth and development, then larvae in the multi-stressor treatment should have had a higher oxygen consumption than pH due to warmer temperatures increasing the rates of physiological processes. Bourgrier et al. (1995) found this in *Crassostrea gigas*, where oxygen consumption increased as temperature increased. Overall, the metabolism data did not support the hypothesis that highly stressed organisms or organisms at a warmer temperature will have higher oxygen consumption rates.

This study describes how OA affects oyster larvae, and it is an important step in understanding how future generations of oysters are going to be affected by rising CO_2 emissions. As important species in the seafood industry and as habitat builders, a decline in oyster growth could result in less survival into adulthood, which would reduce the wild populations. As many hatcheries rely on their local water quality, OA could increase the time it takes to grow oysters and limit hatchery productivity. In addition, future research needs to be done to discover how metabolism will be affected since this study could only get limited insight into what could be happening to the larvae before they settle. Even though these data help understand the effects of OA on Eastern oysters, physiological effects are so extensive that it requires many more studies like this one to investigate and understand the full consequences of OA so that we may find ways to counter them.

Acknowledgements

Thank you to Dr. Emily Rivest for mentoring and guiding me through the entire research process. Thank you to Annie Schatz as serving as a graduate student mentor. Thanks to Anthony Himes, Megan Considine, Hannah Bradley and Grace Vaughn for their contributions in completing the research. Thanks to Jenny Dreyer and Katherine Longmire for coordinating the REU program at VIMS. Program funding for the VIMS Research Experience for Undergraduates was made available through a grant awarded from the National Science Foundation (grant # NSF OCE 1659656) to Drs. Linda Schaffner and Rochelle Seitz. Thank you to the VIMS Aquaculture Genetics and Breeding Technology Center for helping us during the fertilization process.

Literature Cited

Bougrier, S., Geairon, P., Deslous-Paoli, J.M., Bacher, C., Jonquieres, G., 1995. Allometric relationships and effects of temperature on clearance and oxygen consumption rates of *Crassostrea gigas* (Thunberg). Aquaculture, 132, 143-154.

Kennedy, V.S., Newell, R.I.E., Eble, A. F., 1996. "The Eastern Oyster: Crassostrea virginica". Maryland Sea Grant College

Lannig, G., Eilers, S., Pörtner, H.O., Sokolova, I.M., Bock, C., 2010. Impact of ocean acidification on energy metabolism of oyster, *Crassostrea gigas*—Changes in metabolic pathways and thermal responses. Marine Drugs, 8(8), 2318–2339.

Miller, A.W., Reynolds, A.C., Sobrino, C., Riedel, G.F., 2009. Shellfish face uncertain future in high CO2 world: Influence of acidification on oyster larvae Calcification and growth in estuaries. PLoS ONE. 4(5), 1-8.

Murray, T.M. and Hudson, K. "Economic Activity Associated with Shellfish Aquaculture in Virginia – 2012" Virginia Institute of Marine Science, 2013.

Parker, L., Ross, P.M., O'Conner, W.A., Borysko, L., Raftos, D.A., Pörtner, H.O., 2011. Adult exposure influences offspring response to ocean acidification in oysters. Global Change Biology, 18(1) 82–92.

Parker, Laura M., Ross, P.M., O'Connor, W. A., 2010. Comparing the effect of elevated pCO2 and temperature on the fertilization and early development of two species of oysters. Marine Biology, 157(11), 2435–2452.

Pörtner, H.O., 2008. Ecosystem effects of ocean acidification in times of ocean warming: a physiologist's view. Marine Ecology Progress Series, 373, 203–217.

Pörtner, H.O., Farrell, A.P., 2008. Physiology and climate change. Science, 322, 690-692.

Solan, Martin, and Nia M. Whiteley. "Stressors in the Marine Environment". Oxford Univ Press, 2016.

Drivers of herbivory in salt marshes

Anna Bi Ledwin
William & Mary

Mentors: Serina Wittyngham and David Johnson
2 August 2019

Synopsis

The sediment in short-form *Spartina* is most conducive to constructing burrows indicating that the inland movement of the *Sesarma* herbivory front is influenced at least in part by burrow formation potential. Traits beyond nitrogen and protein are likely influencing *Sesarma* consumption preference, including physical factors such as plant height. Predation is omnipresent in creek heads, making predation pressure an unlikely factor in influencing the *Sesarma* herbivory front.

Abstract

Salt marshes and their foundation species, *Spartina alterniflora*, are currently threatened by runaway herbivory and rapid sea level rise. This has lead to a novel geomorphology at the head of creeks along the Atlantic Coast, in which a denuded zone—littered with crab burrows and lacking vegetation—divides the creek from the high marsh, short-form *Spartina*. The denuded zone moves inland overtime, driven by *Sesarma reticulatum* herbivory, killing more *Spartina*. On the Eastern Shore of Virginia, we see a similar creek head structure, but with revegetated tall-form *Spartina* growing in between the denuded zone and the creek. The denuded zone in these areas continues to move inland towards the high marsh, while the

tall-form *Spartina* remains ungrazed. This revegetation allows the marsh to continue vertically accreting, thus keeping pace with sea level rise. We conducted experiments related to plant traits and palatability, predation pressure, and sediment composition to elucidate the drivers of the *Sesarma* herbivory front. We found that *Sesarma* prefer tall-form *Spartina* compared to short-form *Spartina*, and that predation is present in all locations of the creek head. Sediment is most conducive to constructing burrows in the short-form *Spartina* zone, indicating that the *Sesarma* herbivory front is influenced at least in part by burrow formation. Further research is needed to conclude the drivers of the *Sesarma* herbivory front.

Introduction

Salt marshes sequester carbon, provide nursery habitat, and mitigate erosion (Barbier et al. 2011; Davy et al. 2009; Mitsch & Gosselink 2008) but are currently threatened by rapid sea level rise and runaway herbivory, resulting in marsh productivity decline and death (Holdredge 2009; Hughes et al. 2009; Best et. al 2018). *Spartina alterniflora* (henceforth *Spartina*) serves as a foundation species in East Coast marshes and drives marsh morphology through organic matter accumulation, sediment binding, and vertical accretion (Morris et al. 2002; Hughes et al. 2009; Vu et al. 2017). Runaway herbivory induces rapid creek growth through *Spartina* consumption, which reduces the marsh's ability to vertically accrete—a vital process that allows the marsh platform to remain in equilibrium with sea level rise (Hughes et al. 2009). The effects of these threats are emerging through altered geomorphology at creek heads in the southeastern United States. Adjacent to creek heads, there is a semi-circular denuded zone—littered with crab burrows and lacking vegetation—which then transitions steeply to the high marsh (Hughes et al. 2009; Vu et al. 2017). These denuded zones facilitate creek expansion (Hughes et al. 2009).

The purple marsh crab, *Sesarma reticulatum* (henceforth *Sesarma*), greatly contributes to creek head growth, for its herbivory and burrowing can decimate *Spartina* populations and degrade sediment stability (Vu et al. 2017). Similar *Sesarma*-induced denuded zones occur on the Eastern Shore of Virginia; however, there is one stark difference between Virginian and southeastern U.S. marshes. Previous studies reported that following herbivory, the denuded zone remains unvegetated and becomes a mudflat, thus extending the creek head (Hughes et al. 2009; Vu et al. 2017). Moreover, the denuded zone progresses inland towards the short-form *Spartina*, further contributing to creek head expansion. On the Eastern Shore, we see similar inland movement of the denuded zone, but no inland movement of the creek head itself. This is due to a patch of tall-form *Spartina* that revegetates between the denuded zone and the creek head. The revegetated *Spartina* remains ungrazed by *Sesarma*, thus allowing vertical accretion to continue, preventing erosion and creek head extension.

Our objective was to determine what factors are driving the Eastern Shore *Sesarma* front—the denuded zone induced by herbivory—inland. We hypothesize that plant traits are primarily responsible. Alternatively, predation and sediment composition may also play a role, as they are relevant to *Sesarma*'s behavior (Bertness et al. 2009; Vu et al. 2018). Our experiments examined how these factors may influence *Sesarma* herbivory and thus distribution.

Plants are used by herbivores as a source of energy and nutrients, so they've evolved to alter their traits in response to damage and stress (Karban & Baldwin 1997; McArthur et al. 2014). Thus, the analysis of these traits can inform us about *Spartina*'s response to herbivory. We are specifically interested in the influence of nitrogen and protein content on the forage quality of *Spartina*. *Sesarma* have limited time to consume foods that meet their metabolic demands, so we expect that they will seek *Spartina* with high protein and nitrogen content (Pyke et al. 1977; Abrams 1984). We hypothesize that following herbivory by *Sesarma*, the revegetated tall-form *Spartina* is altering its traits, making it less palatable to *Sesarma*, thus driving herbivory inland.

Predation pressure and/or sediment composition may also affect *Sesarma* distribution. *Sesarma* predators include intertidal fish, birds, and carnivorous crabs (Holderedge 2009; Vu et al. 2018). We expect the survival rate to be higher in the short-form *Spartina* and denuded zone, which are furthest from the creek, than in the tall-form *Spartina*, which is closer to the creek, because the tall-form *Spartina* is inundated during high tide, allowing predators access to *Sesarma*. Greater predation closer to the creek may deter *Sesarma* from feeding on the tall-form *Spartina*, thus driving the *Sesarma* herbivory front inland.

Grain size and organic matter influence the stability of *Sesarma* burrows, which defend *Sesarma* against predation and desiccation (Bertness et al. 2009; Coverdale et al 2013). The creekhead has less belowground organic matter (Hughes et al. 2009) and is composed of finer sediment than the high marsh

(Christiansen et al. 1999), indicating that burrow formation potential may be lower in the tall-form *Spartina* and the denuded zone than the short-form *Spartina*, potentially facilitating the inland movement of the *Sesarma* front.

We are hypothesizing that plant trait alteration following herbivory, high predation pressure adjacent to the creek, or low burrow formation potential around the creek are driving the movement of *Sesarma* inland. If one or a combination of these hypotheses is correct, this would explain the revegetation of tall-form *Spartina* and thus its capacity to continue to accrete sediment. This direct response to herbivory may have an indirect, positive effect on marsh-wide protection against sea level rise: by growing and accreting sediment, tall-form *Spartina* halts creekhead movement inland and raises the marsh platform, preventing the drowning of the high marsh.

Methods

Feeding Assays and Plant Traits

We conducted feeding assays to test whether *Sesarma* displays feeding preference between *Spartina* collected from each zone. We collected sixty *Sesarma* and thirty stalks of both tall-form and short-form *Spartina*. Crab carapace widths were measured with calipers (mm), and then crabs were placed into *Rubbermaid* 2.9 cup tupperware containers, with two *Sesarma* per container. A 12 cm segment from both tall-form and short-form *Spartina* was cut (from the fourth leaf counting inward from the outermost living leaf on the stem), weighed, and placed into the containers. Seawater was provided to prevent *Sesarma* and plant desiccation, and was replaced once per day. An additional ten replicate controls containing only plant material and seawater assessed any changes in plant biomass caused by factors other than consumption. After 46 hours, the plant segments were blotted with a paper towel and reweighed. We corrected consumption values using the equation: $(M_i \times C_f / C_i) - M_f$, where M_i and M_f were the initial and final weight of tissue used in the feeding assay, and C_f and C_i were the average final and initial mass of the control plant tissue (Goodman & Hay 2012). Any replicates displaying negative consumption after correcting for controls were set to zero for statistical analyses. Tall-form and short-form *Spartina* were collected in the summer of 2018 for the analysis of total soluble protein and nitrogen content. Protein and nitrogen content were measured using a modified Bradford assay and the combustion method, respectively.

Predation Assays

Predation pressure around creek heads may be altering *Sesarma* behavior and driving them inland. To evaluate this hypothesis, twenty-seven *Sesarma* were collected and measured at Upshur Creek. Each *Sesarma* was tethered around their second and third walking legs using a slip knot loop made from 30 lb fishing line. The fishing line was attached to the carapace using cyanoacrylate glue and duct tape. Tethers were approximately 20cm long and were attached to a clear acrylic rod. Three *Sesarma* were placed per zone—tall-form *Spartina*, denuded zone, and short-form *Spartina*—at three different sites within Upshur Creek. Each crab was placed near a burrow to allow for protection against desiccation and predators. After approximately 24 hours crab presence or absence was assessed. We repeated this trial on three consecutive tides. For the third trial, 10 cameras were randomly deployed across zones at two creek heads to look for predators and examine crab behavior.

Bulk density, organic matter, and sediment strength

We used a Russian Peat Borer to take sediment cores around four creek heads in Upshur Creek, with two cores per zone (tall-form *Spartina*, denuded zone, and short-form *Spartina*). In addition, shear vane measured sediment strength in each zone.

Wet weights were taken and samples were dried at 60°C for 96 hours, then reweighed for dry weight. Samples were ground with a mortar and pestle and homogenized in a coffee grinder, then 5g of each sample was placed into a pre-weighed aluminum tin. Samples were burned in a muffle furnace at 550°C for 6 hours and weights were recorded.

Bulk density (g cm^{-3}) was calculated by dividing the dry oven weight by the fresh sample volume. We used the following equation to calculate organic matter content (Chambers et al. 2011; Roberston 2011).

$$\frac{(5g\ (\pm 0.1g)\ dry\ oven\ weight - muffle\ furnace\ weight)}{5g\ (\pm 0.1g)\ dry\ oven\ weight} \times 100$$

Shear vane data was converted to sediment strength in kilopascals (kPa) using the equation:

25.4 x 50.8mm size vane = value x 0.5

50.8 x 101.6mm size vane = value x 0.0625

Statistical Methods

Data analysis was completed in R (version 3.6.1, R Core Team 2018). All experiments were set up in a randomized block design, with creek head location as the blocking factor.

Response variables were tested for normality and homogeneity of variance; if these conditions were not met, variables were transformed using Box Cox transformations. Plant trait and consumption data were analyzed using ANCOVA, therefore the assumptions of linearity and equality of slopes were also tested. Predation data was analyzed with a binomial logistic regression. A two-way ANOVA was run on all sediment data to test independent and interactive effects of zone and creek head location. Post-hoc tests were used to distinguish significant differences.

Results

Feeding Assays and Plant Traits

Plant type had a significant effect on consumption, with tall-form *Spartina* consumed over three times more than short-form *Spartina* (Figure 1; $p=1.72 \times 10^{-5}$). Despite this, there was no significant difference in protein or nitrogen content between the two plant types (Figure 2a,b). Plant biomass, however, had a significant effect on both protein and nitrogen content ($p=0.0207$; $p=9.67 \times 10^{-5}$). Average crab size between both trials was 19.3 cm.

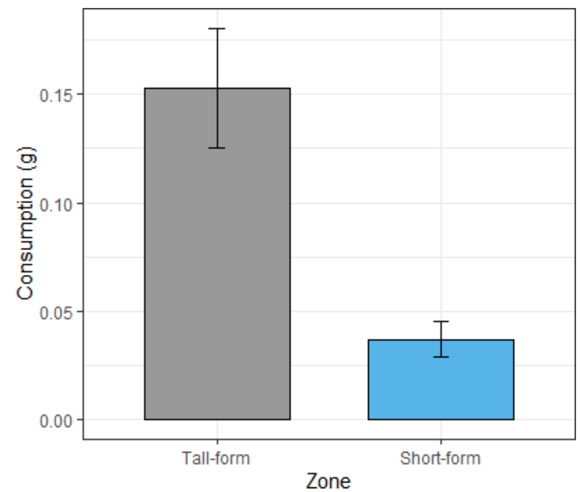

Figure 1: Mean Sesarma consumption of tall-form and short-form Spartina. Error bars represent standard error.

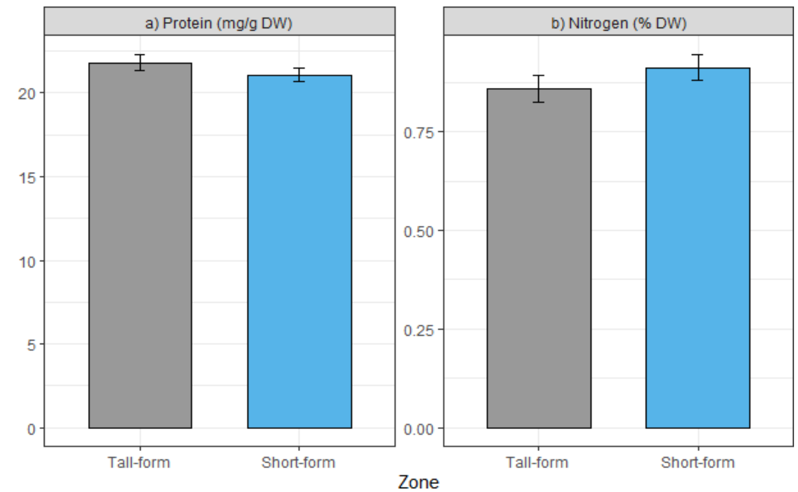

Figure 2: a) Average protein and b) percent nitrogen content for tall-form and short-form Spartina. Error bars represent standard error.

Predation Assays

Less than half of the deployed *Sesarma* survived after 24 hours. At many tethers, we saw strong indicators of predation including remaining carapaces, claws, or other parts. Zone (short-form *Spartina,* denuded zone, and tall-form *Spartina*) had no significant effect on *Sesarma* survival (Figure 3; p=0.1508). Average crab size between the three trials was 21.8cm.

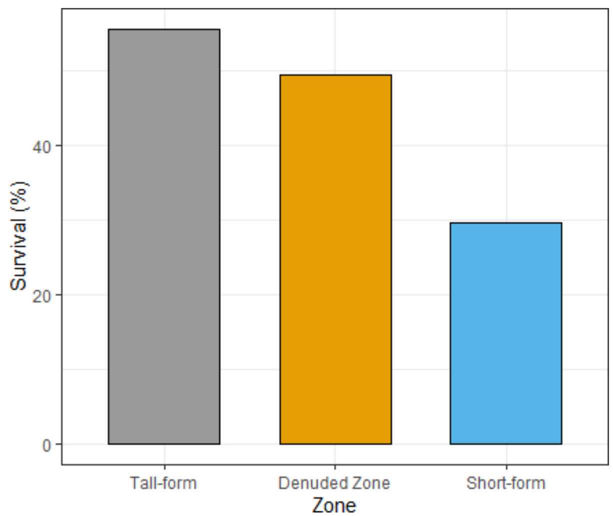

Figure 3: Percent survival of tethered Sesarma in each zone.

Bulk density, organic matter, and sediment strength

There was a significant effect of zone on organic matter content, with short-form *Spartina* sediments having the greatest organic matter content, and tall-form and denuded zone sediments having a similar, lower amount (Figure 4a; $p=2.72 \times 10^{-6}$). In addition, there was a marginally significant effect of zone on bulk density, with the lowest bulk density in short-form *Spartina* zone (Figure 4b; p=0.0916). Shear strength was also significantly different between zones, with the weakest sediments occurring in the tall-form *Spartina* and denuded zone, and the strongest sediment in the short-form *Spartina* zone (Figure 5; $p=3.39 \times 10^{-11}$).

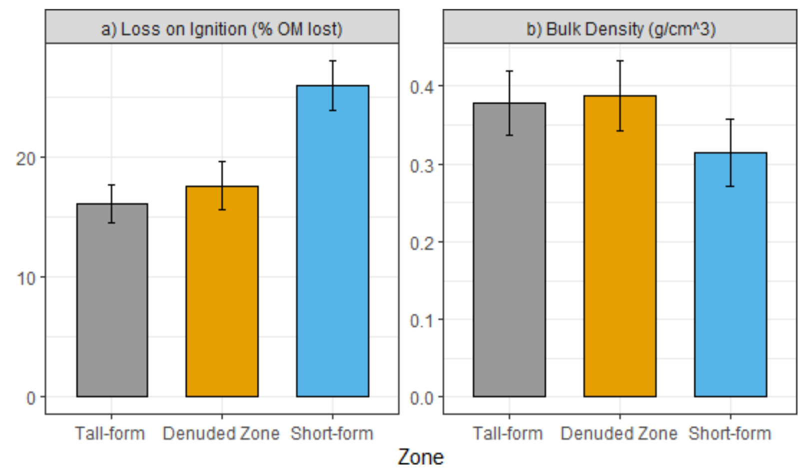

Figure 4: a) Loss on ignition and b) bulk density for each of the three zones. Error bars represent standard error.

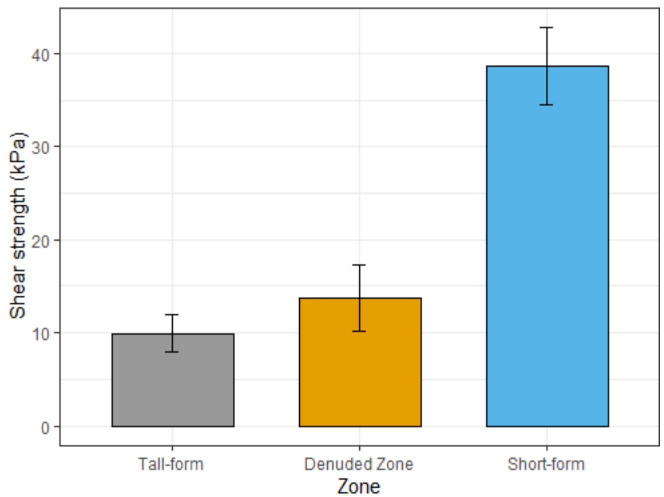

Figure 2: Shear strength measurements for each of the three zones. Error bars represent standard error.

Discussion

Feeding Assays and Plant Traits

Sesarma showed consumption preference of tall-form *Spartina* over short-form *Spartina*, despite there being no significant difference in protein and nitrogen content between them. This result opposes our hypothesis that tall-form *Spartina* had lower protein and nitrogen content than short-form *Spartina*. This indicates that there may be additional plant traits or behavioral responses influencing *Sesarma* preference.

Despite this observation, the altered geomorphology at creek heads remains the same: *Sesarma* are not consuming the revegetated tall-form *Spartina*, and continue to eat away at short-form *Spartina*, pushing the denuded zone inland. A possible explanation for this may be accessibility. In our experiment, we placed each segment of *Spartina* flat on the bottom of the tupperware containers, allowing equal access to each leaf. In nature, however, tall-form *Spartina* has a greater height than short-form *Spartina*. *Sesarma* consume *Spartina* leaves by shredding and consuming small strips off of each leaf, therefore, mechanistically, *Sesarma* may be unable shred and consume the tall-form *Spartina* leaves because they are inaccessible. To elucidate whether access was a confounding factor, natural conditions should be better simulated for future feeding experiments.

Predation Assay

There was greater survival in the tall-form *Spartina* than in the short-form *Spartina* and the denuded zone. This directly contradicts our hypothesis that there would be higher survival in the short-form *Spartina* due to its distance from the creek head. Video footage of tethers was unable to capture which predators were responsible for the consumption of *Sesarma*, so perhaps predation pressure is not increasing with the incoming tides as we had previously hypothesized. One potential predator in our footage was the red-jointed fiddler crab, *Uca minax*, who was seen consuming parts of a *Sesarma* that had previously perished. This finding introduces an additional avenue for future study. In addition, cameras with increased battery life or alternate settings should be deployed in the future to further elucidate which predators are responsible for the consumption of *Sesarma*.

A potential confounding factor in this experiment was the length of the 20 cm tethers. *Sesarma* construct burrow networks that range from 10-40cm belowground (Seiple and Salmon 1982; Bertness et al. 2009); the depth of these tunnels allow *Sesarma* to escape and hide from predators. While all *Sesarma* in our experiment were placed adjacent to burrows, videos indicate that many *Sesarma* could only hide within the first few centimeters of the burrows, potentially leaving them at greater risk for predation.

Bulk density, organic matter, and sediment strength

Organic matter content and shear strength were significantly higher in short-form *Spartina* than the similar, lower values of tall-form *Spartina* and the denuded zone; bulk density only showed marginal significance between zones. These conclusions indicate that burrow formation potential is lower in the tall-form *Spartina* and denuded zone than in the short-form *Spartina*. While we currently see many burrows in the denuded zone, its low organic matter content and shear strength due to *Sesarma* herbivory and burrowing make forming additional burrows in the zone less feasible. Furthermore, since the *Sesarma* front is moving inland, current denuded zones were previously short-form *Spartina* zones—the *Sesarma* created the burrows when the areas were highly supported by vegetation. While bulk density, a proxy for sediment compaction, was only marginally significant, we saw the trend that the tall-form *Spartina* and denuded zone had greater densities compared to short-form *Spartina*. This is a logical progression, for higher amounts of organic matter correlate with lower densities (Morris et al. 2016). High percent organic matter indicates high amounts of peat in the short-form *Spartina*. Peat is integral to the formation of *Sesarma* burrows, and herbivory is higher in areas with high burrow and crab densities (Bertness et al. 2009). This supports our hypothesis that the *Sesarma* herbivory front is influenced at least in part by burrow formation potential in each zone.

From our findings, we still cannot conclude exactly what elements are driving the *Sesarma* herbivory front inland. Sediment composition appears to be a factor influencing *Sesarma* behavior, but this alone does not explain why the *Sesarma* are consuming the short-form *Spartina* over the tall-form *Spartina*, especially considering our results, which found that *Sesarma* have a preference for tall-form *Spartina.*

Runaway herbivory and rapid sea level rise continue to threaten marshes, yet the tall-form *Spartina* still persists in creek heads along the Eastern Shore. This revegetation counters both of marshes' major threats—tall-form *Spartina* regrowth shows no signs of herbivory, thus countering the effects of *Sesarma*, and continues to vertically accrete, thus keeping pace with sea level rise. Understanding the *Sesarma* herbivory front allows us to understand the process the marsh is undergoing to protect itself. These natural defenses can inform management and restoration efforts to facilitate the resilience of salt marshes under future climate change scenarios.

Acknowledgements

Many thanks to JLab—David Johnson, Serina Wittyngham, Manisha Pant, Kayla Martinez-Soto, Caroline Failon, Emily Goetz, and Leah Scott—for your support in the field and in the lab. Special thanks to Serina Wittyngham for mentoring and guiding me through every step of this process; your patience and dedication have made this experience more valuable than I could have ever imagined. Thank you, REU Coordinators Jennifer Dreyer, Katherine Longmire, and Rochelle Seitz, for without you, this opportunity would not have been possible in the first place. I would also like to thank the National Science Foundation for funding my project through the Research Experience for Undergraduates program, which allowed me to further explore my relationship and role within the sciences.

References

Abrams, P. A. (1984). Foraging time optimization and interactions in food webs. *The American Naturalist, 124*(1), 80-96.

Anderson, C. M., & Treshow, M. (1980). A review of environmental and genetic factors that affect height in Spartina alterniflora loisel. (salt marsh cordgrass). *Estuaries, 3*(3), 168-176.

Barbier, E. B., Hacker, S. D., Kennedy, C., Koch, E. W., Stier, A. C., & Silliman, B. R. (2011). The value of estuarine and coastal ecosystem services. *Ecological Monographs, 81*(2), 169-193.

Best, Ü S. N., Van der Wegen, M., Dijkstra, J., Willemsen, P. W. J. M., Borsje, B. W., & Roelvink, D. J. A. (2018). Do salt marshes survive sea level rise? modelling wave action, morphodynamics and vegetation dynamics. *Environmental Modelling and Software, 109*, 152-166.

Chambers, F.M., Beilman, D.W., & Yu, Z. (2011). Methods for determining peat humification and for quantifying peat bulk density, organic matter and carbon content for palaeostudies of climate and peatland carbon dynamics. *Mires and Peat, 7*(7), 1-10.

Christiansen, T., Wiberg, P. L., & Milligan, T. G. (2000). Flow and sediment transport on a tidal salt marsh surface. *Estuarine, Coastal and Shelf Science, 50*(3), 315-331.

Coverdale, T. C., Axelman, E. E., Brisson, C. P., Young, E. W., Altieri, A. H., & Bertness, M. D. (2013). New england salt marsh recovery: Opportunistic colonization of an invasive species and its non-consumptive effects. *PLoS One, 8*(8), e73823.

Davy, A., Bakker, J. P., & Figueroa, E. (2009). Human modification of european salt marshes. In B. Silliman, E. Grosholz & M. Bertness (Eds.), *Human impacts on salt marshes: A global perspective*. Berkeley and Los Angeles, CA: University of California Press.

Goodman, K., & Hay, M. (2012). Activated chemical defenses suppress herbivory on freshwater red algae. *Oecologia, 117*, 921-933.

Holdredge, C., Bertness, M., & Altieri, A. (2009). Role of crab herbivory in die-off of new england salt marshes. *Conservation Biology, 23*(3), 672-679.

Hughes, Z. J., FitzGerald, D. M., Wilson, C. A., Pennings, S. C., Więski, K., & Mahadevan, A. (2009). Rapid headward erosion of marsh creeks in response to relative sea level rise. *Geophysical Research Letters, 36*(3), 1-5.

Karban, R., & Baldwin, I. (1997). *Induced responses to herbivory;* The University of Chicago Press.

McArthur, C., Banks, P. B., Boonstra, R., & Forbey, J. S. (2014). The dilemma of foraging herbivores: Dealing with food and fear. *Oecologia, 176*(3), 677-689.

Mitsch, W., & Gosselink, J. (2015). *Wetlands* (5th ed.). Hoboken, New Jersey: John Wiley & Sons, Inc.

Morris, J. T., Barber, D. C., Callaway, J. C., Chambers, R., Hagen, S. C., Hopkinson, C. S., Johnson, B. J., Mengonigal, P., Neubauer, S. C., Troxler, T., Wigand, C. (2016). Contributions of organic and inorganic matter to sediment volume and accretion in tidal wetlands at steady state. *Earth's Future, 4*(4), 110-121.

Morris, J. T., Sundareshwar, P. V., Nietch, C. T., Kjerfve, B., & Cahoon, D. R. (2002). Responses of coastal wetlands to rising sea level. *Ecology, 83*(10), 2869.

Pyke, G. H., Pulliam, H. R., & Charnov, E. L. (1977). Optimal foraging: A selective review of theory and tests. *The Quarterly Review of Biology, 52*(2), 137-154.

R Core Team (2013). R: A language and environment for statistical computing. R Foundation for Statistical Computing, Vienna, Austria.

Robertson, S. (2011). *Direct estimation of organic matter by loss on ignition: Methods*. Unpublished manuscript.

Vu, H. D., & Pennings, S. C. (2018). Predators mediate above- vs. belowground herbivory in a salt marsh crab.*Ecosphere, 9*(2), 1-10.

Vu, H. D., Wie˛ski, K., & Pennings, S. C. (2017). Ecosystem engineers drive creek formation in salt marshes. *Ecology, 98*(1), 162-174.

Salinity and pH effects on blue crab, *Callinectes sapidus*, cuticle layer structure

Chanté Lively
Nova Southeastern University

Dr. Rochelle Seitz &
Katherine Longmire

2 August 2019

Synopsis

After eight weeks of treatment in experimental ambient and low-salinity and low-pH conditions to stimulate ocean acidification, 15 blue crab, *Callinectes sapidus*, carapace cuticles were analyzed to assess thickness layer (µm) variations based on treatment. Of the four cuticle layers, the epicuticle, the outermost layer, indicated significantly thicker width with the two low-salinity treatments, but no effects of pH.

Abstract

Studies focusing on ocean acidification (OA), an increasing problem have begun to emphasize its effect on marine calcifying organisms. The objective of this project was to assess the effects of various pH and salinity treatments on blue crab, *Callinectes sapidus,* cuticle layer structure. For eight weeks, we raised twenty-four blue crabs, of the inter-molt C4 stage, in differing pH and salinity conditions, split into four treatments of low and high pH and low and high salinity. Then using an Olympus microscope and cellSens software, thickness measurements (µm) were taken for fifteen crab cuticle layers that went through histological processing. A one-way ANOVA indicated a significant effect of salinity on the epicuticle layer

(P-value= 0.028). The Fisher pairwise comparisons indicated statistical differences between a group of T2 and T3 (high-salinity treatments) and a group of T4 and T1 (low-salinity treatments). Since blue crabs form the new carapace inside of their old carapace and the epicuticle is the first layer to be secreted, the impact of salinity variations due to OA may exponentially affect the layer in comparison to others. However, our results are in line with some other studies on OA effects on crabs, but do not completely correlate with some other studies on crab shell calcification, emphasizing the need for more research. Overall, more studies need to be done as understanding the relationship between OA and various factors (salinity, pH, and water temperature) is critical to predicting species responses to a range of climate-change scenarios.

Introduction

Ocean acidification (OA) is a rising problem across marine waters. Driven by rapidly increasing anthropogenic emissions, the resulting addition of carbon dioxide (CO_2) in seawater causes variability in ocean pH, shifts in carbonate speciation, changes to ecosystem structure, and more (Doney et al. 2009, Duarte et al. 2013). OA typically affects the open ocean, but the concept of anthropogenic impacts on marine pH is applicable to all systems, including estuarine ecosystems. Estuarine ecosystems are more complex and dynamic than the open ocean; estuarine organisms are similarly dynamic (Duarte et al. 2013). These ecosystems are dominated by benthic and engineering species with a capacity to be more vulnerable to water chemistry changes (Duarte et al. 2013).

Although this is a relatively new area of research, it is projected that the organisms most affected by OA will be marine calcifying organisms (Dickinson et al. 2013) and potentially crustaceans. OA will directly impact a wide range of marine organisms that build shells from calcium carbonate (the biomineralization and calcification of ions to form shells) (Doney et al. 2009), such as the blue crab. As the anthropogenic impacts on marine areas increase, it is imperative to study the potential effects of OA on marine organisms. The present understanding of potential OA impacts mainly focuses on short-term laboratory and mesocosm experiments, leading to a large gap in understanding the response of individual organisms, populations, and communities (Doney et al. 2009). After all, the potential for marine organisms to adapt to increasing CO_2 and other effects are not well known (Doney et al. 2009).

Blue crabs, *Callinectes sapidus*, are commercially and ecologically valuable organisms in the Chesapeake Bay, the largest estuary in the United States. Blue crabs are benthic, decapod crustaceans found along the Atlantic and Gulf coasts of North America (Glandon et al. 2018). As the main bivalve predator in the Chesapeake Bay, these crabs are an integral part of the benthic food web, highlighting the importance of quantifying the effects of OA on this species (Glandon et al. 2018).

The objective of this project is to assess the effects of various pH and salinity treatments on blue crab cuticle layer structure. Blue crabs are strong osmoregulators with a wide salinity tolerance and strong acid-base regulators with an exoskeleton shielding the carapace from surrounding seawater (Whiteley 2011). With climate change, storm frequency is predicted to increase, which would lower salinity and result in stressful conditions for blue crabs. Though crabs are euryhaline, respiration is increased under low salinities. Blue crabs have an incremental growth cycle achieved through the shedding of the carapace, known as molting (Roer & Dillaman 1984). As part of their skeletal structure and carapace, there are four cuticle layers of diverse thickness and composition: epicuticle, exocuticle, endocuticle, and an inner basal membranous layer connected to the hypodermis (Roer & Dillaman 1984, Kennedy & Cronin 2007). The epicuticle, exocuticle, and endocuticle are mineralized layers, while the membranous layer is not (Roer & Dillaman 1984). The epicuticle also lacks chitin. Since the four cuticle layers are connected to the hypodermis by pore canals, the movement of the carapace's organic and mineral composition are absorbed and deposited during each molt cycle (Roer & Dillaman 1984). In crustaceans, the carapace cuticle resists mechanical loads, provides protection from the environment and predators, and enables mobility, but little is known about how OA affects the structure of the carapace in crustaceans (Whiteley 2011, Coffey et al. 2017).

For this experiment, the chosen pH values reflect the range that estuaries could encounter with rising OA by 2100 (Feely et al. 2009), while the various salinity values are used to address potential effects of increased storm activity with climate change as well as the resulting changes in physiology of estuarine inhabitants (Dickinson et al. 2013). In addition, juvenile crustaceans showcase greater sensitivity to OA (Coffey et al. 2017). The experiment is an integral part of a larger project (already completed in fall 2018), and this project will deal with the results of the crab cuticle histology and microscopy. Histology is the study of living tissue (Windle & Nonidez 1969). Concerned primarily with the microscopic structure, there are three main preparatory steps to making the tissues usable for microscopy: fixation, embedding and sectioning, and mounting and staining (Weiss & Greep 1977). Overall, the histological treatment and microscopy procedure will allow biochemical and physiologic characteristics of tissue (i.e. cuticle thickness) to be measured, supporting the objective.

Methods

For eight weeks, we raised twenty-four blue crabs, of the inter-molt C4 stage, in differing pH and salinity conditions, split into four treatments of low and high pH and low and high salinity. For the experiment, the low pH had a range of 7 to 7.2, while the high pH had a range of 8 to 8.3. The low salinity was 16 ppt, while the high salinity was 30 ppt. The exposure conditions were crossed into four treatments with two tanks per treatment.

T1: Low pH, high salinity
T2: Low pH, low salinity
T3: High pH, low salinity
T4: High pH, high salinity

Crab size (mm), as well as days since molt, were recorded.

Table 1: Fifteen individual blue crab treatment data indicating crab sex, crab size (mm), and days since the last molt.

Treatment	ID	Sex	Size (mm)	Days since last molt
T1	T1E	F	84.5	69
T1	T1G	F	87.9	70
T2	T2C	M	74.5	35
T2	T2E	F	90	0
T2	T2G	M	82.5	70
T3	T3A	F	68.7	1
T3	T3B	M	86.3	7
T3	T3C	M	79.1	70
T3	T3F	M	97.8	70
T3	T3G	F	83.9	70
T4	T4A	M	69.7	70
T4	T4B	F	84.7	70
T4	T4C	M	111.1	70
T4	T4E	F	70.2	70
T4	T4G	M	90.8	7

After eight weeks, the crab carapace tissue went through histological processing. Doubles of each 15 crab carapaces were made into slides (thirty slides in total). Using an Olympus compound microscope and cellSens software, I took three measurements of each of the four layers at 20x magnitude per slide section. The thickness measurements were recorded in µm. I then chose two different slide sections for each layer, for an average of measurements, with a total of twenty-four measurements per crab.

Experimental data was analyzed with five response variables (thickness of each of the four cuticle layers, plus whole cuticle thickness), for each crab. All analyses were conducted in Minitab 18, including mean, significance, and variance. An alpha level of $P < 0.05$ was used for all analyses. A one-way Analysis of Variance (ANOVA) was used to test for the effects of treatment type on each response variable. Response variables included epicuticle layer thickness, endocuticle layer thickness, exocuticle layer thickness, membranous layer thickness, and total cuticle layer thickness. Significance of the interactions was assessed using the ANOVA test, Tukey's test, and Fisher's method. Each response variable was also tested against crab size and days since last molt with scatterplot regression analysis. In addition, bar/line graphs were created using SigmaPlot Version 13.

Results

The carapace thicknesses of 15 individual blue crabs were determined for this experiment. Some differences can be seen in the crab size and days since last molt of each crab as well as the mean measurements of the whole cuticle, epicuticle, exocuticle, endocuticle, and membranous layer thickness of the crabs by salinity-pH treatment (Tables 1-2). A one-way ANOVA indicated a significant treatment effect on the epicuticle layer (P-value= 0.028) (Table 3). However, the one-way ANOVA indicated no significant treatment effect on exocuticle, endocuticle, basal membrane, and whole cuticle thickness (P-value= 0.710, 0.618, 0.512, and 0.548, for the exocuticle, endocuticle, basal membrane, and whole cuticle thickness, respectively) (Table 3).

Table 2: Fifteen individual blue crab treatment data indicating the mean of the epicuticle, exocuticle, endocuticle, basal membranous layer, and whole cuticle layer thickness (μm).

Treatment	ID	Epicuticle	Exocuticle	Endocuticle	Basal membrane	Whole
T1	T1E	4.05	43.84	225.66	11.63	285.17
T1	T1G	4.22	51.26	187.21	9.29	251.98
T2	T2C	5.45	24.73	242.79	15.46	288.43
T2	T2E	5.85	61.00	100.83	3.41	171.08
T2	T2G	4.70	33.40	172.02	4.59	214.71
T3	T3A	6.22	26.22	116.31	2.88	151.64
T3	T3B	5.93	56.97	205.30	2.61	270.81
T3	T3C	4.64	70.62	209.99	24.07	309.32
T3	T3F	4.79	45.89	186.57	22.58	259.83
T3	T3G	4.49	42.34	182.13	21.43	250.39
T4	T4A	3.77	64.60	271.23	4.70	344.31
T4	T4B	4.06	48.29	202.60	21.15	276.10
T4	T4C	4.47	46.21	189.09	13.50	253.27
T4	T4E	4.30	49.68	205.54	24.18	283.70
T4	T4G	4.42	48.52	174.20	2.46	229.61

Table 3: One-way ANOVA results for the effects of treatment on epicuticle, exocuticle, endocuticle, membranous layer, and whole cuticle layer thickness (μm). For significance levels, $\alpha = 0.05$. Significant p-values are shown in bold. It indicated no significant treatment effect on exocuticle, endocuticle, basal membrane, and whole cuticle thickness, but there was a significant effect of treatment on the epicuticle layer.

Layer	P-value
Epicuticle	**0.028**
Exocuticle	0.71
Endocuticle	0.618
Basal membrane	0.512
Whole	0.548

In addition for the epicuticle, the Tukey pairwise comparisons, which covered grouping information on a 95% confidence interval, indicated no statistical differences between the means of all four treatments (5.333, 5.214, 4.204, and 4.1341 for T1, T2, T3, and T4 respectively) (Table 4). The Fisher pairwise comparisons, which covered grouping information using the Fisher LSD method on a 95% confidence interval, indicated statistical differences between a group of T2 and T3 and a group of T4 and T1 (Table 5), with low-salinity treatments having thicker epicuticle width. Both T2 and T3 were high salinity treatments. Both T4 and T1 were low salinity treatments. The groupings were not statistically different between each individual in the salinity group, but are different between the salinity treatments in the other group (e.g. low-salinity treatment differed from high salinity treatment) (Figure 1). For comparison to the epicuticle, the Tukey's test and Fisher's method were run on the other cuticle layers, specifically the basal membranous layer. There were no differences in groupings between the different salinity treatments (Figure 2)

Table 3: One-way ANOVA results for the effects of treatment on epicuticle, exocuticle, endocuticle, membranous layer, and whole cuticle layer thickness (µm). For significance levels, α = 0.05. Significant p-values are shown in bold. It indicated no significant treatment effect on exocuticle, endocuticle, basal membrane, and whole cuticle thickness, but there was a significant effect of treatment on the epicuticle layer.

Layer	P-value
Epicuticle	**0.028**
Exocuticle	0.71
Endocuticle	0.618
Basal membrane	0.512
Whole	0.548

Table 4: Tukey pairwise comparison for the epicuticle layer thickness (µm) using the Tukey method on a 95% confidence interval based on treatment groupings. It indicated no statistical differences between the means of all four treatments. Means that do not share a letter are significantly different.

Treatment	N	Mean	Grouping
T2	3	5.333	A
T3	5	5.214	A
T4	5	4.204	A
T1	2	4.1341	A

Table 5: Fisher pairwise comparison for the epicuticle layer thickness (µm) using the Fisher LSD method on a 95% confidence interval based on treatment groupings. It indicated statistical differences between a group of T2 and T3 (high salinity) and a group of T4 and T1 (low salinity). Means that do not share a letter are significantly different.

Treatment	N	Mean	Grouping
T2	3	5.333	A
T3	5	5.214	A
T4	5	4.204	B
T1	2	4.1341	B

Figure 1: The crab epicuticle layer thickness (µm) by treatment group using the ANOVA and Fisher comparison results on a bar graph. The treatments are in a pH to salinity format where the letter L refers to low and the letter H refers to high. The graph indicates a difference in treatment based on salinity, where low salinities grouped by the letter B have wider thicknesses than high salinities grouped by the letter A. The thicknesses by treatment were not different by pH.

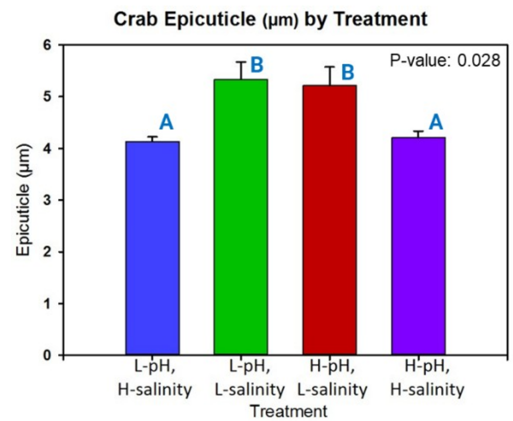

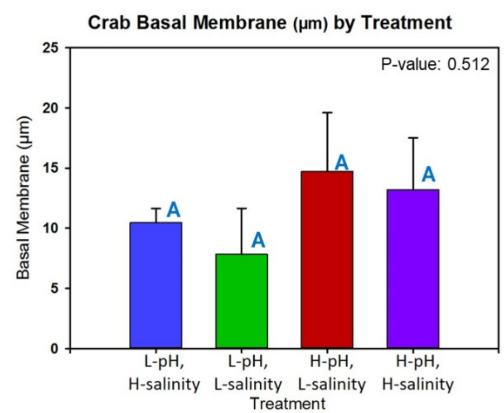

Figure 2: The crab basal membranous layer thickness (µm) by treatment group using the ANOVA and Fisher comparison results on a bar graph. The treatments are in a pH to salinity format where the letter L refers to low and

the letter H refers to high. The letter A refers to grouping comparisons. The basal membranous layer is not statistically different by treatment.

When testing the cuticle response variables against crab size and time since last molt, the correlations were analyzed on a scatterplot with a fitted linear regression line. Crab size did not statistically affect the cuticle layers (Figures 3-7) as the R^2values were all less than 10% (0.9%, 1.8%, 4.8%, 0.1%, and 2.4% for the epicuticle, exocuticle, endocuticle, membranous, and whole layer measurements, respectively), and p-values were non-significant. There was no correlation between days since last molt and the exocuticle (Figure 8). However, there were positive correlations between days since last molt for the endocuticle, basal membrane and whole layer measurements (Figures 9-11) and a negative correlation between days since last molt and the epicuticle layer (Figure 12). Lastly, the data was rerun omitting the crabs that had recently molted (0-7 days since last molt), but that did not change the outcome of significance.

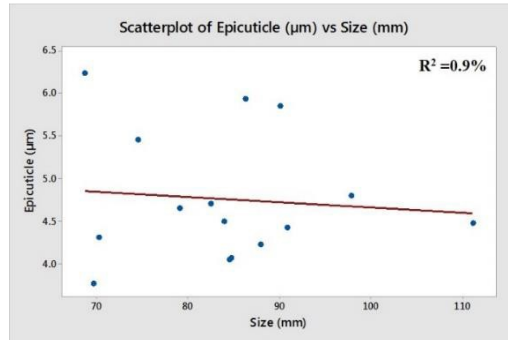

Figure 3: The epicuticle layer thickness (µm) versus crab size (mm) on a scatterplot with a fitted linear regression line.

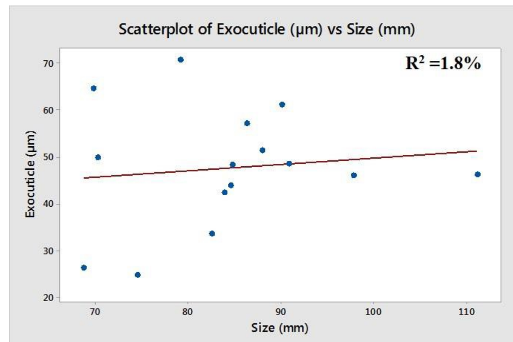

Figure 4: The exocuticle layer thickness (µm) versus crab size (mm) on a scatterplot with a fitted linear regression line.

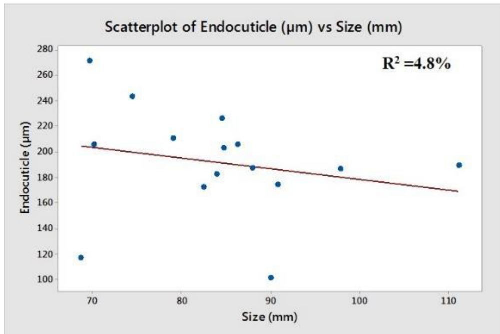

Figure 5: The endocuticle layer thickness (µm) versus crab size (mm) on a scatterplot with a fitted linear regression line.

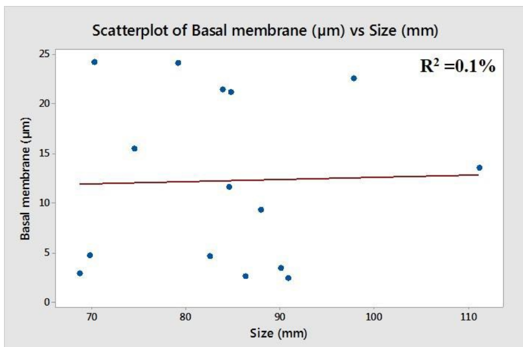

Figure 6: The basal membranous layer thickness (µm) versus crab size (mm) on a scatterplot with a fitted linear regression line.

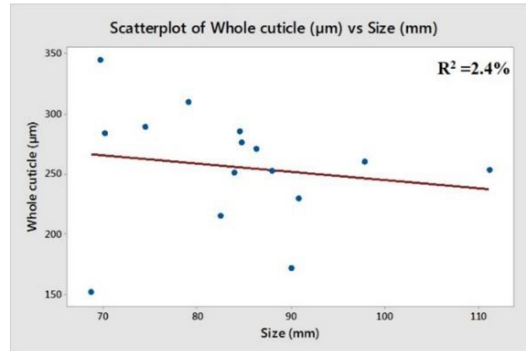

Figure 7: The whole cuticle layer thickness (µm) versus crab size (mm) on a scatterplot with a fitted linear regression line.

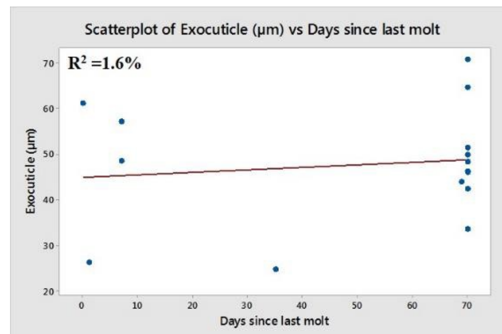

Figures 8: The exocuticle thickness (µm) versus days since last molt on a scatterplot with a fitted linear regression line.

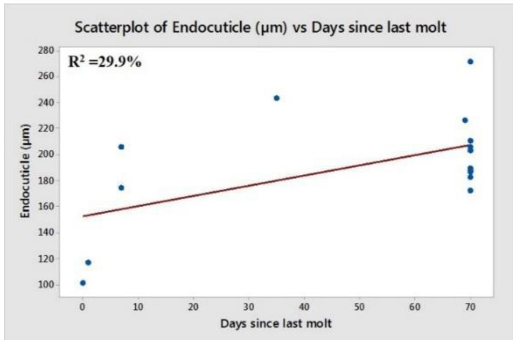

Figure 9: The endocuticle thickness (µm) versus days since last molt on a scatterplot with a fitted linear regression line. There was a positive correlation.

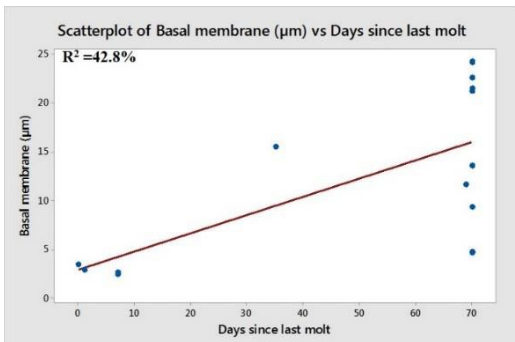

Figure 10: The epicuticle thickness (µm) versus days since last molt on a scatterplot with a fitted linear regression line. There was a positive correlation.

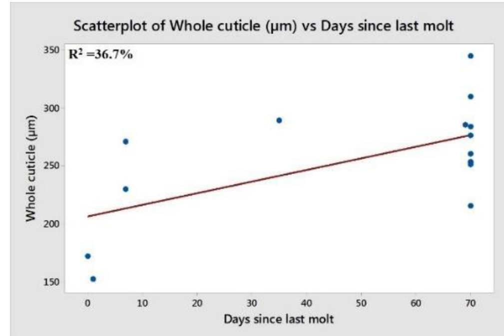

Figure 11: The whole cuticle layer thickness (µm) versus days since last molt on a scatterplot with a fitted linear regression line. There was a positive correlation.

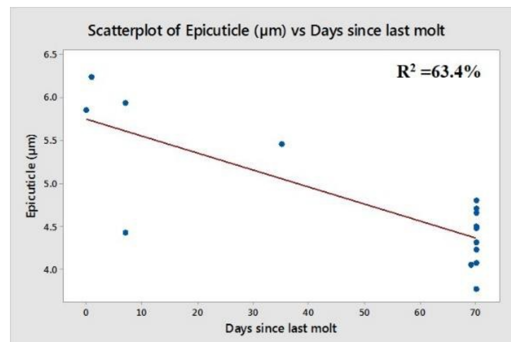

Figure 12: The epicuticle layer thickness (µm) versus days since last molt on a scatterplot with a fitted linear regression line. There was a negative correlation.

Discussion

The data from this experiment reveal an interesting effect of salinity-pH treatments on the carapace cuticle layers of juvenile blue crabs. In a similar methodology, Glandon et al. 2018 examined the effects of increased water temperature and pCO_2 on blue crab carapace thickness, correlating increased temperature with average declines in carapace layer thickness, and increased pCO_2 having no impact. However though other studies have analyzed the effects of water temperature, pCO_2, or pH on various crab species, this specific OA methodology with the multiple stressors of pH and salinity has not been previously conducted.

For this experiment, the epicuticle layer was the only cuticle layer to indicate a statistically significant effect between salinity treatments, regardless of pH. In agreement with Glandon et al. 2018, which tested temperature $\times$ pCO_2 interactions with a slightly different methodology, increased pH did not indicate a statistically significant effect on the thickness of the exocuticle, endocuticle or the whole cuticle. They did not analyze effects on the epicuticle or basal membranous layer. Yet, our results conflict with previous studies where there was a positive net calcification response under elevated pCO_2 (Ries et al. 2009). Since their study focused on calcification and we did not examine calcification, this could explain why the results do not match.

Blue crabs are a euryhaline species, whose frequent movements require them to adjust for differing salinity. For epicuticle thickness, the different salinity treatment groupings were significantly different, with thicker epicuticle layers in lower salinities. Thus, salinity-based climate changes may affect cuticle layer thickness. Some marine calcifying organisms are enclosed within a protective external covering from seawater and for crustaceans, this is the epicuticle (Ries et al. 2009). Crabs in low-salinity treatments had thicker epicuticle layers, possibly as a protective shield for the other cuticle layers against the stressful low-salinity conditions. Furthermore, the days since last molt factor was deemed significant in reference to the epicuticle layer. In the scatterplot (Figure 11), the epicuticle width had a high R^2 as well as a negative correlation with days since last molt. As the days since last molt increased, the shorter the mean thickness of the epicuticle.

During molting, blue crabs form their new carapace inside of the old carapace and the epicuticle is secreted prior to molting (Glandon et al. 2018, Waugh et al. 2009). In addition, though all layers of the cuticle are deposited in the C_4 molt stage, internal tissue still continues to grow (Roer & Dillaman 1984, Kennedy & Cronin 2007). Vertical pore canals help to keep the hypodermis in contact with all the cuticle layers, running from the epicuticle downwards (Roer & Dillaman 1984). Since the four cuticle layers are connected to the hypodermis by pore canals, the movement of the carapace's organic and mineral composition are absorbed and deposited during each molt. With a continuous exchange of nutrients, the epicuticle would continue to be affected by the surrounding water (i.e. salinity) ever since molting. Salinity tolerance and subsequent increased layer thickness would then be a result of acclimation to the new conditions (Tankersley & Richard 2007). Furthermore, the epicuticle does not calcify until the end of ecydsis (Roer & Dillaman 1984).

Overall, the effects of the multiple stressors, OA, and salinity, on crab carapace cuticle have not been previously examined. The results of the experiment agree with some previous studies showing no effects of OA on cuticle layer thickness, but do not completely correlate with other studies showing increased calcification. This emphasizes the need for more research. However, overall understanding of the relationship between ocean acidification and various factors (salinity and water temperature) is critical to predicting species responses to a range of climate-change scenarios. In reference to salinity by 2100, increased sea level rise is predicted to continue, causing more oceanic water to flow into the estuaries and increasing salinity (Glandon et al 2018). On the other hand, an increase of storms, is predicted to increase with climate change, leading to a lowering of salinity. Low salinity and lower pH could be a potential stressor for blue crabs. For *Callinectes sapidus*, more research needs to be done, especially with carapace cuticle. Future studies that focus on blue crab carapace cuticle need to increase sample size, analyze other aspects of the cuticle (besides thickness or calcification), and delve more into the function of the epicuticle. With an increased sample size, it is possible that we may see significant correlations between days since last molt, crab size, and cuticle layer thickness. Lastly by understanding the function of each individual cuticle layer, the importance of our results could be highlighted.

Acknowledgements

Thank you to my mentors, Dr. Rochelle Seitz and Katherine Longmire for the research ideas, materials, and encouragement. Thank you to Dr. Jeff Shields for the usage of his Olympus microscope and software as well as assistance with the crab cuticle slide measurements. Thank you to our lab tech Kathleen Knick for data analysis assistance on Minitab 18 and SigmaPlot Version 13. Lastly, thank you to Jenny Dreyer and Katherine Longmire for coordinating the REU program at VIMS. Program funding for the VIMS Research Experience for Undergraduates was made available through a grant awarded from the National Science Foundation (grant # NSF OCE 1659656) to Drs. Rochelle Seitz and Linda Schaffner.

Literature Cited

Coffey, W. D., Nardone, J. A., Yarram, A., Long, W. C., Swiney, K. M., Foy, R. J., Dickinson, G. H. 2017. Ocean acidification leads to altered micromechanical properties of the mineralized cuticle in juvenile red and blue king crabs. *Journal of experimental marine biology and ecology* 495: 1-12.

Dickinson, G.H., Matoo, O.B., Tourek, R.T., Sokolova, I.M., Beniash, E. 2013. Environmental salinity modulates the effects of elevated CO_2 levels on juvenile hard-shell clams, *Mercenaria*. *The Journal of Experimental Biology* 216 (14): 2607-2618.

Doney, S. C., Fabry, V. J., Feely, R. A., Kleypas, J. A. 2009. Ocean acidification: The other CO_2 problem. *Annual Review of Marine Science* 1: 169-197.

Duarte, C.M., Hendriks I.E., Moore, T.S., Olsen, Y.S., Steckbauer, A., Ramajo, L., Carstensen, J., Trotter, J.A, McCulloch, M. 2013. Is ocean acidification an open-ocean syndrome? Understanding anthropogenic impacts on seawater pH. *Estuaries and Coasts* 36(2): 221-236.

Feely, R.A., Doney, S.C, Cooley, S. R. 2009. Ocean acidification: Present conditions and future changes in a high-CO_2 world. *Oceanography* 22: 36-47.

Glandon, H.L., Kilbourne, K.H., Schijf, J., Miller, T.J. 2018. Counteractive effects of increased temperature and pCO2 on the thickness and chemistry of the carapace of juvenile blue crab, *Callinectes sapidus*, from the Patuxent River, Chesapeake Bay. *Journal of Experimental Marine Biology and Ecology* 498: 39-45.

Kennedy, V.S., Cronin, L.E. 2007. Anatomy of post-larval blue crab. Pp. 56 In V.S. Kennedy, L.E. Cronin, eds., *The Blue Crab: Callinectes sapidus*. College Park, MD: Maryland Sea Grant College.

Ries, J. B., Cohen, A. L., & McCorkle, D. C. 2009. Marine calcifiers exhibit mixed responses to CO_2-induced ocean acidification. *Geology* 37(12): 1131-1134.

Roer, R., Dillaman, R. 1984. The structure and calcification of the crustacean cuticle. *American Zoologist* 24(4): 893-909.

Tankersley, R.A., Richard, B.F., Jr. 2007. Environmental physiology. Pp. 460-462 In V.S. Kennedy, L.E. Cronin, eds., *The Blue Crab: Callinectes sapidus*. College Park, MD: Maryland Sea Grant College.

Waugh, D. A., Feldmann, R. M., Burrell, J. L., Hull, A. L., Hein, K., & Schweitzer, C. E. 2009. Ontogenetic variations in cuticle morphology in the blue crab *Callinectes sapidus*. *Journal of Crustacean Biology* 29(2): 141-156.

Weiss, L., Greep, R.O. 1977. The Cell. Pp. 3-14 in *Histology.* 4th ed. New York, NY: McGraw-Hill, Inc.

Whiteley, N. M. 2011. Physiological and ecological responses of crustaceans to ocean acidification. *Marine Ecology Progress Series* 430: 257-271.

Windle, W.F., Nonidez, J.F. 1969. Tissues. Pp. 1-2 in *Textbook of Histology.* 4th ed. New York, NY: McGraw-Hill, Inc.

The Effect of Varied Substrates on Community Development and Oyster Reef Restoration in Chesapeake Bay

Josephine Hall
University of Arkansas

Mentor(s): Rom Lipcius, Gabby Saluta, Katie Knick

2 August 2019

Synopsis

As the structural complexity of a settlement tile increases, species richness, abundance, and biodiversity also increase. If current seawalls and manmade coastal structures were to be enhanced, the quality of the surrounding ecosystem would also be improved.

Abstract

The goal of this project was to determine how varied substrate (pH-balanced concrete, oyster shell, bulkhead polymer) and structural complexity (0cm relief, 2.5cm relief, 5cm relief) affected community development in the subtidal zone of the York River. Twenty tiles, composed of 5 treatments with 4 replicates each, were placed at a 45° angle on a series of rebar racks for 3.5 weeks. The tiles were then rinsed to collect the residing macrofauna which underwent many statistical analyses following identification. 16 total species were identified among the treatments, percent composition varying between treatments. As structural complexity increased, so did species richness, abundance, and biodiversity.

Introduction

Though oysters have always been a treasure of the Chesapeake Bay, years of commercialized dredging and harvesting have severely depleted this native species' population. These ancient mollusks that have survived 25-30 million years have been brought to approximately 1% of their initial population since the late 19th century by human exploitation (Lawrence 1971). This is not only a problem for commercial fisheries, but also for the fate of Chesapeake Bay. As a community-based, species, oysters aggregate together into reefs which provide habitats for a plethora of other native species, including commercially viable crabs and fishes (Bahr and Lanier 1981). Although the significance of other filter-feeding bivalves is not considered in this factoid, it was once believed the Chesapeake Bay could be filtered in one week, but following the oyster's exploitation, the process now takes one full year (Chesapeake Bay Foundation 2019, Kreeger 2018). This drastic decrease in filtration rate has, and will continue to have, detrimental effects on the water quality in the Bay if proper measures are not taken to restore the oyster's population. Though filtration is one of the most widely acknowledged benefits of oysters, there are many other "ecosystem services" provided by this mollusk. These services include providing a habitat for other marine species, promoting biodiversity, stabilizing marsh environments, and intaking carbon (Coen et al. 2007).

Oysters play a significant role in stabilizing marsh environments and coastlines because they provide a hard substrate in a primarily loose-sediment environment. Considering that habitat loss is one of the primary concerns for commercial fisheries, oyster reef restoration would aid the Chesapeake Bay's ecosystem and economy as now depleted fish stocks would return, supporting the plethora of fisheries that surround the Bay. Restoration efforts would also assist in preventing coastal erosion as reefs provide a natural seawall, rather than commercial bulkhead or other manufactured alternatives (Coen *et al*. 2007). These structures tend to lack the complexity needed for adequate recruitment as they do not provide enough protection against predation for juvenile oysters. Eco-engineering has now taken rise to improve the functionality of seawalls near urban coastlines. By providing both a habitat for oysters and the diversity of marine life associated with reefs, in addition to reinforcing shorelines, this practice may be the best option for restoration efforts. (Strain *et al.* 2017)

Nearly all major coastlines have become urbanized, due to roughly 70% of the world's population living on the coast (Strain *et al*. 2017). This has major implications for the coastlines themselves, due to runoff, erosion, and the subsequent hardening of coastlines, as well as the neighboring marine ecosystems as the aforementioned hardening replaces natural shorelines with unnatural substrates. These additions can include wooden piers, concrete, and rock, among other things. Not only do these hardening mechanisms introduce new substances and chemicals to the environment, but they also decrease the amount of living space available. Typically oriented in a vertical fashion, coastal-hardening practices especially decrease the amount of intertidal space, leading to overcrowding, as there is no gentle slope for the intertidal zones to transition. It has also been observed that though hardened coastlines do harbor significant marine populations, many of the attracted species are either nuisance or invasive (Chapman and Underwood 2011).

Though most coastlines have already been hardened, and therefore eco-engineering was not initially a concern, current methods can be applied to existing coastlines in order to improve their conditions and restoration potential. Elisabeth Strain and the Reef Design Lab in Australia have tested the importance of structural complexity and crevice availability on juvenile oyster recruitment and survivorship as part of a larger Green Harbour Project. Three sets of tiles were manufactured by the Reef Design Lab using pH-balanced concrete with relief heights ranging from zero to five centimeters. Strain's study shows that as complexity and crevice space increased, the settlement and survivorship also increased (Strain *et al.* 2017). If the Reef Design Tiles were applied to existing seawalls, as they were done in Sydney Harbor for this study, then biodiversity would increase, and native populations would return to the area. Similar studies which varied structural complexity have also been done, all with the same results; as structural complexity increases, biodiversity and presence of native rather than invasive species increases.

One such study by Ido and Shimrit in Israel focused on the effects of coastal and marine infrastructure (CMIs) on an ecosystem by comparing the standard concrete based CMI to one of ECOncrete. Their results showed a significant change in ratio of invasive to native species between the two types of antifer blocks. In addition to increased presence of native fish species, the ECOncrete breakwater section also had a more diverse recruitment of engineering species such as oysters, barnacles, and bryozoans. These creatures are significant due to the fact that they contribute to the biogenic build-up of their substrate, increasing its structural integrity. Eco-engineers, such as oysters, deposit $CaCO_3$ (calcium carbonate) which adds to the surface complexity of the breakwater section, creating more living space for other species, adding to the biodiversity of the area. (Ido and Shimrit 2015) Although the ECOncrete is also a manmade structure, and essentially "unnatural", the eco-engineering techniques applied to this design, such as including indents in the sides in contrast to the smooth sides of standard antifer blocks and using a pH-neutral substrate rather than the alkaline Portland-based concrete, made this breakwater section more successful ecologically.

Two related studies in Beaufort, NC used settlement tiles to assess the stable points in a fouling community should certain niche species be excluded, or environmental factors shift. With primary cover dominated by the tunicate species *Styela* and *Schizoporella,* spat recruitment was negatively affected by disturbance date, though biodiversity and community evenness on the settlement plates increased throughout the study. In the 2017 study done to see the changes in the Beaufort fouling community after nearly 50 years, Theuerkauf witnessed the affect exotic species have on community development and associated biodiversity as the invasive tunicate, *C. oblonga* dominated the available substrate. Although both studies resulted in the short-term pattern of disturbance date affecting the settlement plate community, the 2017 study showed a decrease in biodiversity due to the introduction of a nonnative species. (Sutherland 1974, Theuerkauf *et al*. 2017)

This study aims to apply the results from the aforementioned experiments to oyster reef restoration in the Chesapeake Bay estuary. To inform oyster restoration efforts, the goal of this project is to determine the best medium (plastic, pH-balanced concrete, rock, oyster shell) and level of structural complexity (no grooves, 2.5-centimeter groove height, 5-centimeter groove height) for maximizing oyster recruitment in a high energy area. This experiment hopes to compare the efficiency of eco-engineered substrates with those already present in the Chesapeake Bay. Questions this project will address are: How much of an affect does substrate and structural complexity have on recruitment? Will subtidal environments show improved recruitment as they as farther from shore than the previously tested intertidal zone of the York River? In the event that spat recruitment does not occur within the short timeframe of this experiment, how does the biodiversity associated with each treatment differ?

Methods

In an effort to determine which substrate receives the best recruitment, five varieties of tile were chosen for analysis. Each tile had a footprint of $600.25cm^2$. The chosen variety includes three Reef Design Lab tiles of varying groove height; low, medium, and high relief of 0cm, 2.5cm, and 5cm. The composition of these tiles was specially crafted to attract settlement due to their neutral pH. The other tiles tested included bulkhead polymer and a synthetic "reef" composed of native oyster shell adhered to one of the pH-balanced tiles with epoxy to present a natural environment for settlement. Sense 3D imaging software and Fusion 360 were used to calculate the surface area of each treatment. The tiles were first scanned into the Sense 3D system, creating a digital representation of the tile. These files were then imported into the Fusion 360 AutoCAD software where surface area was calculated. (Figure 1)

Figure 1: Digital renditions of low, medium, high relief Reef Design Lab tiles and oyster shell tile. Top row depicts 3D Sense imagery. Bottom Row depicts Fusion 360 models.

The twenty tiles were placed onto rebar racks at approximately a 45^{o} angle with cable ties at each corner and bungee cord so that they could be easily removed for analysis. We used block randomization to ensure that each treatment was represented equally, and so that one treatment was not given preference in terms of location. A series of five rebar racks was used to support the tiles and was placed in the subtidal zone in the York River behind Andrews Hall. The rebar racks were approximately 8 feet long, with four tiles attached to each rack. These tiles represent a variety of material people may use whilst reconstructing an oyster reef.

The tiles were placed in the subtidal zone in June 2019 and left for two weeks in order to adjust to the new environment before initial data was taken. A randomly chosen subset of tiles representing each treatment were removed to check for spat recruitment and then replaced. Unfortunately, in the short time frame of this experiment, spat were not visibly present and could not be accounted for. Though the target of the project was to recruit oyster spat, many other species which support reefs were attracted to the provided environment. Some of these species included various tunicates, naked gobies, amphipods, and mud crabs. As the communities present on each type of tile appeared to differ greatly in abundance, the focus of this project changed to understand how an oyster reef would begin to develop prior to recruitment.

Approximately 3.5 weeks after placement, all tiles were removed with a 500-micron mesh bag placed overtop to enclose any mobile macrofauna residing on the settlement tile. To refrain from destructive sampling, the tiles were lightly rinsed into the mesh bag and replaced on the rebar rack. The contents of each bag were preserved in ethanol and stained with Rose Bengal (10%) prior to sorting. Each sample was initially sorted by naked eye, separating fish species, worms, and amphipods, with a second check being performed under Nikon 10x magnifying microscopes. To further sort key species, amphipods were separated into groups Gammarus, Gammarid sp. 1, Gammarid sp. 2 and Corophium. Worms were sorted between Alitta and Spionid. Following separation, the abundance of each species was counted and stored into separate vials of ethanol.

Various programs including Excel, Minitab, Sigma Plot, and R were used to analyze species richness, biodiversity, and abundance for each treatment and individual tile.

Results

The sixteen identified species included Mud Crab, Blue Crab, various Megalopae, Gammarus, Gammarid 1, Corophium, Ampithoe, Pill Bug, Neanthes Worm, Spionid Worm, Naked Goby, Skilletfish, Feathered Blenny, Grass Shrimp, Skeleton Shrimp, and Dog Welk. Overall, abundance was greatest for the high relief tile, followed by medium relief, oyster shell tile, low relief, and bulkhead in that order. There was a direct negative linear relationship between tile complexity and abundance for the high, medium, and low treatments (Figure 2). For individual tiles, worm, amphipod, and crab species were grouped to determine percent composition in relation to abundance. Composition among the tile was dominated by worms, amphipods, crabs, and naked goby. Percent composition averaged approximately 42.5% for the Alitta worm, followed by the Spionid worm, various Amphipod species, Naked Gobies, and Mud Crabs. (Table 1) All other species were less significant but present throughout the various treatments.

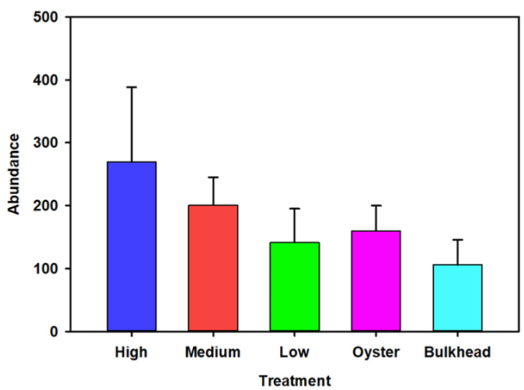

Figure 2: Comparison of average abundance between treatments. Direct linear relationship seen between complexity and abundance in high, medium, low relief tiles.

Table 1: Species list and percent contribution relative to total abundance.

Species	Common name	No. of individuals	Percent Contribution
Alitta succinea	Clam worm	1493	42.49
Spionidae	Spionid worm	494	14.06
Corophium	Corophiid amphipod	472	13.43
Gammarus mucronatus	Gammarid amphipod	341	9.70
Gobiosoma bosci	Naked goby	266	7.57
Eurypanopeus depressus	Mud crab	226	6.43
Gammarid sp. A	Gammarid amphipod	95	2.70
Palaemonetes pugio	Grass shrimp	54	1.54
Gammarid sp. B	Gammarid amphipod	20	0.57
Callinectes sapidus	Blue crab	19	0.54
Gobiesox strumosus	Skilletfish	12	0.34
Caprellidae	Skeleton shrimp	7	0.20
Ilyanassa obsoleta	Eastern mud snail	6	0.17
Hypsoblennius hentz	Feather blenny	5	0.14
Sphaeroma quadridentatum	Isopod	4	0.11
		3514	100.00

Considering that the footprint of each tile was equal, surface area was used as a proxy for complexity. The higher the ridges or available faces increases the living space and complexity of the tile. Sense 3D and Fusion 360 images are shown in Figure 1 of the high, medium, low, and oyster shell tiles with associated surface areas. Using R Studio, a statistical analysis and Log(10) transformation and rarefaction curve was performed to show how tile richness increases as available surface area increases, richness eventually plateauing. (Figure 3) Comparing species richness of 16 tiles, excluding the bulkhead treatment, the frequency of number of species present is depicted in Figure 3, the variable y1 being equivalent to species richness. A richness of 13 species present was the most frequent.

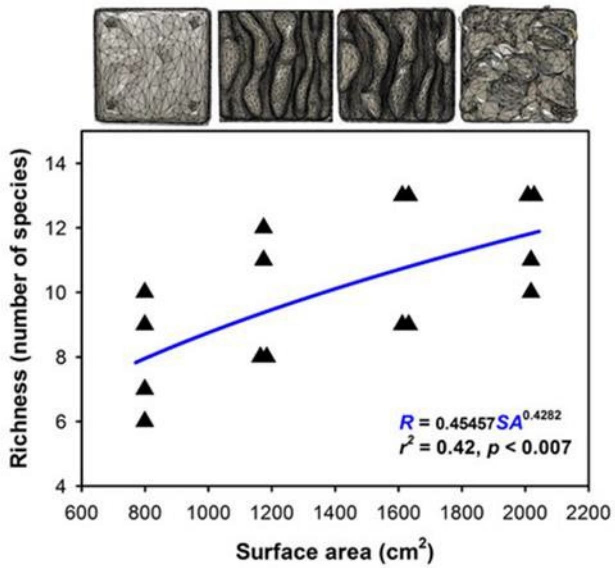

Figure 3: Log(10) transformation and rarefaction curve of surface area versus species richness.

Multivariate analysis was also performed on the species assemblage as a whole (Figure 4). The high, medium, and oyster shell treatments were much more similar than the low relief and bulkhead treatments, as seen by their proximity to each other. Though the p-value resulting from the associated PERMANOVA proved this data to be insignificant for the total species assemblage, the statistics were significant when the MDS analysis was restricted to fish assemblage. Clear clustering among higher complexity tiles and lower complexity tiles is now apparent. (Figure 5) A pair-wise post-hoc analysis was also performed showing how specific treatments correspond to one another. The bolded rows highlight which comparisons were significant, $p < 0.05$. (Table 2)

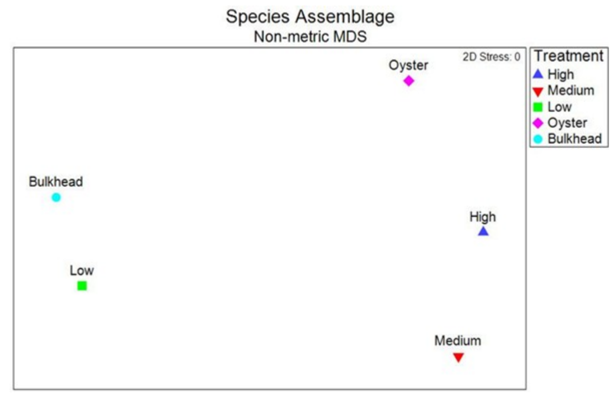

Figure 4: Multivariate analysis with Bray-Curtis similarity matrices of non-transformed community data.

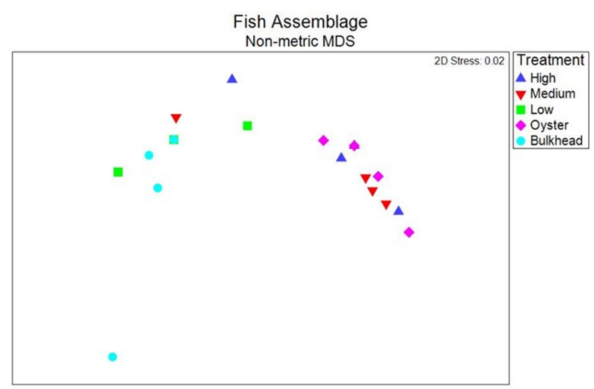

Figure 5: Multidimensional Scaling of Fish Assemblage includes Naked Goby, Feather Blenny, Skilletfish (p=0.003).

Table 2: Pair-wise post-hoc comparison of fish assemblage between treatments. Significant comparisons are bold.

Groups	t	p-value
High, Medium	0.456	0.625
High, Low	3.033	**0.046**
High, Oyster	0.779	0.547
High, Bulkhead	2.765	**0.030**
Medium, Low	2.542	0.062
Medium, Oyster	0.746	0.649
Medium, Bulkhead	2.656	**0.029**
Low, Oyster	4.568	**0.019**
Low, Bulkhead	1.134	0.333
Oyster, Bulkhead	3.716	**0.042**

Discussion

Unfortunately, in the short time frame of this experiment, spat were not visibly present and could not be accounted for. However, the community development on the settlement tiles was quite profound given the 3.5 weeks they were in the subtidal zone. At the beginning of the project, it was hypothesized that complexity would have a positive linear relationship with abundance, richness, and biodiversity. This belief roved to be true, aside from a few caveats.

Species richness, abundance, and biodiversity are restricted based on the number of present resident nekton in the subtidal zone of the York River. This causes the aforementioned measures of productivity to plateau at a given point, seen in the asymptotic relationship in Figure 4.

There was also significant error and standard deviation in this experiment due to several factors. Since there were more treatments than replicates, the statistical analyses were difficult to perform given the structure of the programs being used. Our field work methods also contained variation across the treatments. As the tiles were merely rinsed rather than begin destructively sampled, not every specimen residing on the tile was collected. The complexity of the tiles also affected how effective our method was; the bulkhead tile for example was flat and slick, making it much easier to rinse than the oyster shell tile which would have significant effects on our abundance measurements.

Although error is present, these results are important because the variance in community associated with each treatment show that biodiversity increases with complexity. This correlates to previous work with the Reef design Lab tiles that were trying to enhance existing seawalls; by placing more complex tiles onto seawalls, the biodiversity of the existing shoreline can be increased, benefiting the marine ecosystem as a whole. All species collected from these tiles are also native to the Chesapeake Bay, showing that the ratio of native to invasive species can be improved by providing a more hospitable habitat.

The communities that developed with this 3.5-week interval also represent the initial development of an ecosystem prior to spat settlement. The community will continue to develop as the tiles remain in the subtidal zone of the York River for another year. Future analyses will compare this initial growth to how the community has been affected by the recruitment of oysters.

Acknowledgements

I thank everyone who contributed ideas, technical help, equipment, and advice throughout my time at VIMS. Special thanks to my mentor, Dr. Romuald Lipcius, lab managers Gabby Saluta and Katie Knick, as well as lab technicians Mike Seebo and Alison Smith who helped make this research experience phenomenal. I am also grateful to Rachel Wilson, Sarah Monica, and Chante Lively, fellow interns with whom I worked closely that all aided in my project design and implementation as well as Governor School students Emma Lambert, Jessie Steadman, Logan Flanagan and summer aide Jordan DeBerry. Thank you to Jenny Dreyer and Katherine Longmire for coordinating the REU program at VIMS. Program funding for the VIMS Research Experience for Undergraduates was made available through a grant awarded from the National Science Foundation (grant # NSF OCE 1659656) to Drs. Linda Schaffner and Rochelle Seitz.

Literature Cited

Bahr, L. M. and W. P. Lanier (1981). The ecology of intertidal oyster reefs of the south Atlantic coast: a community profile. Technical report, U.S. Fish and Wildlife Service.

Chapman, M. G., & Underwood, A. J. (2011). Evaluation of ecological engineering of "armoured" shorelines to improve their value as habitat. Journal of Experimental Marine Biology and Ecology, 400(1-2), 302-313.

Chesapeake Bay Foundation (2019). Oyster Fact Sheet. Retrieved from https://www.cbf.org/about-the-bay/more-than-just-the-bay/chesapeake-wildlife/eastern-oysters/oyster-fact-sheet.html

Coen, L. D., R. D. Brumbaugh, D. Bushek, R. Grizzle, M. W. Luckenbach, M. H. Posey, S. P. Powers, and S. G.

Tolley (2007). Ecosystem services related to oyster restoration. Marine Ecology Progress Series 341: 303–307.

Ido, S., & Shimrit, P. (2015). Blue is the new green – Ecological enhancement of concrete based coastal and marine infrastructure. *Ecological Engineering,84*, 260-272.

Kreeger, D. A., Gatenby, C. M., & Bergstrom, P. W. (2018). Restoration potential of several native species of bivalve molluscs for water quality improvement in Mid-Atlantic watersheds. Journal of Shellfish Research, 37(5), 1121-1157.

Lawrence, D. (1971). Shell orientation in recent and fossil oyster Communities from the Carolinas. Journal of Paleontology, 45(2), 347-349.

Strain, Elisabeth & Morris, Rebecca & Coleman, Ross & Figueira, Will & Steinberg, Peter & Johnston, Emma & Bishop, M.J.. (2017). Increasing microhabitat complexity on seawalls can reduce fish predation on native oysters. Ecological Engineering.

Sutherland, J. (1974). Multiple stable points in natural communities. The American Naturalist, 108(964), 859-873.

Theuerkauf, K. W., Eggleston, D. B., & Theuerkauf, S. J. (2018). An exotic species alters patterns of marine community development. Ecological Monographs, 88(1), 92-108.